10-21

Argonne Physics Division
Informal Report PHY-1971A
June 1971

A STUDY OF THE ^{50}V NUCLEUS WITH THE (^{3}He,d), (^{3}He,α), (^{3}He,p), AND (^{3}He,pγ) REACTIONS*

by

James W. Smith†

Argonne National Laboratory, Argonne, Illinois 60439

*Work performed under the auspices of the U.S. Atomic Energy Commission.

†Present address: Ohio State University, Columbus, Ohio 43212.

DISCLAIMER

The facilities of Argonne National Laboratory are owned by the United States Government. Under the terms of a contract (W-31-109-Eng-38) between the U. S. Atomic Energy Commission, Argonne Universities Association and The University of Chicago, the University employs the staff and operates the Laboratory in accordance with policies and programs formulated, approved and reviewed by the Association.

MEMBERS OF ARGONNE UNIVERSITIES ASSOCIATION

The University of Arizona
Carnegie-Mellon University
Case Western Reserve University
The University of Chicago
University of Cincinnati
Illinois Institute of Technology
University of Illinois
Indiana University
Iowa State University
The University of Iowa
Kansas State University
The University of Kansas
Loyola University
Marquette University
Michigan State University
The University of Michigan
University of Minnesota
University of Missouri
Northwestern University
University of Notre Dame
The Ohio State University
Ohio University
The Pennsylvania State University
Purdue University
Saint Louis University
Southern Illinois University
The University of Texas at Austin
Washington University
Wayne State University
The University of Wisconsin

Argonne Physics Division
Informal Report PHY-1971A
June 1971

A STUDY OF THE ^{50}V NUCLEUS WITH THE (^{3}He,d), (^{3}He,α), (^{3}He,p), AND (^{3}He,pγ) REACTIONS*

by

James W. Smith†

Argonne National Laboratory, Argonne, Illinois 60439

The author has a limited number of copies for general distribution. Anyone who desires a copy should contact him directly; the PHY Informal Reports are not handled through the ANL Technical Publications Department.

---

*Work performed under the auspices of the U.S. Atomic Energy Commission.

†Present address: Ohio State University, Columbus, Ohio 43212.

TABLE OF CONTENTS

LIST OF TABLES

LIST OF FIGURES

ABSTRACT

The nucleus ^{50}V with a ground-state configuration $(\pi f_{7/2})^3(\nu f_{7/2})^{-1}$ has been studied with the $^{49}Ti(^3He,d)^{50}V$, $^{51}V(^3He,\alpha)^{50}V$, $^{48}Ti(^3He,p)^{50}V$, and $^{48}Ti(^3He,p\gamma)^{50}V$ reactions induced by the $^3He^{++}$ beam from the tandem Van de Graaff at the Argonne National Laboratory. The angular distributions from $(^3He,d)$, $(^3He,\alpha)$, and $(^3He,p)$ reactions induced by 22-MeV ^3He were studied with overall energy resolution widths of 20, 30, and 42 keV, respectively. The reactions $(^3He,p)$ and $(^3He,p\gamma)$ were also studied at an incident energy of 13 MeV to obtain the γ decay of ^{50}V levels (including two 0^+ isobaric analog states) in which the neutron-proton pair is transferred with zero angular momentum.

The angular distributions of the charged-particle reactions have been analyzed with the distorted-wave Born approximation (DWBA), and spectroscopic factors have been extracted for the one-nucleon transfer reactions. The two-nucleon transfer reaction $(^3He,p)$ has been analyzed with the DWBA on the assumption that the neutron-proton pair is transferred as a deuteron. The angular momentum L_{np} of the transferred deuteron is established for most of the levels, and the possibility that several levels might have spin and parity 1^+ is discussed.

This work has resulted in the assignment of $J^\pi = 1^+$ to levels at 1.333 and 1.490 MeV and supports the previous tentative spin assignments of 5^+, 4^+, 3^+, and 2^+ for the first four excited states. Seven states—these four states and the 6^+ ground state, the 7^+ state at 0.911 MeV, and the 1^+ state at 1.333 MeV—are identified as members of the $(\pi f_{7/2})(\nu f_{7/2})^{-1}$ octet. The γ decay of the two 0^+ isobaric analog states is observed to proceed by M1 transitions to low-lying states. The γ decay of several levels between 1.3 and 4 MeV excitation energy (some of them being possible candidates for a collective 1^+ excitation) are seen to decay in part to

the same levels that are populated by decay of the two 0^+ analog states.

Two models are evaluated with respect to the known data: (1) the truncated $1f_{7/2}$ shell model of McCullen, Bayman, and Zamick (MBZ) and (2) the rotational particle coupling (RPC) model of Wasielewski and Malik. The MBZ model predicts the energy levels and allows the calculation of spectroscopic factors which may be compared with experimental data. The results of the RPC model can be compared only with the experimental energy levels at this time.

I. INTRODUCTION

A. Purpose of This Work

A scan of the current nuclear physics journals will reveal very many studies of $1f_{7/2}$-shell nuclei with one or two nucleons outside a closed shell (e.g., outside the closed shells of ^{40}Ca or ^{48}Ca) but fewer studies of nuclei such as ^{50}V with several nucleons outside a closed shell (Ri69). This situation arises because adequate shell-model calculations for nuclei farther from the closed shells are not generally available. The view taken in this work is that further measurements on these more complicated nuclei should be made in order to find the direction new calculations should take. The particular nucleus chosen is ^{50}V, which has three proton particles $(\pi f_{7/2})^3$ and one neutron hole $(\nu f_{7/2})^{-1}$ outside a ^{48}Ca core and so has four free particles and a core. It is not so complicated as ^{48}Cr $(\pi f_{7/2})^4(\nu f_{7/2})^{-4}$, for example, but not so simple as ^{49}Sc $(\pi f_{7/2})$. The purpose of this work is to study the nature of the levels in the ^{50}V nucleus experimentally and to compare the predictions of the current models against the results of this study.

One of the most powerful methods for studying the nature of nuclear states is the distorted-wave Born-approximation (DWBA) analysis of the angular distribution of charged-particle transfer reactions, developed for the most part in the last decade (Ba62). The shape of the angular distributions of stripping and pickup reactions are dependent on the orbital angular momentum of the transferred particle and may also depend on the total angular momentum of the state in which the residual nucleus is left (Br69). Further, the spectroscopic factor obtained from comparing experimental angular distributions with DWBA predictions is a measure of the extent to which the final nuclear state is an inert core and the

transferred nucleon is in a single-particle state. As a result, the DWBA is a more sensitive probe of the nature of the nuclear states than is the determination of excitation energies. The spectroscopic factors may be calculated directly from model wave functions, and a comparison with experimental values provides a direct test of the model.

The requirement that the target be a stable nuclide restricts the study of ^{50}V by single-nucleon-transfer reactions to proton stripping and neutron pickup. The reactions chosen in this work were (^{3}He,d) and (^{3}He,α) in order to measure proton particle and neutron hole excitations in levels of ^{50}V. On the other hand, the two-nucleon transfer reactions often excite a different type of nuclear state than do the one-nucleon transfer reactions. The excitation of pairing-vibration states has received considerable attention recently, and evidence for pairing vibrations is found in the 1f-2p shell (Sh69 and Sh69a) by use of the (^{3}He,p) reaction. In the present work, the ^{48}Ti(^{3}He,p)^{50}V reaction is used to excite levels not reached by the (^{3}He,d) and the (^{3}He,α) reactions.

The γ decay of nuclear states is another sensitive test of nuclear wave functions. In particular, the γ decay of isobaric analog states (IAS) has received some attention lately (Er66, Ku68, Me70) because the IAS are highly excited states whose nuclear configurations can be known approximately by studying their parent states. The approach taken here has been stated best by Kurath (Ku68). "If the analog state is . . . simple, in the sense that it can be described as a single core state coupled to an odd nucleon [for ^{50}V, two nucleons], then the study of its decay to more complicated intermediate states reveals one aspect of their structure while the subsequent decays to the simple low-lying states provide further information about their nature." In the case of ^{50}V there are two

($J^\pi = 0^+$) particle-bound IAS that are populated by (^{3}He,p) and whose nuclear configurations are approximately known because their parent states in ^{50}Ti at 0.0 and 3.88 MeV have been studied by the (p,t) reaction (Hi67). These IAS appear strongly in the (^{3}He,p) reaction and their γ decay may be studied by the (^{3}He,pγ) reaction. Only those γ rays that are in time coincidence with protons populating levels in ^{50}V are recorded. The (^{3}He,p) reaction transfers a neutron-proton pair either with S = 0, T = 1 (singlet state) or S = 1, T = 0 (triplet state). Starting with a target of ground-state spin 0^+ and isospin T, if the n-p pair is transferred with orbital angular momentum $L_{np} = 0$, the singlet state populates 0^+, T + 1 ($T_>$) and 0^+, T ($T_<$) levels and the triplet state populates 1^+, T ($T_<$) levels. The orbital angular momentum $L_{np} = 0$ is easily selected by positioning the proton detector at 0^o with respect to the incoming beam; at this position, only $L_{np} = 0$ has a very strong maximum in its angular distribution.

B. Survey of Previous Work on ^{50}V

The ^{50}V ground-state spin, parity, magnetic dipole moment, and electric quadrupole moment have been established for some time (Li64, Wa62). Figures I-1A and I-1B show the correct early measurements of the level scheme. An attempt to measure the spins of some excited states by exploiting the total-angular-momentum dependence of the angular distributions from the ^{50}Ti(^{3}He,t)^{50}V reaction (Br69) is shown in Fig. I-1C. Three of the four assigned states are not resolved from nearby states and hence are not reliable. However, the state at 911 keV is established to be 7^+. A larger cross section for neutron pickup to this state than for that to the 6^+ ground state (Ba65) supports this assignment by the 2J + 1 rule, which predicts that the ratio should be 15:13.

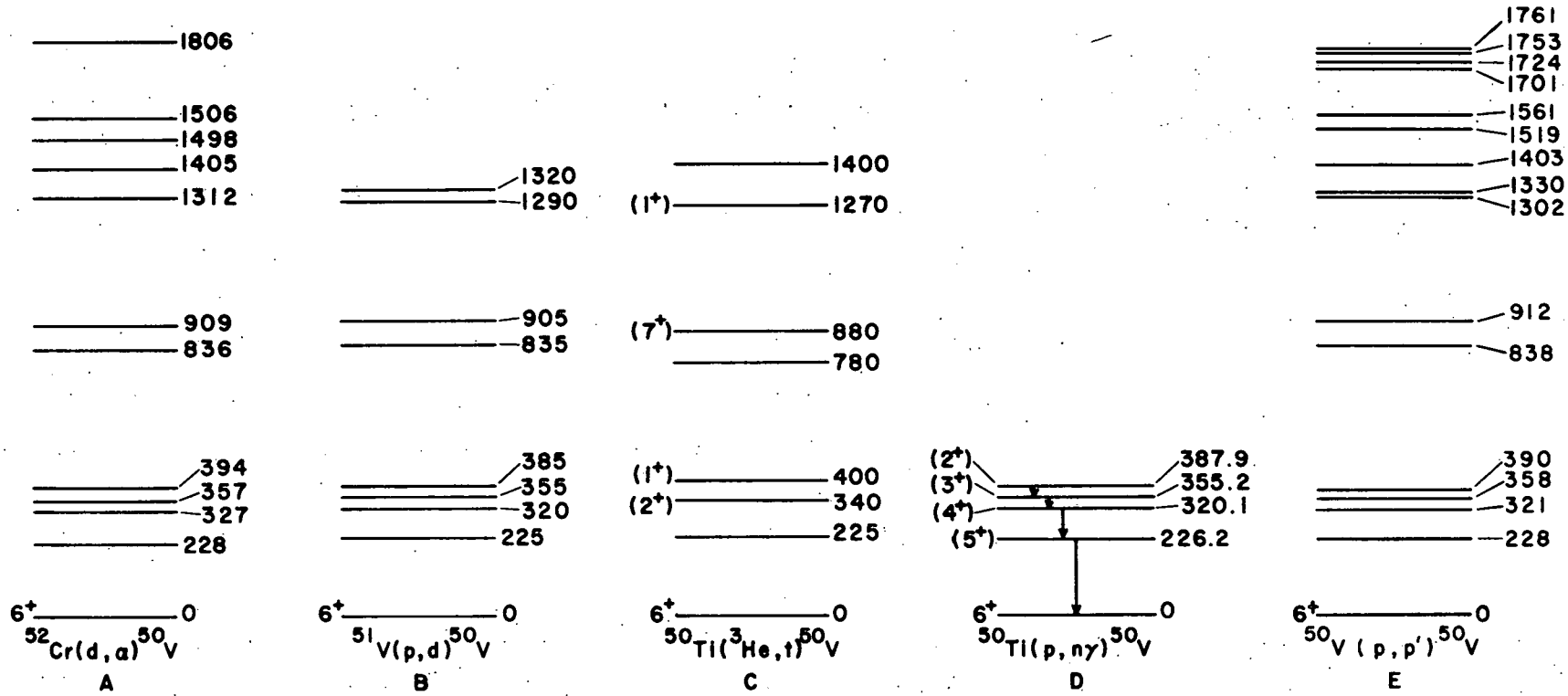

Fig. I-1. ^{50}V energy levels, spin assignments, and γ-ray decay scheme from the reactions A) ^{52}Cr(d,α)^{50}V, B) ^{51}V(p,d)^{50}V, C) ^{50}Ti(^{3}He,t)^{50}V, D) ^{50}Ti(p,nγ)^{50}V, and E) ^{50}V(p,p')^{50}V.

The latest measurement of the ^{50}V energy levels, a high-resolution (8 keV FWHM) study of the inelastic scattering of protons, is shown in Fig. I-1E. This spectrum includes all previously observed levels except the one at 1498 keV, which was seen only in the (d, α) reaction.

Studies of the γ-ray decay of levels below 400 keV by use of the $^{48}Ti(t,n\gamma)^{50}V$, $^{49}Ti(p,\gamma)^{50}V$ (Se69), and by $^{50}Ti(p,n\gamma)^{50}V$ (Bl69) have led to conflicting reports. Of the two reports, the $^{50}Ti(p,n\gamma)^{50}V$ by Blasi is thought to be correct and the γ decay (M1 tentatively) is shown in Fig. I-1D with the (tentatively) assigned spins. Crossover transitions are measured to be less than 2% of the cascade intensity.

Turning to the theoretical situation, shell-model calculations that attempt to reproduce the results of experimental measurements are beset by uncertainties, which may be divided into two principal types (Mc64): (1) the number of shell-model configurations necessary to adequately represent the nuclear state and (2) the nucleon-nucleon residual interaction. Correspondingly, the choice between the two principal approaches to shell-model calculations depends on which type of uncertainty is felt to be the most serious. If type (1) is felt to dominate the problem one might assume a detailed residual interaction and use wave functions of the single-particle shell-model states. It is then possible to calculate the matrix elements between states of as many configurations as can be diagonalized with the available facilities. In principle, then, one has only uncertainties of types (2).

In some regions of the periodic table, however, shell closures drastically limit the number of important configurations and thereby minimize the uncertainties of type (1). The $1f_{7/2}$ orbital satisfies this condition, being separated from the lower 2s1d shell

and the upper $2p_{3/2}$ orbital by a few MeV. In this case the nucleon-nucleon two-body interaction matrix is determined by a few energy-level differences which may be extracted from the experimental data.

The latter approach has been adopted by McCullen, Bayman, and Zamick (Mc64) in order to get wave functions of some of the $1f_{7/2}$ nuclei including ^{50}V. (The results are traditionally known as MBZ wave functions, MBZ magnetic moments, etc.) MBZ do not propose that pure $1f_{7/2}$ configurations and two-body interactions are necessarily valid assumptions, but rather that those phenomena that cannot be explained by a pure $1f_{7/2}$ shell and two-body interactions point the way for future extended calculations.

Although often tacitly assumed, the shell model is not the only model to be successful in the nuclei usually known as 1f2p-shell nuclei. The strong-coupling symmetric-rotor model, including rotational particle coupling or Coriolis coupling between bands, has been developed by Malik and Scholz (Ma66, Sc66) and has had considerable success in predicting ground-state spins and level densities in odd-mass nuclei in the 1f2p shell. In a recent calculation (Wa70) on ^{55}Mn and ^{57}Fe, the excitation energies, magnetic and quadrupole moments, lifetimes, B(E2) values, mixing ratios, and branching ratios differ somewhat from the best current shell-model calculations but agree as well with experiment, and the parameters used are no more "free" than are the shell-model parameters (Co70). This model has been extended to the odd-odd nucleus ^{56}Mn by including a neutron-proton residual interaction (Wa70a) and has produced results in good agreement with experimental quantities (Wa70). The calculation for odd-odd nuclei is readily adapted to calculations for ^{50}V.

At first sight there appears to be a basic contradiction if both the symmetric-rotor model and the shell model agree with

experiment, inasmuch as they are based on entirely different views of the nucleus. However, in each case the model parameters chosen are those that lead to a best fit to the experimental data. Clearly, comparisons between the models will be difficult since each is basically a parameterization of the experimental data and since there is no way to state whether excitation energies or quadrupole moments, for example, are more important. Rather, the discrepancies between each theory and experiment results should be examined separately to establish in what manner that parameterization fails to be congruent with nature. Despite the equal claims of the models, most of the discussions that follow will be in terms of the shell-model for clarity.

C. Summary

The purpose of this work is to extend the experimental knowledge of the ^{50}V nucleus by studying the proton-stripping (^{3}He,d) and neutron-pickup (^{3}He,α) reactions and also through the neutron-proton pair-transfer reaction (^{3}He,p) and the γ decay of particle bound levels (including two 0^{+} isobaric analog states) that are strongly populated by it. The nucleus ^{50}V is subject to calculations by two different models, although each of the models is preliminary and limited in scope. The experimental results will be compared with the predictions of the model calculations.

II. $^{48}Ti(^{3}He,p\gamma)^{50}V$ PARTICLE-GAMMA COINCIDENCE MEASUREMENT

A. Beam Handling

The ^{3}He nuclei used in these measurements were accelerated by the Argonne model-FN tandem Van de Graaff, which was built by High Voltage Engineering Corp. (Wa64). The accelerator and beam-transport system are shown in Fig. II-1. Singly-charged negative ^{3}He ions are injected into the tandem from an Ortec Duoplasmatron ion source. The $^{3}He^{-}$ are then accelerated from ground potential toward the center terminal of the tandem. In this terminal, whose voltage is variable from 2.5 to about 8 MV, the ions pass through oxygen gas or a carbon foil where their electrons are stripped off. The resulting $^{3}He^{++}$ ions then leave the terminal and are accelerated to ground potential; and since they are now doubly charged, they gain 2 eV for each volt of terminal potential. After leaving the tandem tank, the $^{3}He^{++}$ ions are deflected 90^{o} by an analyzing magnet and enter into the experimental area. Control slits at the exit of the 90^{o} magnet measure the amount of beam bent more than 90^{o} (too low an energy) and less than 90^{o} (too high an energy). The two currents are then balanced by a (negative) feedback system that controls the voltage on the terminal. In this way the particle energy is maintained accurately. The energy spread of the particles in the beam is less than 5 keV, and the energy is reproducible to about 25 keV.

B. Target-Chamber Hardware

The ^{3}He beam emerging from the tandem is spacially divergent and difficulties arise in forming a well-defined beam spot on the target. A quadrupole magnetic lens is used to focus

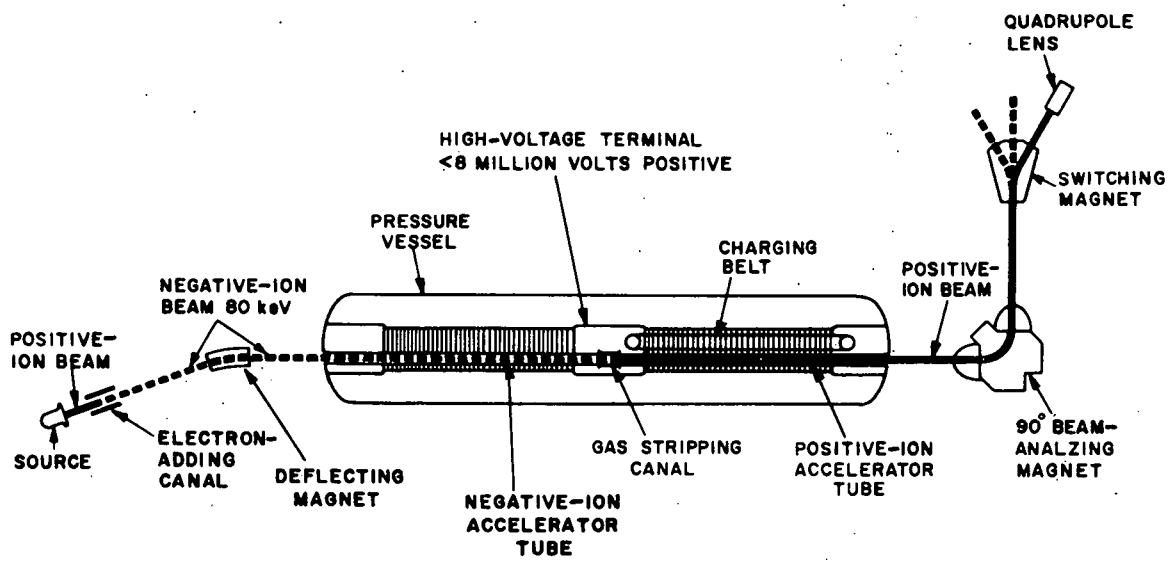

Fig. II-1. Essential features of a tandem Van de Graaff ion accelerator and its beam-handling system.

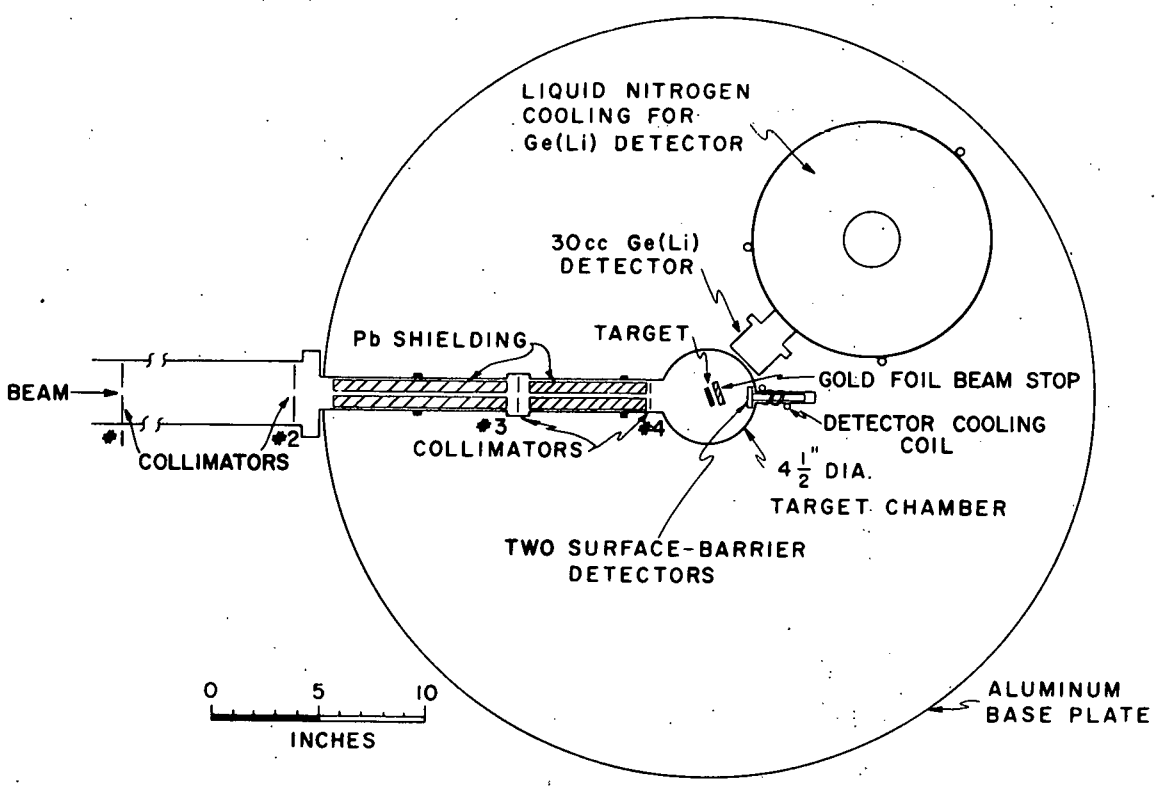

Fig. II-2. Target-chamber hardware and beam-collimation system for the particle-gamma coincidence measurement.

the beam through sets of collinear apertures to form a collimated beam. The size and separation of the apertures determines the degree of collimation. The physical size of the beam profile at the collimators may be made circular and about $\frac{1}{16}$ in. in diameter; collimator apertures smaller than this were found to reduce the target current seriously.

The beam collimation for γ-ray experiments was designed to achieve two necessary or desirable conditions: 1) the beam spot on the target often must be made small so that the angle between the emitted γ ray and the beam axis could be accurately determined, and 2) the flux of γ rays and neutrons striking the collimators and scattering to the γ detector must be kept to a minimum. These γ rays and neutrons would cause unwanted background in the spectrum accumulated, and in Ge(Li) gamma detectors such neutrons may induce charge-trapping centers in the germanium crystal and eventually end the usefulness of the crystal as a γ detector. The first condition is best achieved by an aperture close to the target and detector, whereas the second requires an aperture (to stop the unfocused part of the beam) far from the target and detector.

The collimator arrangement used in this experiment is shown in Fig. II-2. Collimator No. 1 is a square aperture formed by four tantalum slit jaws that are independently movable by two mutually perpendicular pairs of micrometers. Thus the size and/or position of the aperture can be adjusted, or the jaws can be retracted out of the beam path. Collimator No. 2 is a fixed circular aperture $\frac{1}{16}$ in. in diameter. Collimator No. 3, a tantalum disk with a circular aperture $\frac{1}{16}$ in. in diameter, can be swung out of the beam path without opening the beam line. Collimator No. 4 is placed close to the target chamber in order to intercept the beam

scattered from the edges of the other collimators. It is a fixed aperture $\frac{1}{4}$ in. in diameter. To get the beam on target, collimators No. 1 and 3 are removed from the beam path and the beam reaching the target via No. 2 and 4 is maximized. Next, collimator No. 3 is inserted and the target current is remaximized. Finally, collimator No. 1 is closed down until the beam spot is of the desired size. The unfocused part of the beam is intercepted by these slit jaws, which are far from the target and the Ge(Li) detector. Typical currents are 150 nA on target, 150 nA intercepted by collimator No. 1, 2—10 nA on No. 2, and 0.1—0.2 nA on No. 3.

After collimation, the beam strikes the target (a 1-mg/cm^2 metallic foil). The transmitted beam and the reaction products emitted in the forward direction encounter a 0.003-in. gold-foil beam stop (Fig. II-2), where the $^3He^{++}$ beam and the heavy reaction products are stopped and their charge is measured by a current integrator system (Model 1000, Brookhaven Instruments Corp., Brookhaven, N.Y.). Light, highly-energetic reaction products—from such reactions as (^{3}He,p) which has a high Q—penetrate the foil and are energy analyzed in a pair of 2000-μm Ortec silicon surface-barrier detectors in tandem.

Because the surface-barrier detectors draw several microamperes of reverse current at room temperature, they are cooled to well below 0°C by circulating alcohol at -72°C around the outside of the tube in which the detector is mounted, as shown in Fig. II-2. The very small heat load (200 V operating voltage × a few microamperes of detector current) allows the temperature of the detectors to be almost equal to the temperature of the coolant. Since the alcohol is wholly outside the vacuum chamber, the vacuum is protected from accidental leaks or breaks in the circulating tubes. The alcohol from a reservoir cooled by a bath of alcohol

and solid CO_2 is circulated by a small squirrel-cage pump submerged in the reservoir. A stainless steel shaft connects the pump to an electric motor located outside the cold jacket.

The Ge(Li) γ detector slides on an aluminum base plate fastened rigidly to the target chamber, and its angular position with respect to the beam can be varied from 0 to 140° in 5° steps. However, the requirement that the Ge(Li) detector be very close to the target (to maximize the detection efficiently) usually restricts the angular range to $30-135^{\circ}$. The Ge(Li) detector used was purchased from ORTEC. Its volume is 30 cm^3 and it has 3 keV resolution for 1.33-MeV gamma rays.

A good vacuum is required in the target chamber and the beam line for two reasons. First, scattering in residual gas would increase the difficulty in achieving a small intense beam spot on the target. Second, and most important, contamination of the target would introduce background in the observed spectra. The most serious of the target contaminants for the measurement under consideration here are carbon, oxygen, and hydrogen. By mounting a 4-in. T-M Mini-Imp diffusion pump (T-M Vacuum Products, Riverton, New Jersey) with a liquid-nitrogen cold trap immediately below the target chamber (diameter $4\frac{1}{2}$ in.) a vacuum of 10^{-6} Torr in the target chamber is achieved. This is sufficient to eliminate the first problem and to bring the second under control. The use of rolled self-supporting metallic foils as targets has further reduced the troubles with these contaminants.

C. Experimental Problems and Methods

A two-parameter pulse-height analysis provides the best method of accumulating particle-gamma coincidence information. One parameter is taken as the particle energy as analyzed by

the surface-barrier detector and the other parameter as the γ-ray energy as analyzed by the Ge(Li) detector. The events of the γ decay of a level in the residual nucleus then appear as a row of peaks along the gamma-energy axis and the particle emission is represented by a similar row of peaks along the particle-energy axis. The result is a two-dimensional plane surface. From the positions of peaks on the particle-energy axis, the excitation energies of the levels populated in the nucleus may be obtained. From the position of the peaks in the row parallel to the gamma-energy axis and from the numbers of events in the peaks, the gamma decay scheme of the nuclear level corresponding to the position on the particle-energy axis may be determined. One such row of gamma-energy peaks will appear for each nuclear level populated by the charged-particle reaction.

However, for a case in which events corresponding to true particle-gamma coincidences have small cross sections, as is shown to be the case here, the measurement can be obscured by large numbers of random coincident events. At an emission angle of 5^{o}, the cross section for the $^{48}Ti(^{3}He,p)^{50}V$ reaction leading to the lowest isobaric analog state (IAS) is known to be about 100 μb/sr (Sh69). For the experimental arrangement shown in Fig. II-2, a proton detector subtending a solid angle of 100 msr, a beam current of 100 nA, and Ti targets with a thickness of 1 mg/cm^{2}, reactions leaving the ^{50}V in the lowest IAS will lead to 40 protons/s entering the proton detector. Then if the 30-cm^{3} Ge(Li) detector is placed 13 cm from the target (where it will have a detection efficiency of 4% at 1 MeV for the full-energy peak) and if the gamma rays are distributed isotropically (a valid assumption for the J = 0 lowest IAS), then the coincidence rate recorded in the apparatus will be about 0.006 events/s = 21 events/h. Note that the

values used in the above calculation are the maximum possible values of the quantities involved. With the values in this example the event rate in the surface-barrier detector is 20 000 s^{-1} and the events rate in the Ge(Li) detector is 35 000 s^{-1}.

Simply stated, the experimental difficulties all arise because the number of events of interest are a small portion of the total number of events occurring. Experimentally, this difficulty shows up in two requirements on the electronic circuitry. First, the electronics must reject enough random coincident events to yield a spectrum in which the peaks of interest stand out against the background. The random coincidences look like a fairly smooth background because they are the sum of a large variety of γ decays, whereas the true coincidences for each γ ray are collected together because of the high resolution of the Ge(Li) detector. Therefore a 20:1 true-to-random ratio in a true coincidence peak can correspond to about a 0.1:1 true-to-random ratio over the whole spectrum.

Second, the electronics must reject those events that result in pileup of the energy pulses in the amplifier and in the analog-to-digital converter and consequently lead to spectral distortion. Because some gamma lines of interest are separated by only 25 keV in energy, the spectral distortion in the gamma spectrum must not get worse than $\sim$10 keV. This last requirement is especially important in the present investigation because the resolution width in the proton spectrum is about 300 keV as a result of the target thickness (1 mg/cm^2) and the straggling in the gold-foil beam stop. This poor resolution precludes the separation of proton groups which leave the residual nucleus in a specific level.

The rest of this subsection is devoted to the steps taken to solve these two experimental problems, namely (1) to maximize the true-to-random ratio, and (2) to minimize the spectral distortion due to pile-up.

1. Maximization of the True-to-Random Ratio

The pulses from the detection of the proton which leaves the ^{50}V nucleus in a given state and the pulses from the detection of the gamma rays resulting from the decay of that state appear at the pulse-handling system within a few nanoseconds of each other (barring metastable states). By measuring the time interval between the detection of the proton and the gamma event to sufficient precision, the ratio of true to random coincident events can be increased to an arbitrary value. Let R be the true-to-random ratio, T the width of the time window within which the timing system accepts events as coincident ($T = 2\tau$, where τ is the pulse width for overlap coincidence), $N_{p\gamma}$ the true coincidence rate, N_p the proton rate, and N_γ the gamma rate. Then the desired time window is given by

$$T = N_{p\gamma}/(N_p N_\gamma R).$$

For a true-to-random ratio of 0.1:1 (over the whole spectrum), a true coincidence rate of 9 s^{-1} (over the whole spectrum), a proton rate of 20 000 s^{-1} (over the whole proton spectrum) and a gamma rate of 35 000 s^{-1} (over the whole gamma spectrum), the necessary time window T is $\sim$125 ns. If T could be reduced below 125 ns, a further improvement in R will result.

There are two general methods for electronically marking, or picking off, the time at which a pulse from a detector occurs. The two, called leading-edge pickoff and cross-over pickoff, are diagrammed in Fig. II-3. For cross-over pickoff (Fig. II-3b), a doubly-differentiated bipolar pulse is put into a circuit capable of responding when the pulse voltage passes through zero after an initial threshold (the discriminator setting) has been reached. In principle, the zero crossing of a pulse should be

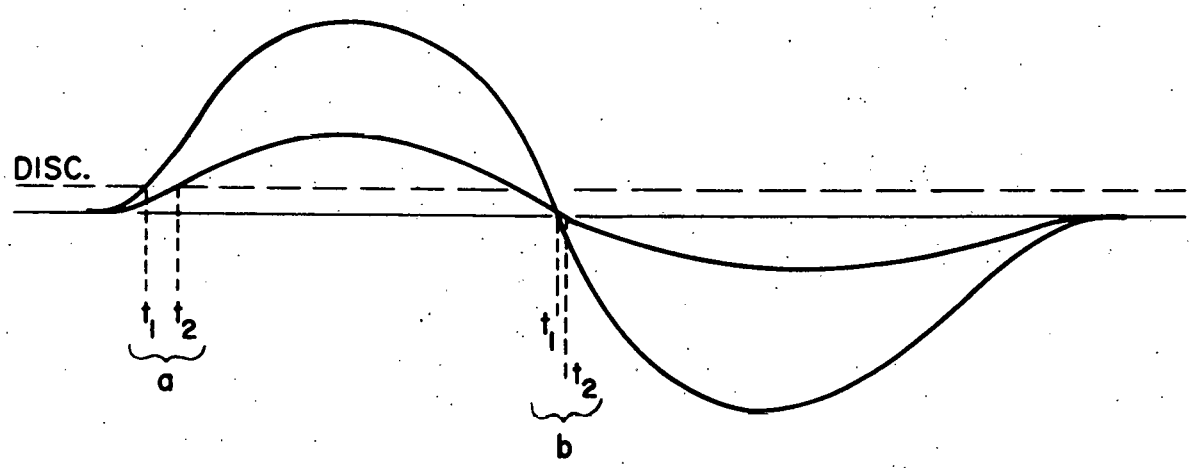

Fig. II-3. Diagram explaining the meaning of leading-edge- and crossover-time pickoff.

independent of pulse amplitude (although noise in the circuit will cause some "jitter" in the signal and will result in some uncertainty in the time of zero crossing). If the amplitude or rise time affect the measured time of zero crossing, the resultant variation $(t_2 - t_1)$ is called "walk."

For leading-edge pickoff (Fig. II-3a), the discriminator level is set above the noise level; and whenever a signal increases beyond that level, a timing signal is generated. Clearly jitter causes uncertainty in leading-edge pickoff to the same extent as in cross-over pickoff. Figure II-3a, which shows leading-edge pickoff on a slowly rising pulse, indicates the walk that accrues from the difference in the rise time of pulses with different amplitudes. This walk is exaggerated in Fig. II-3a because the rise-time is so slow; in practice, one uses a steeply rising pulse such as is available at the output of a detector or a preamplifier. Nonetheless, amplitude-dependent walk is a significant problem with leading-edge pickoff. This walk problem may be enhanced in the case of a coaxial Ge(Li) detector, whose nonuniform charge-collecting fields lead to risetime-dependent effects due to the different positions at which the γ rays are incident on the Ge(Li) crystal.

In the first attempt to avoid amplitude-dependent walk, standard Ortec equipment designed for cross-over pickoff was used for the signals from both the Ge(Li) and the surface-barrier detectors. The resulting pulses proportional to the interval between the two time marks were pulse-height analyzed to obtain a time spectrum of true events. A full width at half maximum (FWHM) of 60—80 ns, corresponding to a full width of 200—250 ns, was achieved with a 20:1 dynamic range for the energy pulses. Although this resolving time (full width) could be considered acceptable, a value more like 100 ns was desired. The pulse-shape variation

due to uneven charge collection in the coaxial Ge(Li) have defeated our attempts to attain zero walk with cross-over pickoff. That is, cross-over pickoff may be independent of amplitude but not of pulse shape. Ortec has recently marketed a "constant-fraction timing discriminator" which compensates for the effects of amplitude and rise time in cross-over pickoff, but this device was not yet available for evaluation at the time of this study.

It is inadvisable to do leading-edge timing on the output of the main amplifier because the pulse integration (necessary for energy resolution) introduces walk of the order of a microsecond. The best place to do leading edge timing is immediately after the detector (by using a pulse transformer). Unfortunately, this would worsen the energy resolution significantly in the case of the Ge(Li) detector. Instead, a buffered pulse output of the preamplifier was used as the input to a low-level leading-edge fast discriminator. The preamplifier has a fast rise time and a very wide bandwidth so that a minimum of time information from the detector is lost. The output of the fast discriminator from the proton detector and from the gamma detector are fed into the start and stop, respectively, of a time-to-pulse-height converter. The time spectrum, the pulse-height analyzed output of the converter, is shown in Fig. II-4b. The FWHM is 28 ns, with a dynamic range of 100:1 for the γ energy pulses. If the output of the converter were put into a single-channel analyzer in order to set a time window T on the proton-gamma pulse pair, a window about 200 ns wide would be needed because of the asymmetric shape of the spectrum. This shape is a result of the large number of low-energy gammas, which have considerable walk as shown in Fig. II-3a. Inasmuch as this work will be concerned only with gammas from about 300 keV to 7.5 MeV, the gammas

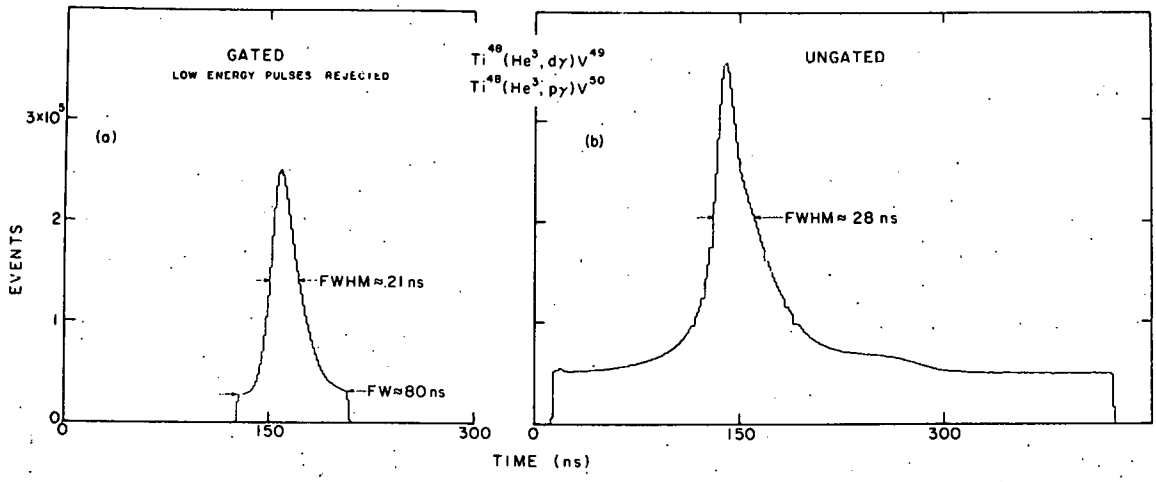

Fig. II-4. Time spectra from leading-edge-time pickoff a) for protons from 6 to 22 MeV and gammas from 0.300 to 8 MeV and b) for all protons and all gammas incident on their detectors.

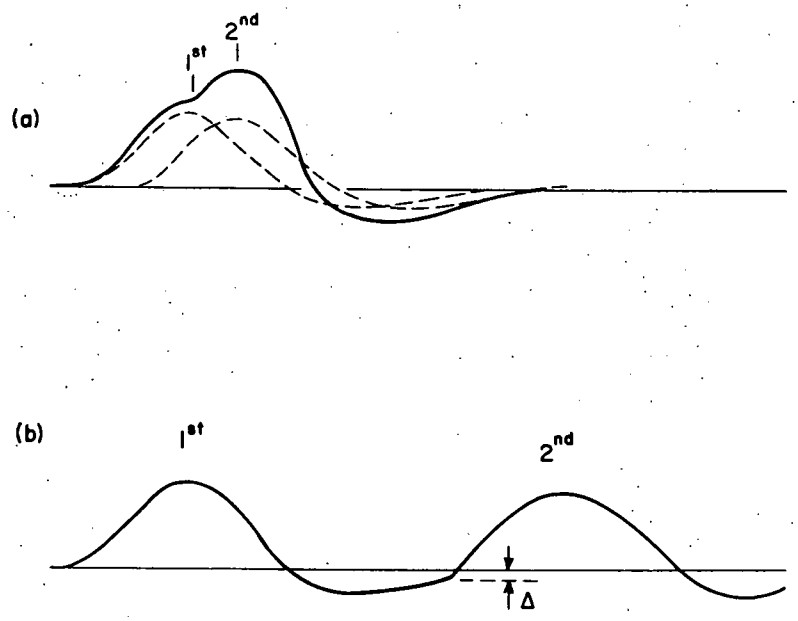

Fig. II-5. Diagram explaining the meaning of pileup and the distinction between a) peak pileup and b) tail pileup.

(from real coincident events) below 300 keV unnecessarily broaden the time window. By gating the output of the time-to-pulse-height converter with an energy window covering the range from 300 keV to 7.5 MeV before putting it into the multichannel pulse-height analyzer, the time spectrum shown in Fig. II-4a is obtained. The FWHM has been improved by 7 ns, but more importantly, the shape of the peak is more symmetric and the full width of the peak is less than 80 ns. Figure II-4a is in fact the time spectrum accumulated during the measurement of the gamma decay to be presented at the end of this chapter. The true-to-random ratio is 2.3:1 over the whole spectrum.

2. Minimization of Spectral Distortion

Having decided how the events of interest are to be selected from the great number of random coincident events, one must ensure that the pulses from the events that are rejected by the timing system are not allowed to distort the pulse height of the unrejected pulses before they get to the pulse-height analyzer. This distortion arises from the pulse pile-up, which may be classified as either peak pile-up or tail pile-up, as illustrated in Fig. II-5a and b, respectively.

In the case of tail pile-up, one pulse rides on the tail of an earlier pulse (Fig. II-5b) and as a result the pulse height is incorrect by the amount Δ, the pulse defect. If this pulse is accepted into the final spectrum, it will miss its correct position in the spectrum by an amount corresponding to Δ. The best solution to the tail pile-up is to eliminate the tail by direct coupling all the electronics from the detector to the analyzer. Unfortunately this is not within the present state of the art for electronic pulses. However, Δ can be minimized by forcing the pulse back to the

base line in the shortest possible time by the use of pole-zero cancelation and base line restoration. These devices use active elements to force the pulse to return to the base line with as little as possible effect on the pulse height. Also, using the smallest possible time constants in the shaping amplifier tends to expand the time scale and thus reduces Δ. On the other hand, a reduced time constant worsens the energy resolution. For the Ge(Li) detector, a pulse-shaping time constant of 2 μs produces good energy resolution (at low counting rates) but 0.5 and 1 μs may be used in many cases in which the very highest resolution is not required. With the poor proton-energy resolution expected in this measurement, time constants of 0.5 μs are entirely satisfactory in the shaping circuit. Another device used supresses tail pile-up by automatically rejecting a pulse that follows another by less than some preset time. Such methods, called paralysis methods, may greatly increase the deadtime of the system.

Peak pile-up (Fig. II-5a) produces a pulse of unusual shape, and such shapes (easily detected by sensing the zero crossing of the derivative of the pulse) may be used to reject events related to such pulses. Pulses with defective shapes may also occur as a result of poor charge collection in the detectors—e.g., because of neutron-induced trapping centers in the Ge(Li) detector. We take the Elizabethan view that any unusual shape is unnatural and should be rejected.

3. Electronic Pulse Handling

Figure II-6 is a block diagram of the electronics. All the analog signal-processing equipment except the time-to-pulse-height converter was designed and built by the Argonne Electronics Division. This section describes the electronic units

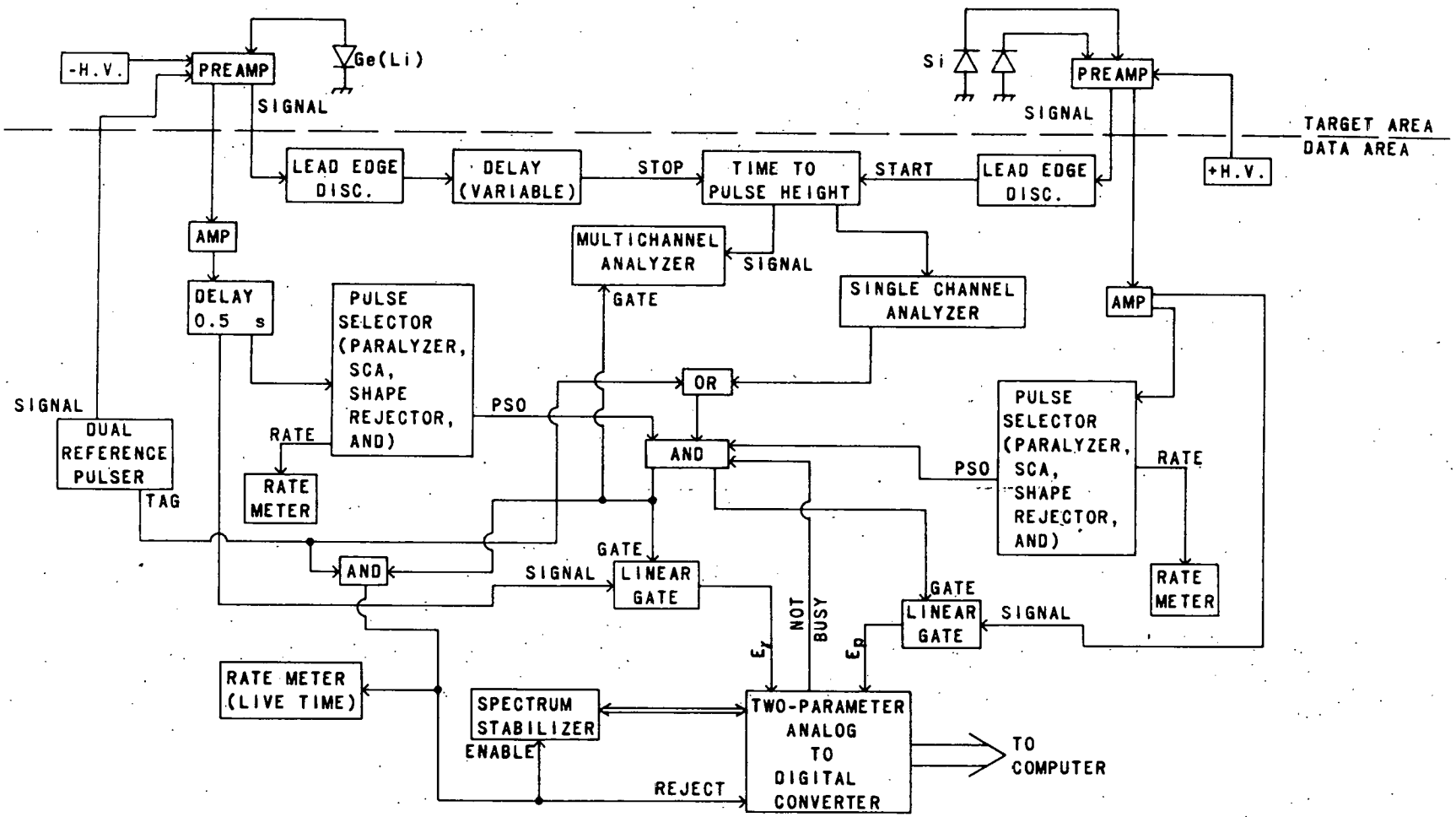

Fig. II-6. Block diagram of the electronics used for the particle-gamma coincidence measurement.

and their use in this measurement. The fast-timing section has already been described in Sec. II C1.

The preamplifiers are connected to the detectors with as short a lead as possible to minimize the capacitance on the charge-sensitive input of the preamplifiers, this precaution decreasing the rise time and minimizing the noise of the first stage. A large dynamic range is available to provide the option of using several detectors on the same preamplifier to absorb the reaction products and avoid the difficulties of summing amplified pulses.

The linear pulses from the two preamplifiers (proton and gamma) go first into the main shaping amplifiers and then into linear gates and pulse selectors. The gamma energy pulse is delayed by 0.5 μs immediately after amplification to allow the pulse selection to be done on the proton-energy pulse first. The pulse-selector box consists of four circuits: 1) a single-channel analyzer, 2) a pulse-shape discriminator to reject misshaped pulses, 3) an input paralyzer to stop a second pulse from riding in on the tail of the first pulse, and 4) an inclusive coincidence gate called an AND gate. Logical outputs from the single-channel analyzer and pulse-shape discriminator are fed into the AND gate and no output pulse from the AND occurs if any of the inputs are absent.

Because of the very high resolution of the Ge(Li) detector, the amplification and linear-gate system must be stabilized against amplification drift which could wash out the high resolution. In order to accomplish this stabilization, the output of a highly stable reference pulser is put into the front end of the preamplifier and a Nuclear Data spectrum stabilizer is used to provide base-line and gain stabilization to 20 parts per million per day through the whole gamma system. To inform both the spectrum stabilizer and

the analog-to-digital converter that the pulse being processed by the latter is a stabilizing pulse from the reference pulser, the reference pulser generates a tag pulse on the external ENABLE input of the stabilizer and on the REJECT input of the converter. When a tag is present, the pulse height analysis continues but the result is not stored as an unrejected pulse would be.

A measure of the live-time of the system is the fraction of the reference pulses that actually are used for stabilization. This fraction, which is measured with a rate meter, is used to continuously monitor the percent live-time of the system. Failure of a device in the system is usually reflected in a dramatic change in the live-time.

Refinements are also incorporated in the AND circuit. Three (ganged) two-position switches instruct the logic section either (a) to allow only time-coincident events (coincidence spectrum) or (b) to allow all events (singles spectrum). Each pulse selector drives a rate meter with a signal triggered by every input pulse whose amplitude exceeds the noise level. A multichannel analyzer forms a pulse-height spectrum corresponding to the converted time spectrum with and without the gate that accepts or rejects a coincidence.

D. Data Accumulation

After digitizing the desired analog pulse-height information into as many as 1024 proton-energy channels and as many as 1024 gamma-energy channels, the events must be stored as a 1024×1024-channel array. But core memories of 10^6 words are not generally available. The solution to this dilemma is to execute the two parts of the pulse-height analysis at different times. Ordinarily a pulse-height analyzer first performs an analog-to-digital

conversion on the input analog pulse and second adds one unit to the address in a memory array specified by the digitized analog pulse. There is no a priori reason why the second step in pulse-height analysis (which will be referred to as sorting) must be performed immediately upon the completion of the first step. Instead, the digitized input pulse is recorded on magnetic tape for later sorting into ten 96×1024-channel subarrays of the total 1024×1024-channel array. The subdivision is necessitated by the availability of a 96 000-word core memory.

The on-line computing system for the Argonne tandem (Fig. II-7) is designed to allow this manner of data acquisition. A large program, named GROUP, has been written to accumulate, manipulate, and analyze data in the form of two-parameter 1024×1024-channel arrays as just described. The program GROUP is fully described in Appendix A, and only those general aspects necessary for the accumulation and analysis of 1024×1024-channel arrays will be presented here.

During data accumulation, the program GROUP will accept the analog-to-digital signals as words into an array in the computer memory. After 256 such words are accumulated, another array of 256 is opened to store the digital information while the first block is written onto a magnetic tape. Next these words are interrogated to see if they lie within limits (lower and upper channel numbers) previously stored in the program on either the proton or gamma spectrum. If, for example, the program has been given the proton limit pair (500, 515), then a 1024-channel gamma spectrum is accumulated in coincidence with protons between channels 500 and 515. Up to 50 such spectra may be accumulated simultaneously. Any one of these spectra may be displayed on the DD16B memory display oscilloscope while data continue to be accumulated. Changes

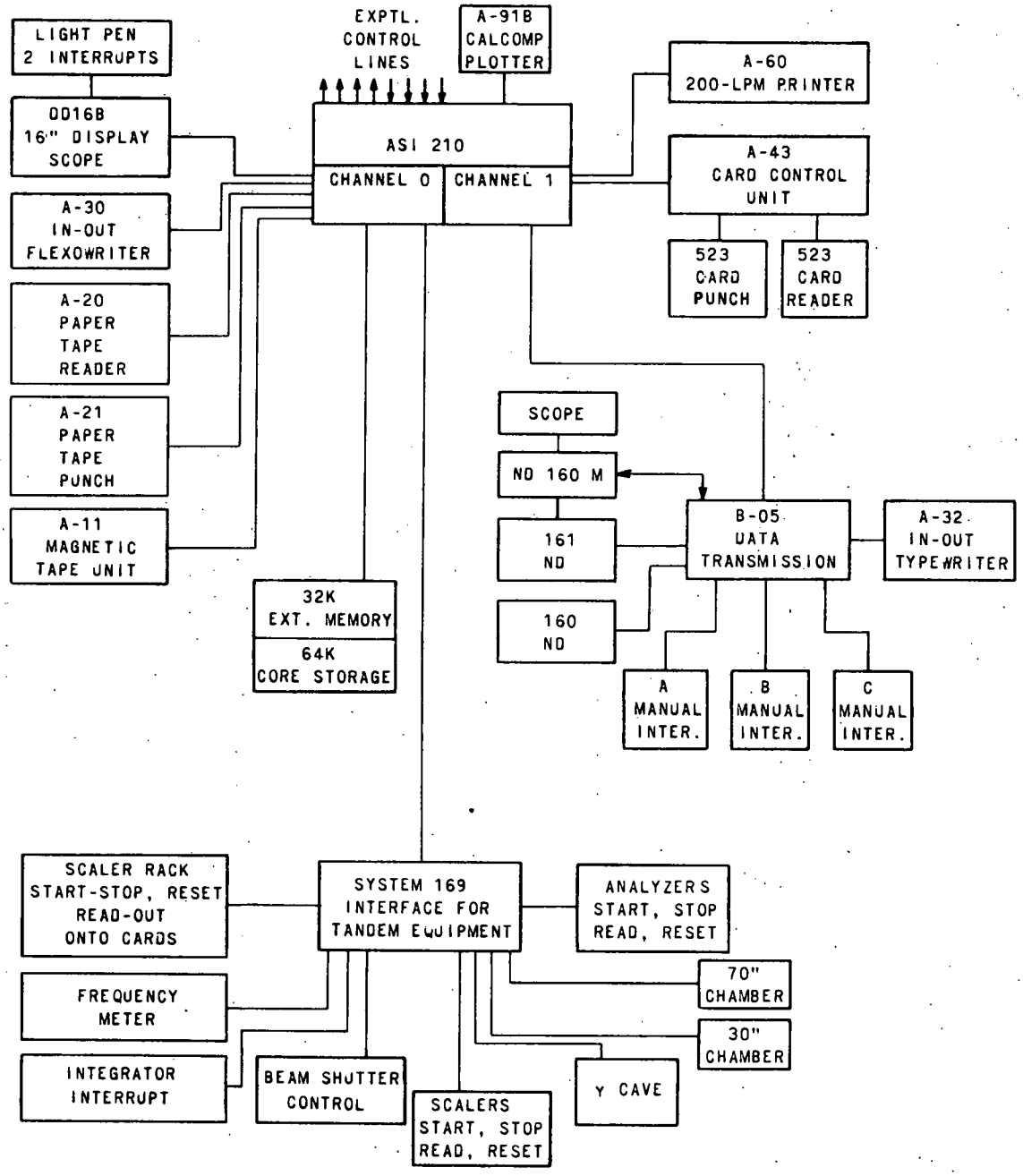

Fig. II-7. Block diagram of the ASI-210 computer and peripheral devices at the ANL tandem Van de Graaff.

in the display (either to a different selection from the 50 spectra or to a different scale) have no effect on the data accumulation. By watching the displayed spectrum, the experimenter may monitor the data quality and quantity just as he would with a conventional pulse-height analyzer. Other provisions for controlling the beam, the current integrator, the monitor one-parameter multichannel analyzers, and the scalers are discussed in Appendix A. Program GROUP also has provisions for printing spectra or limits on a line printer and for plotting spectra on a Calcomp plotter, but none of these may be done while data are accumulating.

E. Data Reduction

Once several reels of magnetic tape full of analog-to-digital data have been accumulated, the 1024×1024-channel array may be sorted in much the same way as the fifty 1024-channel spectra were sorted by GROUP, except that the input is from the magnetic tape instead of from the analog-to-digital converter. Twenty-one 50×1024-channel subarrays of the whole 1024×1024-channel array would have to be sorted. However, days of computer time are saved by using the faster and more convenient program DIMWIT, as explained in Appendix A, Sec. D.

After the 10^6 channel array is formed, GROUP is used to analyze the two-parameter spectrum. Recalling that the resolution in the gamma spectrum is good while that in the proton spectrum is bad, a contour plot of the two-parameter data would be similar to the one shown schematically in Fig. II-8a. The two-dimensional peaks are very narrow in the E_γ direction and very broad along the E_p direction. The contour plot shown might represent the proton-gamma coincidences from two closely-spaced nuclear levels that gamma decay to the same nuclear level. (Close spacing

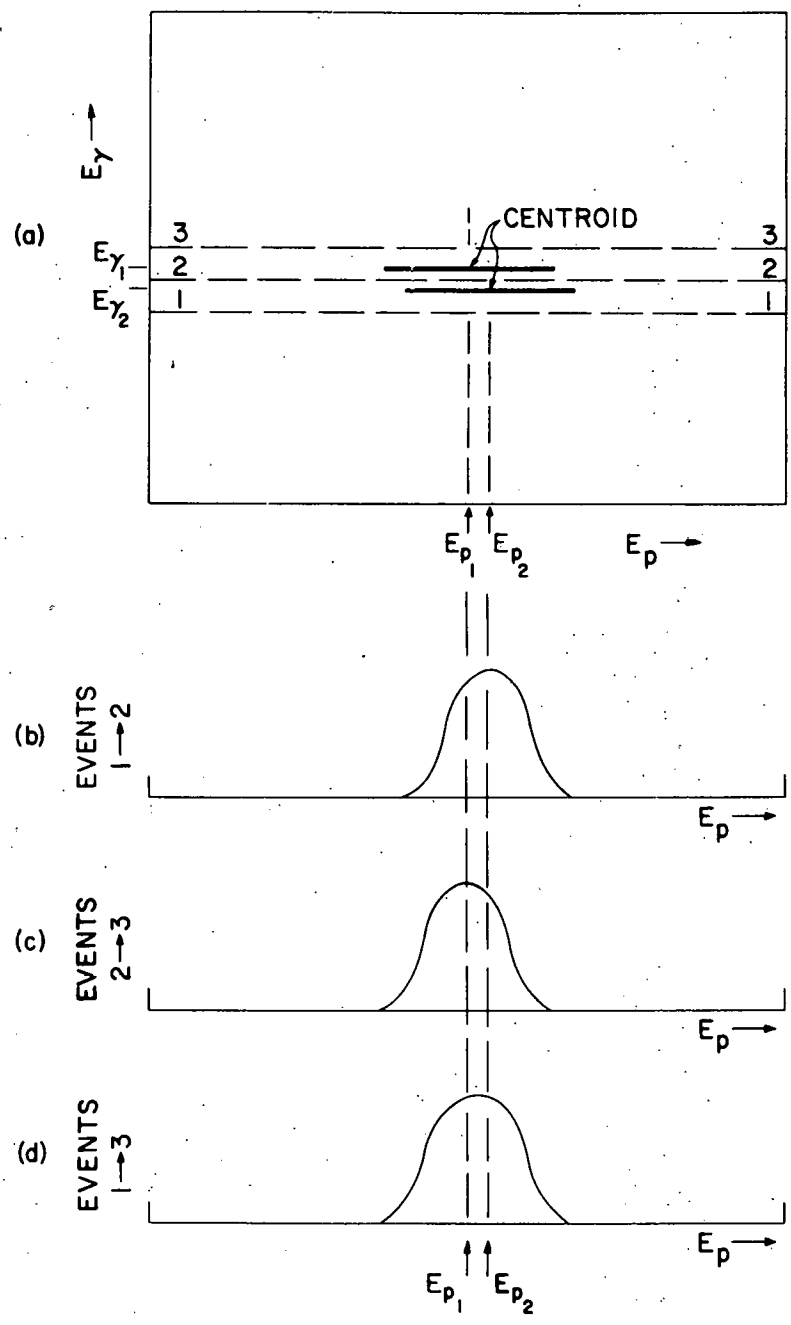

Fig. II-8. The reduction of two-parameter pulse-height-analyzer data for peaks that overlap in the particle spectrum but are resolved in the gamma spectrum. a) A contour plot of the two-parameter spectrum. b) The protons in coincidence with γ rays falling between lines 1 and 2. c) The protons in coincidence with gammas falling between lines 2 and 3. d) The protons in coincidence with γ rays falling between lines 1 and 3.

means that the difference δ between the excitation energies is greater than the resolution width for γ energies but less than that for proton energies. That is, $15 < \delta < 150$ keV.) The peaks corresponding to levels 1 and 2 at excitation energies E_{x_1} and E_{x_2} have their centroids at E_{p_1}, E_{γ_1} and E_{p_2}, E_{γ_2}, respectively, where $\delta = E_{x_1} - E_{x_2} = E_{\gamma_1} - E_{\gamma_2} = E_{p_2} - E_{p_1}$. Along the scale of proton energies, the peaks overlap beyond any hope of separating them without some additional clue; but their projections onto the gamma axis are easily separated by eye.

Asking the program GROUP to plot the proton spectrum coincident with all γ rays falling between the lines marked 1 and 2 in Fig. II-8a would result in the spectrum shown in Fig. II-8b. The proton spectrum coincident with gammas between 2 and 3 is Fig. II-8c and that for gammas between 1 and 3 is Fig. II-8d. (The problem of γ-ray background arising from Compton scattering of higher energy gamma rays is discussed in Appendix A.) The spectra in Figs. II-8b and c show how the decomposition is accomplished. Program GROUP allows such an analysis, and the lines analogous to 1, 2, and 3 in Fig. II-8 can be drawn not only in the proton direction but also (separately) in the gamma direction; and the resulting spectra of protons coincident with specified ranges of γ energies and the spectra of gammas coincident with specified ranges of proton energies are displayed side by side on the DD16B memory display oscilloscope. The results of this decomposition may be plotted, printed, or stored on magnetic tape for later use—just as can any other spectrum in program GROUP.

To get the area under a peak in a spectrum such as that in Fig. II-8b or II-8c, GROUP can perform the integration at computer speed. Because the whole 10^6 channels cannot be stored in fast-access core memory at the same time, it is convenient to

use subarrays of 50 proton channels by 1024 gamma channels stored in the external core memory. This means that only one region (with a width of about 2.5 MeV) of the nuclear excitation may be examined at a time.

The processes by which electromagnetic phenomena interact with matter add some complications to the analysis of particle-gamma experiments. For example, interactions due to the photoelectric effect and multiple Compton scattering make up the full-energy peak shown in Fig. II-9. The pair-production effect, which becomes important at higher energies (above the 1.022-MeV threshold) where the photoelectric effect and Compton scattering are small, introduces the possibility that one or both of the 511-keV gamma rays from the positron annihilation may escape from the detector. This gives rise to the so-called single- and double-escape peaks, as shown in the γ spectra of Fig. II-9. Presented with a spectrum such as Fig. II-9, the experimenter must decide whether he has observed 2, 3, or 4 or more γ rays. Program GROUP will use a previously determined calibration to calculate and display the energies of each peak in Fig. II-9 upon request. If any of these peaks are separated by 511 keV or 1022 keV, they are probably the single- or double-escape peaks of the same gamma ray. By measuring the area under the proton spectrum in coincidence with each of the related gamma peaks (by the process outlined above) and by knowing the relative detection efficiencies, the experimenter can determine what γ-ray energies and how many γ-ray events are in coincidence with what proton peaks.

F. Extensions and Limitations of the Measurements

Certain simplifying assumptions have been made in Secs. II C and D. In the work reported here, two Ge(Li) detectors

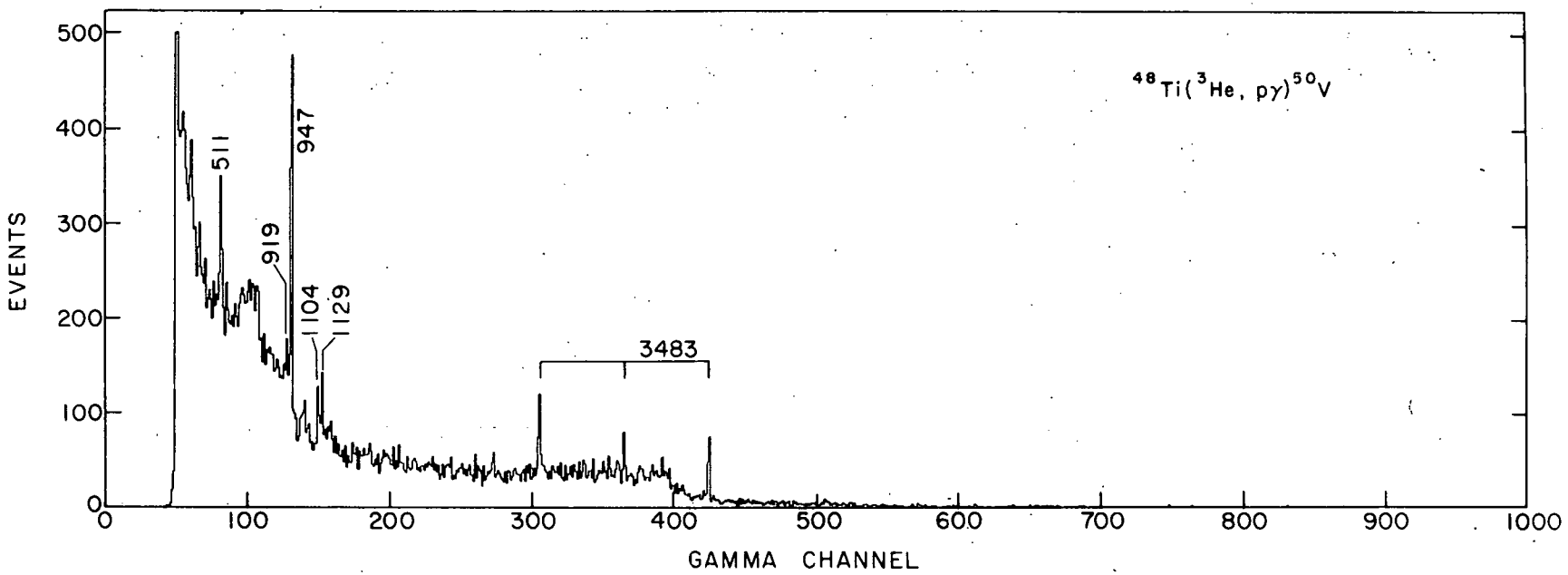

Fig. II-9. The gamma spectrum observed in coincidence with protons from the ^{50}V isobaric analog state at 4.820 MeV. The bracket connects a full-energy, single-escape, and double-escape peak of the 3483-keV gamma ray. The full-energy peaks of the 0.947- and 0.511-MeV gammas are also observed.

(each with its own independent electronics) have been used at different angles. The program GROUP is written to accept two-parameter data simultaneously from the two systems and to keep track of the parameters associated with each.

The $^{48}Ti(^{3}He,d\gamma)^{49}V$ particle-gamma coincidence measurement may be carried out simultaneously with the $^{48}Ti(^{3}He,p\gamma)^{50}V$ measurements as a result of a fortuitous combination of Q values and cross sections for the two reactions. The $^{48}Ti(^{3}He,d)^{50}V$ reaction has a much lower Q value and a much higher cross section. The yield of deuterons leading to levels in ^{49}V then falls in the lower part of the particle spectrum and masks the yield of protons leading to ^{50}V levels above $\sim$9 MeV excitation. The proton yield from the reaction to ^{50}V lies in the upper part of the particle spectrum and is uncontaminated by deuterons. The results of the $^{48}Ti(^{3}He,d\gamma)^{49}V$ measurement will be presented elsewhere.

Bombarding ^{48}Ti with 13-MeV ^{3}He produces a considerable number of neutrons, which induce trapping centers in the Ge(Li) crystal and thus eventually destroy the excellent energy resolution of the Ge(Li). The Ge(Li) crystals can be rejuvenated to some extent by various means, but they all are costly. Hence, the aim has been to minimize the electronic dead time associated with the accumulation of a given number of true coincidences, and thereby to minimize the neutron dose while the necessary amount of data is collected. The rate at which the Ge(Li) is damaged by neutrons has prevented the accumulation of the number of events necessary for a Litherland-Ferguson method-II correlation study. Such a study might have led to spin assignments of more levels.

G. Results of the Measurements

When a target of ^{48}Ti, whose ground state is $J^{\pi} = 0^{+}$, is bombarded with a 13-MeV beam of ^{3}He and the protons from the reaction are detected at 0° with respect to the beam, the protons observed are from reactions in which states in ^{50}V are populated by a neutron-proton pair being absorbed into the ^{48}Ti nucleus with orbital-angular-momentum transfer $L_{np} = 0$. (Such states must have either $J^{\pi} = 0^{+}$, 1^{+} and $T_{<}$ or else $J^{\pi} = 0^{+}$ and $T_{>}$.) This selection is a result of the very strong forward peaking of the $L_{np} = 0$ angular distribution. Note that the γ rays following the decay of a level populated by a reaction with a zero orbital-angular-momentum transfer must be isotropic. In this work the gamma decays of eleven levels are observed. The particle detector is at 0° and the gamma detector is at 100° with respect to the beam. In addition, the isotropy of the γ decay was checked by short runs with the γ detector at three other angles (45°, 60°, and 90°). No significant anisotropy was observed.

1. Observed Particle and Gamma Spectra

Figure II-10a is the singles spectrum of particles incident on the particle detector at 0° with respect to the beam. The peak farthest to the right in the spectrum (near channel 750) corresponds to the excitation of ^{50}V states at 1.333 and 1.490 MeV. No ^{50}V states of lower excitation are excited. Clearly a number of ^{50}V states above 1.490 MeV are excited as evidenced by the structure in the spectrum to the right of channel 400. At channel numbers below 400, the peak structure is due to ^{49}V excited states populated by the ^{48}Ti(^{3}He,d)^{50}V reaction. The very strong peak at channel 280 results from hydrogen in the target being knocked out elastically into the particle detector by the beam.

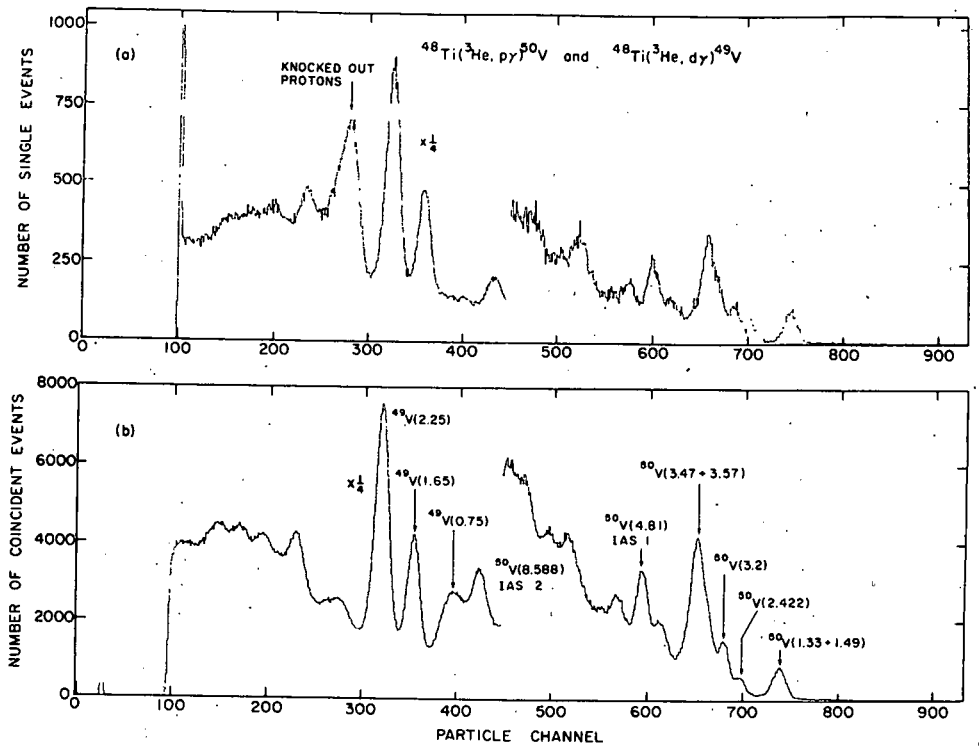

Fig. II-10. The particle spectrum a) with no coincidence requirement and b) with the 80-ns coincidence requirement.

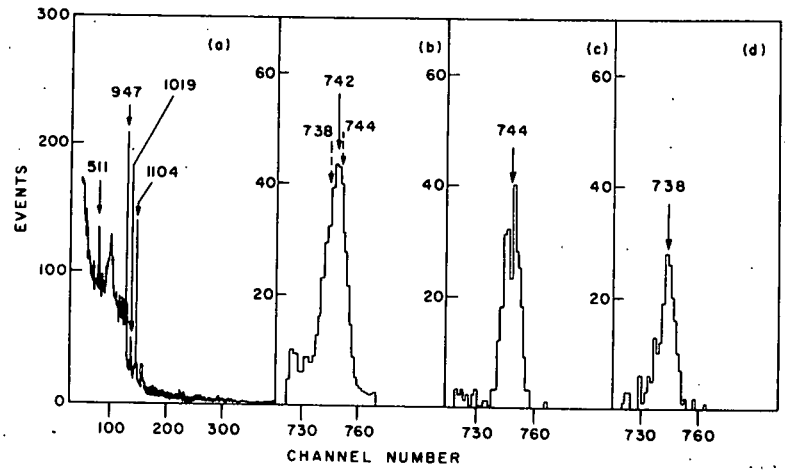

Fig. II-11. The analysis of the gamma decay of the 1.333- and 1.490-MeV levels in ^{50}V. a) The gamma spectrum in coincidence with protons from the 1.333- and 1.490-MeV levels. b) The protons from the 1.333- and 1.490-MeV levels in coincidence with all the γ rays. c) The spectrum of protons in coincidence with the 0.947-MeV gamma ray. d) The spectrum of protons in coincidence with the 1.104-MeV gamma ray.

Figure II-10b is a similar particle spectrum with the particle-gamma time-coincidence requirements in force. That is, the two-parameter particle-gamma spectrum has been integrated over all gamma energies. The two particle spectra are similar in structure as expected. The knocked-out proton peak just described is not observed in the coincidence spectrum because no γ ray is associated with the hydrogen knock-on. Many of the ^{50}V peaks above channel number 400 are seen quite clearly, but only eleven of these are strong enough that their gamma decay can be obtained. The poor energy resolution in the particle spectrum explains why the proton groups to the 1.333 and 1.490 MeV levels of ^{50}V are not resolved.

Figure II-11a is the gamma spectrum in coincidence with the proton peak at channel 750 (Fig. II-11b) that was identified with the 1.33- and 1.49-MeV levels of ^{50}V. Two strong gamma lines are seen at 947 and 1104 keV. By constructing the particle spectrum in coincidence with each of these gamma lines, we obtain the two proton spectra shown in Fig. II-11c and d. The centroids of these two peaks fall at different channels. One peak is the protons leading to the 1.33-MeV level in ^{50}V and the other is the peak of the protons leading to the 1.49-MeV level. By this procedure the decay of the 1.33-MeV level in ^{50}V is seen to be by a 947-keV gamma, and the decay of the 1.490-MeV level is seen to be by a 1104-keV gamma. The analysis of the remaining ^{50}V levels proceeds by a similar procedure.

Figure II-9 shows the gamma spectrum in coincidence with protons from the 4.816-MeV level, the lowest isobaric analog state of ^{50}V. The γ decay of this IAS proceeds by a 3483-keV and 947-keV cascade. The three lines from channel 300 to 420 are the double-escape, single-escape, and full-energy peak of the

3484-keV gamma. Several other small gamma lines due to the gamma decay of neighboring levels may be observed. Also a 511-keV gamma line is present as a result of positron annihilation.

2. Gamma Decay and Branching of Observed Levels

Figure II-12 shows the observed gamma decay of the eleven levels directly populated (darker lines) and the secondary gamma decay of two levels excited by the gamma decay of levels directly populated. No gamma decay from levels lower than 388 keV is observed because the system is sensitive only to gamma energies greater than 300 keV.

The two analog levels at 4.816 and 8.588 MeV decay entirely to the levels shown, to within a 20% uncertainty. Likewise the levels at 1490 and 1333 keV decay wholly by one γ ray, to within 20%. In the decay of all other levels, a branch as intense as 40% of the strongest observed γ ray from that level could be missed due to statistical uncertainties.

The uncertainty in the energy of the observed gamma ray is 10 keV, and therefore the uncertainty in the exact excitation energies of the levels is about equivalent to that in the high-resolution spectrographic work of Buhl et al. (Bu69) who studied the $^{50}V(p,p')^{50}V$ reaction.

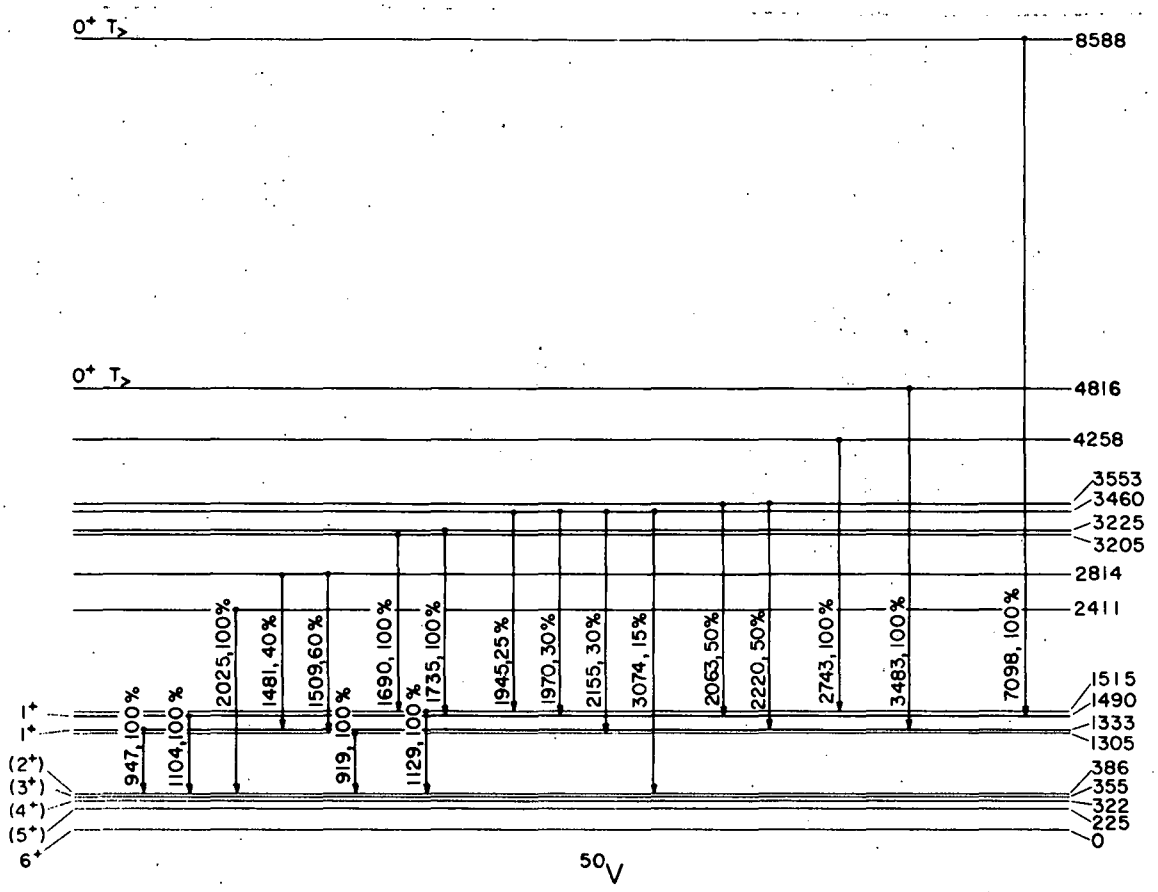

Fig. II-12. The observed γ decay of levels in ^{50}V. Levels populated by the (^{3}He,p) reaction with $L_{np} = 0$ are shown as dark lines. Light lines are levels that participate in the cascade but are not populated directly by the (^{3}He,p) reaction.

III. SPECTROSCOPIC MEASUREMENTS

A. Beam Handling

The beam-transport system up to the collimation system is as described in Chap. II. The beam to the split-pole spectrograph is defined by two collimators placed 3 in. and $6\frac{1}{2}$ in. from the target. The final collimator is rectangular, with dimensions of 1×3 mm. (Collimators measuring $\frac{1}{2} \times 3$ mm and $1\frac{1}{2} \times 3$ mm are also available.) Typical ^{3}He target currents of 250—350 nA are obtained by using a quadrupole lens to focus the beam onto the target.

The number of particles in the incident ^{3}He beam is measured, after it has passed through the target, by catching it in a Faraday cup. The charge deposited in the Faraday cup is measured with Model 1000 current integrator system manufactured by the Brookhaven Instruments Corporation, Brookhaven, New York.

B. Charged-Particle Spectroscopy in the Split-Pole Magnetic Spectrograph

The use of silicon surface-barrier detectors to energy analyze the reaction products is impossible because of the large number of elastically scattered ^{3}He ions at the scattering angles of interest. On the other hand, momentum analysis of reaction products from charged-particle reactions provides excellent energy resolution of reaction products regardless of elastic scattering, but at the price of small solid angles of acceptance and therefore slow data accumulation. The recent use of the transverse focusing properties of split magnetic poles has allowed a tenfold increase in the solid angle accepted by magnetic

spectrographs. Figure III-1 is a diagram of the double focusing (transverse and momentum focusing) split-pole spectrograph at the Argonne tandem. The magnet consists of two separate pairs of pole pieces, with a gap between the pairs, and the magnetizing coils enclose both. The broad-range momentum focusing is indicated in Fig. III-1, in which representative particle trajectories converge to two spots on the focal plane—corresponding to two particle momenta.

First-order transverse focusing is achieved over the whole momentum range by the fringing fields in the pole gaps, and second-order aberrations are minimized by the choice of the position and shape of the final pole boundary. (Pole boundaries are rounded to minimize saturation effects.) Second-order transverse aberrations are quite small over the whole range of momenta (Sp67). Momentum focusing and transverse focusing may not be achieved at the same spacial position but it should be realized that the purpose of the transverse focusing is not to produce an exact image of the source on the focal plane but to allow an enlarged entrance aperture. Reaction products are accepted over solid angles of 1, 2, π, and 4 msr (defined by four standard entrance slits) are are focused onto the focal plane in a line about 1 mm wide and less than 1 cm long (transverse to the nuclear-track plate).

Reaction products emitted at angles of 7—160^{o} to the beam can be studied with this spectrograph. A nuclear-magnetic-resonance device is used to measure the field strength. An extensive description of the hardware associated with the Argonne split-pole spectrograph is given elsewhere (Er69).

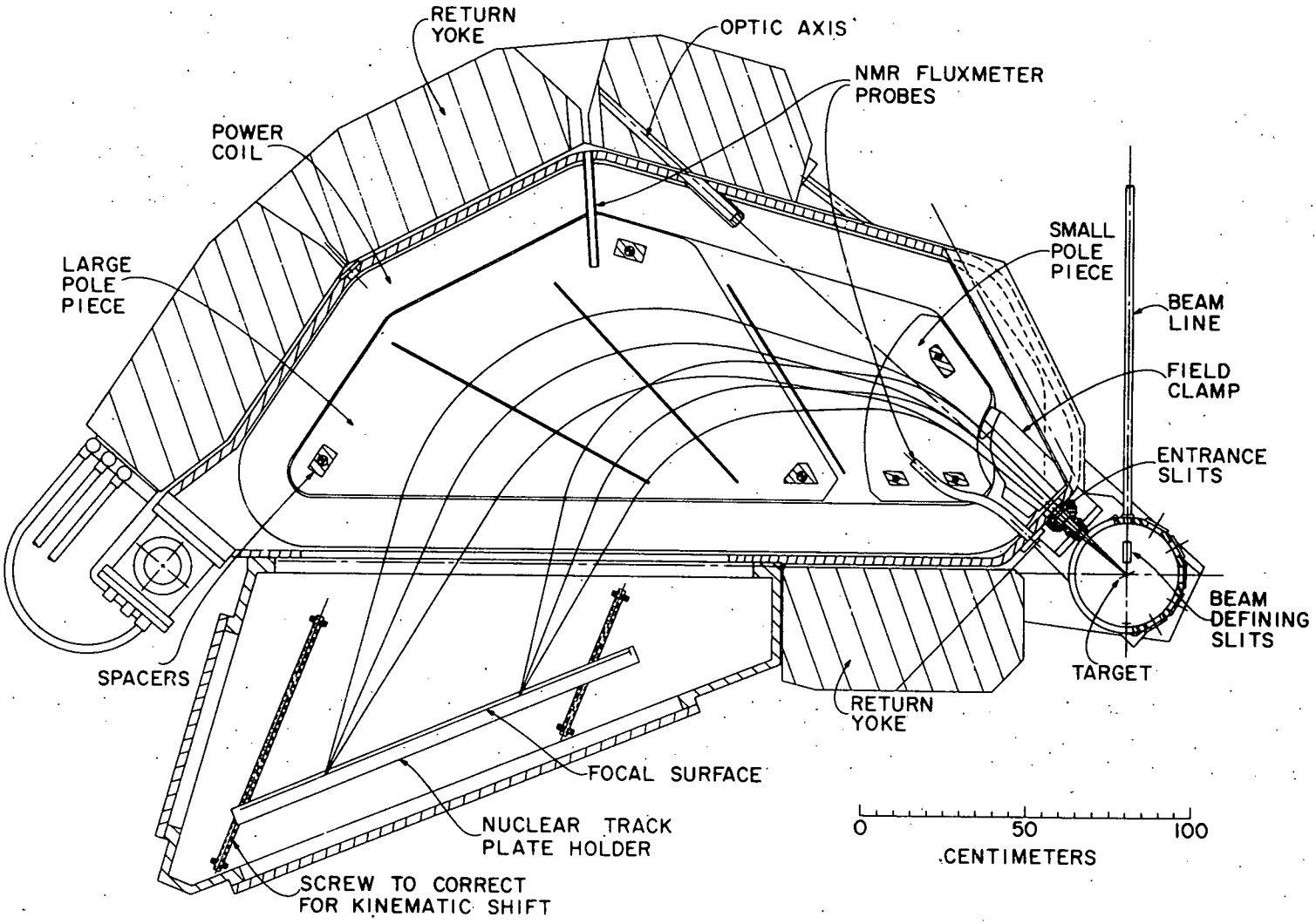

Fig. III-1. The split-pole magnetic spectrograph at the Argonne tandem Van de Graaff.

C. Nuclear-Track Emulsions as Recording Devices

The recording device is placed on the focal plane of the spectrograph. Because this focal plane moves (as a result of kinematic effects which are more important with the larger entrance aperture) the recording device is mounted on two screws and its position may be changed without disturbing the evacuated region. We have used Kodak NTB 50-micron photographic plates to record reaction products from the (^{3}He, p) and (^{3}He, d) reactions. A proton or deuteron leaves a track in the emulsion about 1 μm wide and 50—75 μm long. The emulsion is developed by a procedure due to Erskine (Er70). In order to stop the products of uninteresting reactions and to slow the reaction products of interest so they leave high-contrast tracks in the emulsion, moderating foils of cellulose triacetate are used immediately in front of the emulsion. The low average Z of these foils minimizes angular straggling.

For the (He^3, α) reaction we have used Ilford K-1 plates in order to take advantage of the specific ionization of the α^{++} being greater than that of a singly-charged nucleus. High-energy (> 7 MeV) singly-charged nuclei leave no track in the K-1 plates.

D. Extraction of Spectra from Nuclear-Track Emulsions

In order to obtain the spectra, one must scan the plates and find the number of tracks per unit length along the plate in the direction of changing momentum. The Argonne automatic plate scanner (PAULETTE) developed by Erskine (Er70) was used to scan the NTB-50 plates. PAULETTE consists of a high-resolution (5-μm) camera tube which views a $\frac{1}{4} \times 10$-mm section of the plate (or alternatively one may choose a $\frac{1}{2} \times 10$-mm section of the plate). The $\frac{1}{4}$ mm is broken into 50 scan lines each 10 mm long.

An analog signal-processing unit, in the form of a peak-finding circuit, identifies the position of bright points (observed under dark-field illuminations) to within 2—3 μm in the scan line. This information is transmitted to a PDP-9 Computer (Digital Equipment Corp., Maynard, Mass.) which performs the pattern-recognition and control functions. The computer recognizes a pattern by keeping track of the number of times the same point (within 2—3 μm) has been bright in consecutive scans (the scan line is perpendicular to the track length). The number of scan lines in which the same point is seen bright is then taken as the length of the track. More accurately, the pattern-recognition program is a one-skip correlator. That is, a track is considered ended after two consecutive scan lines have failed to see the bright spot. Of course, the program correlates for all bright points in the scan line.

The track-length spectrum for a $\frac{1}{4}$-mm strip, accumulated in one complete 50-line scan, is a plot of the number of tracks having a given length versus track length (expressed as the number of bright spots that form the line). Such a spectrum is shown in Fig. III-2. The large number of tracks with lengths of 1 or 2 are due to light-scattering centers in the plates — e.g., glass blemishes, dust, or bits of dirt in the emulsion. The few very long tracks (lengths much greater than 70 μm) are scratches in the emulsion. In the example shown in Fig. III-2, the average track length is 6 and the number of events would be taken as the 308 between 3 and 9. (The measured track length — actually the component in a direction parallel to the surface of the emulsion and perpendicular to the scan lines — is subject to some real variation because the particles may enter the emulsion in somewhat different directions.) Further details on PAULETTE, including the exact

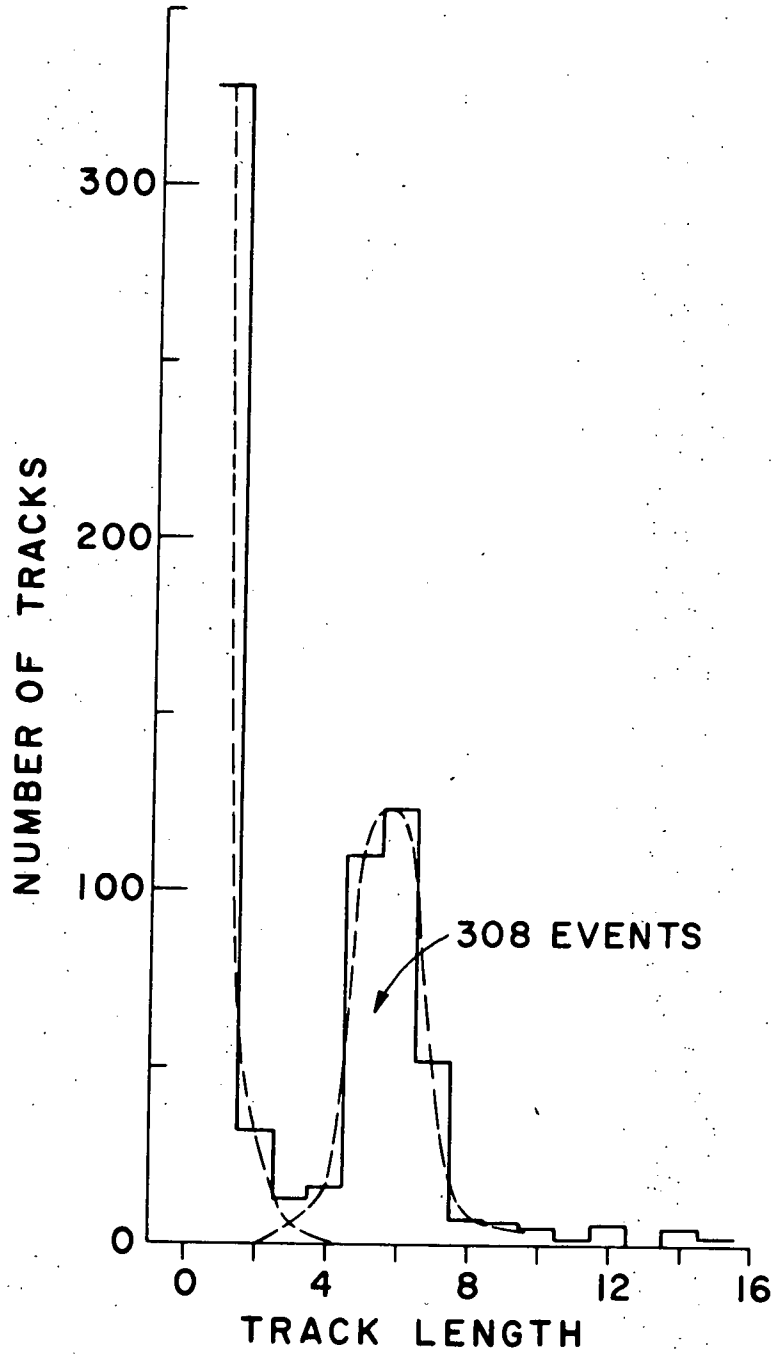

Fig. III-2. The track-length spectrum from the PAULETTE automatic plate scanner. This spectrum is for a $\frac{1}{4} \times 10$ mm strip of an emulsion exposed to protons from a (^{3}He, p) reaction.

criterion on which the number of events is determined, have been given by Erskine (Er70).

The results of the plate scanning are shown in Figs. III-3 to III-6. Figure III-3 displays a typical deuteron spectrum from the reaction $^{49}Ti(^{3}He, d)^{50}V$, while Figs. III-5 and 6 are typical proton spectra from the $^{48}Ti(^{3}He, p)^{50}V$ reaction. For the $(^{3}He, \alpha)$ reaction, the track-to-background contrast in the Ilford K-1 plates was so low that PAULETTE did not produce reliable results; so the plates from the $^{51}V(^{3}He, \alpha)^{50}V$ reaction were counted by human scanners. A typical spectrum is shown in Fig. III-4.

E. Spectrum Decomposition

Spectrum decomposition was simplified by the use of the program AUTOFIT written by Spink (Sp65). The inputs to the program were a standard peak shape from a well isolated peak in the spectrum, the positions on the emulsions of all the significant peaks, and a background curve. The results produced by AUTOFIT include the yield (area under peak minus background), yield error, position, and position error of each peak. Peaks spaced not more than 30 keV apart overlap and must be separated by fitting the standard peak shape to the experimental spectrum. After doing this, AUTOFIT also produces a graphic output of the individual fitted peaks as a smooth curve (atop the given background) superimposed over the original data points. From this graph it is obvious if the fitting has gone awry.

The yield errors calculated by AUTOFIT are larger than the statistical uncertainty in the yield. However, they are a consistent measure of the uncertainty in the yield of one peak with respect to the yield of another peak. The advantage of these error

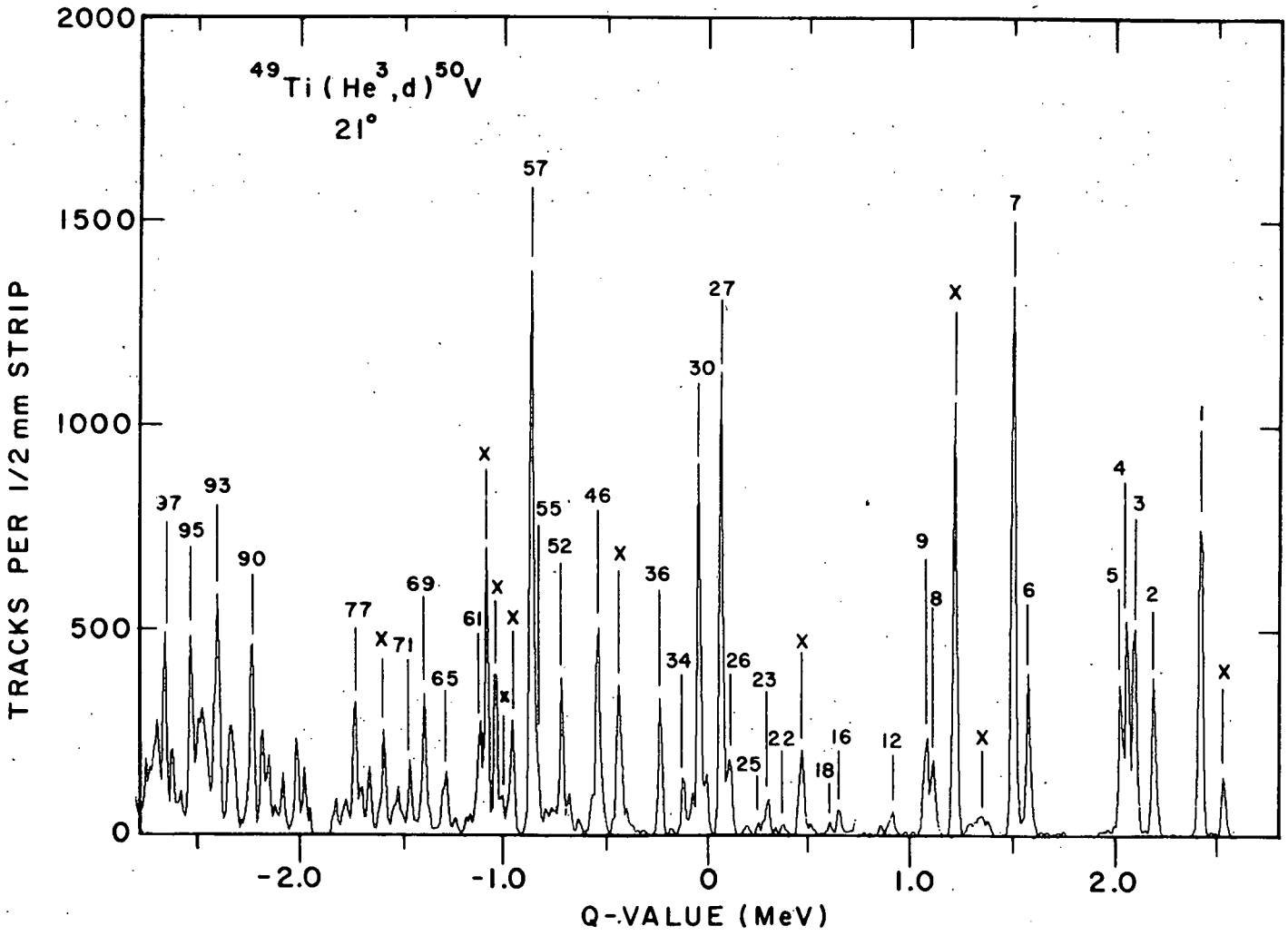

Fig. III-3. A typical deuteron spectrum from the ^{49}Ti(^{3}He,d)^{50}V reaction.

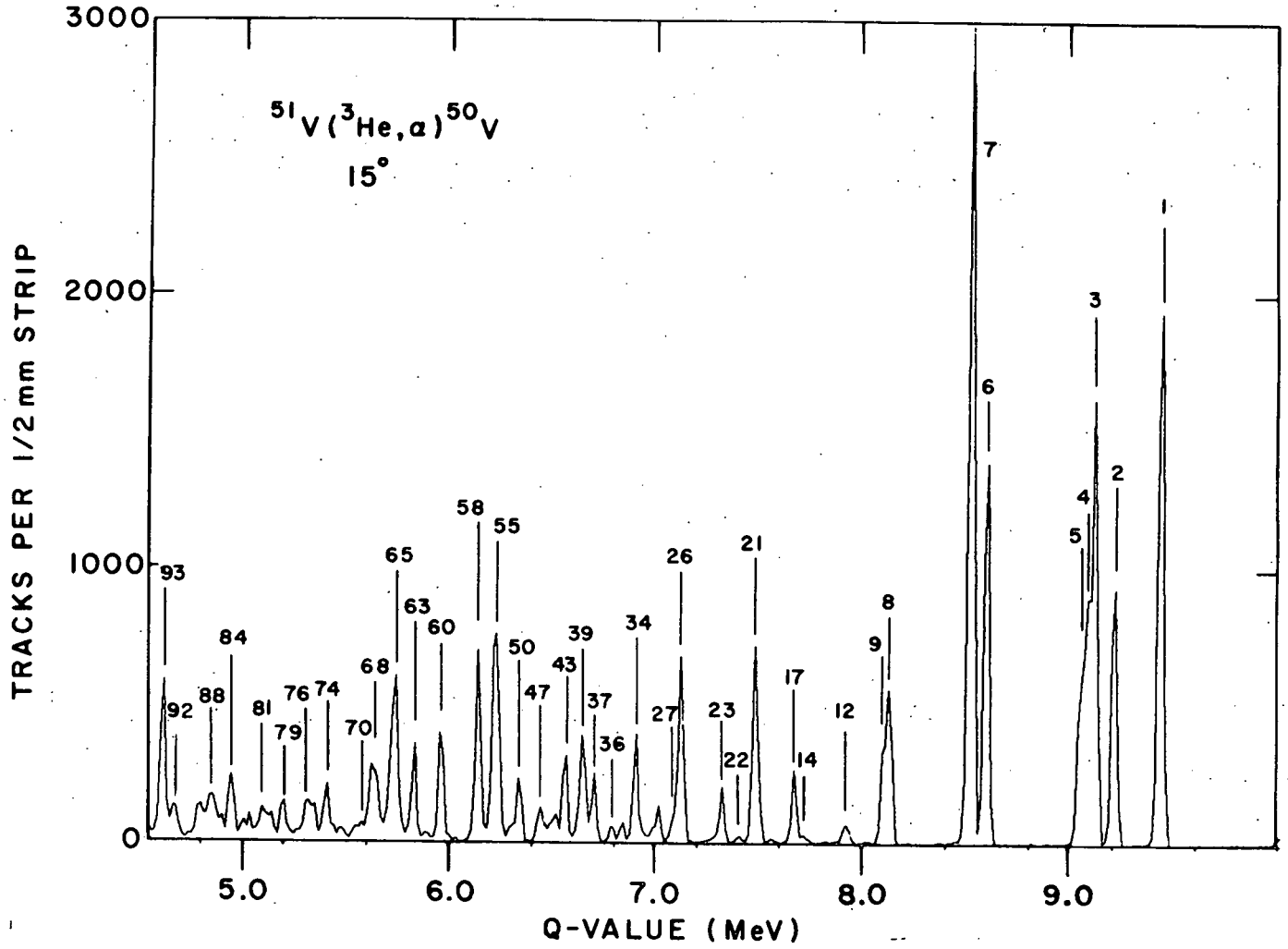

Fig. III-4. A typical α spectrum from the $^{51}V(^{3}He,\alpha)^{50}V$ reaction.

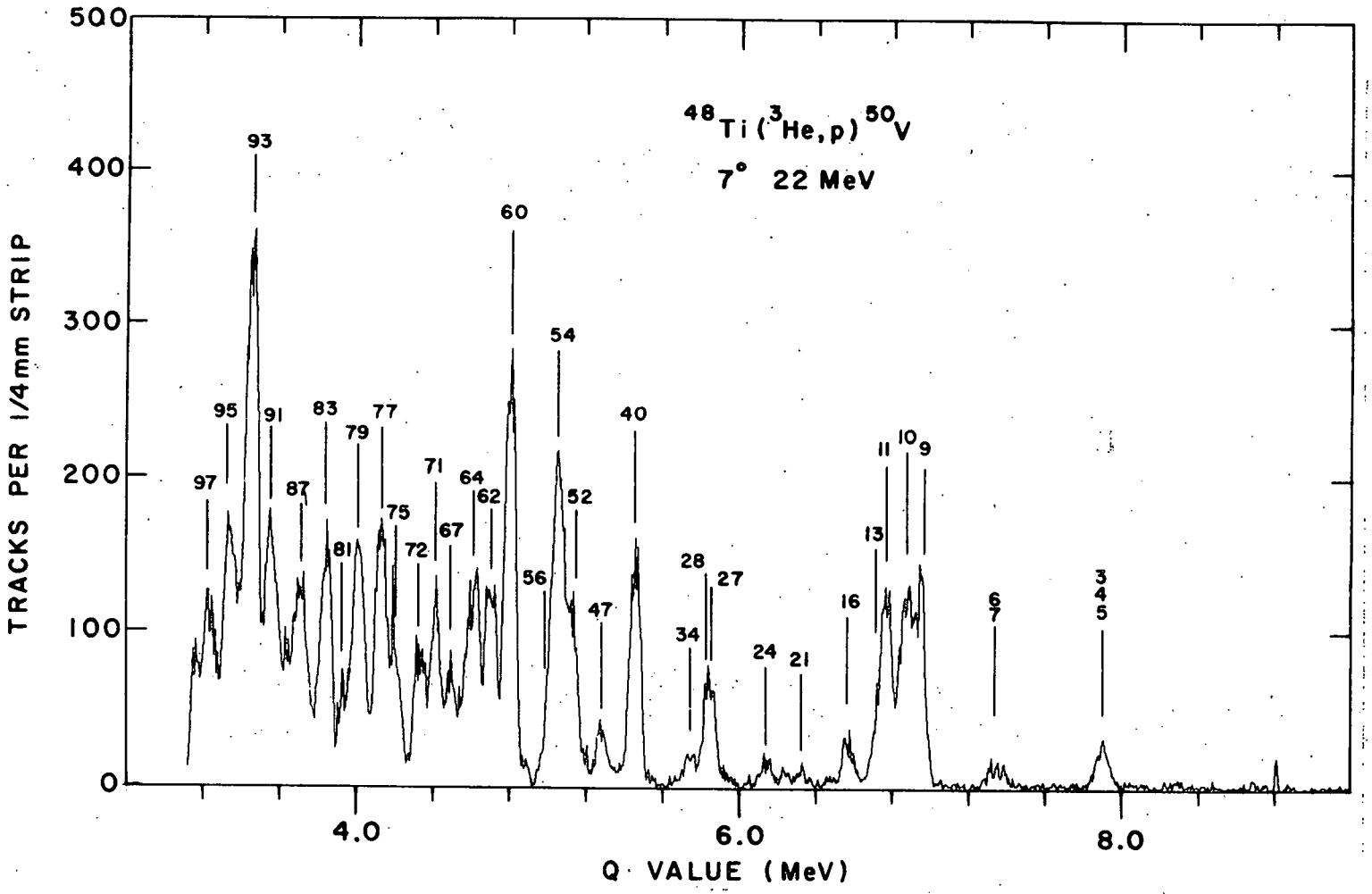

Fig. III-5. A typical proton spectrum from the ^{48}Ti(^{3}He,p)^{50}V reaction induced by 22-MeV ^{3}He particles.

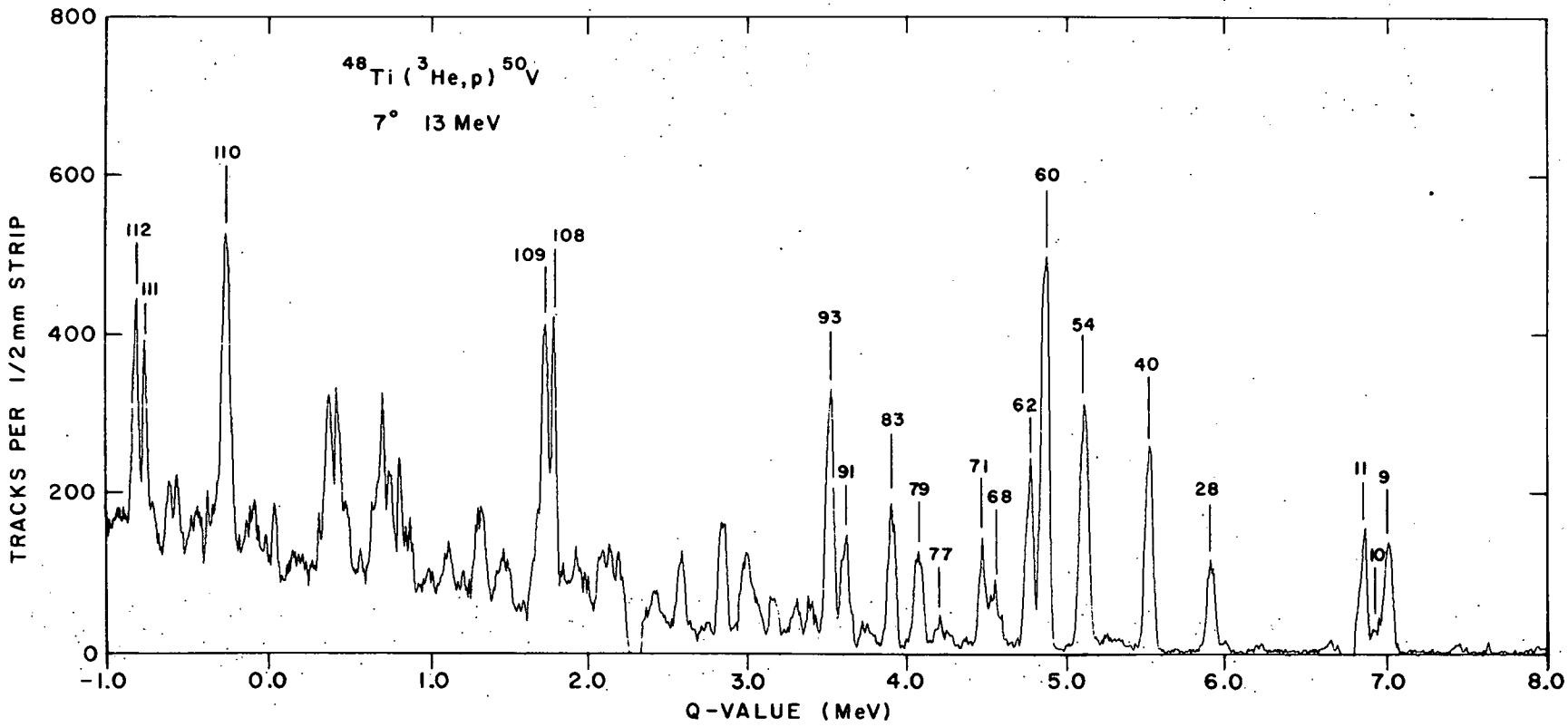

Fig. III-6. A typical proton spectrum from the ^{48}Ti(^{3}He, p)^{50}V reaction induced by 13-MeV ^{3}He.

estimates is that they include the uncertainty of the fits not only to the peak with which they are associated but also to neighboring peaks and to the background.

F. Normalization of the Yield to Absolute Cross Sections

In order to establish the absolute cross section of a reaction, the number of scattering centers in the target must be determined, e.g., by measuring the elastic scattering of charged particles from the target of interest under conditions in which Rutherford scattering dominates. To this end the elastic scattering of 8-MeV $^{3}He^{++}$ ions from the targets ^{48}Ti, ^{49}Ti, and ^{51}V was measured. Since the $^{3}He^{++}$ Coulomb barrier for these nuclei is about 9 MeV, and since the measurements were carried out at forward angles (12°, 17°, and 22° lab.), we assume that the scattering is entirely Coulomb in nature. Further, using three angles provided a check that no interference phenomena were present.

The uncertainty in the normalization is due to several factors: 1) Counting errors may occur in scanning to convert tracks in the emulsion into spectra. These are expected to be no worse than similar errors in scanning the emulsions from the reactions. 2) Target nonuniformity may contribute significantly to the normalization error inasmuch as the beam spot may not always fall on the same place on the target. 3) Uncertainties in beam-charge integration for the very low exposures necessary in the elastic scattering may contribute significantly to the normalization error. 4) The extent of deviation from Rutherford scattering is unknown. However such deviation, if present, is expected to be small. As a result of the above, an overall normalization uncertainty of 20% is set.

G. Results of the Spectroscopic Measurements

This section will present the results of the measurements in the split-pole spectrograph in the form of 1) excitation energies and 2) angular distributions from the $^{49}Ti(^{3}He, d)^{50}V$, $^{51}V(^{3}He, \alpha)^{50}V$, and $^{48}Ti(^{3}He, p)^{50}V$ reactions induced by 22-MeV incident ^{3}He and from the $^{48}Ti(^{3}He, p)^{50}V$ reaction induced by 13-MeV incident ^{3}He.

The uncertainty in the excitation energy is estimated to be 15 keV for the $^{49}Ti(^{3}He, d)^{50}V$ and $^{51}V(^{3}He, \alpha)^{50}V$ reactions; and the peak widths (FWHM) are 22 keV in the former spectrum (Fig. III-3) and 30 keV in the latter (Fig. III-4). The peak width is larger for the latter than for the former because the straggling in coming out of the target is greater for the alphas than for the deuterons. The 15-keV uncertainty in excitation energy is small enough to allow unambiguous identification of levels below 2 MeV in the two reactions. At higher excitation energies, however, the nuclear levels become so closely spaced that one cannot be certain of correspondence.

The $^{48}Ti(^{3}He, p)^{50}V$ reaction has a very low cross section which has made the use of a very thin target for angular distribution impractical. The FWHM observed in Figs. III-5 and 6 is 75 keV. However, to check for closely spaced levels, a thin ^{48}Ti target for which the resulting peak width was 42 keV (FWHM) was used and an exposure was taken at one angle (7°).

The experimental angular distributions are shown as the points in Figs. III-7 to III-10; error bars are shown except when they are smaller than the points. The smooth curves are the results of the distorted-wave Born approximation calculations and will be discussed in Chapter IV.

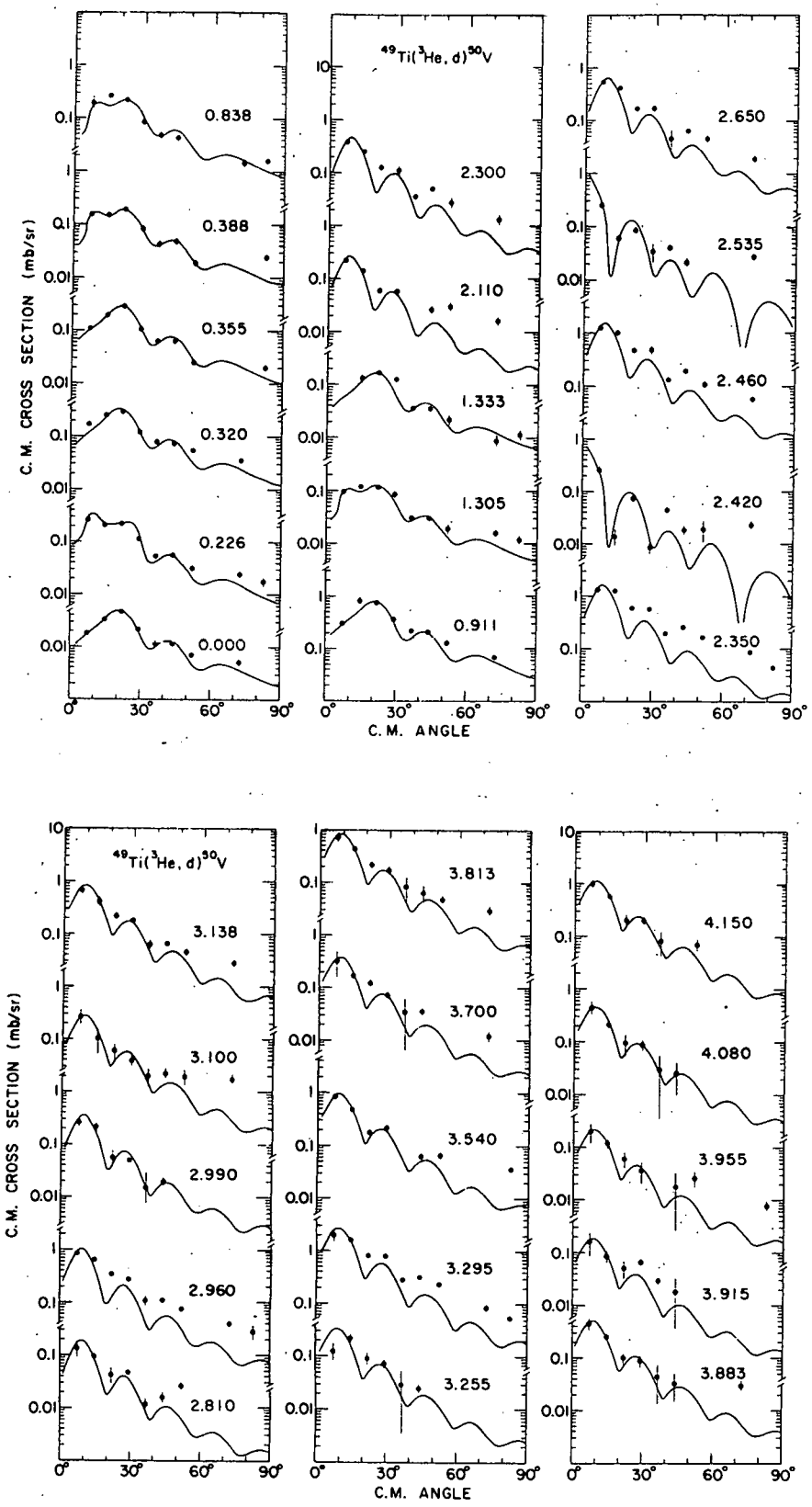

Fig. III-7. Angular distributions and DWBA fits from the ^{49}Ti(^{3}He, d)^{50}V reaction.

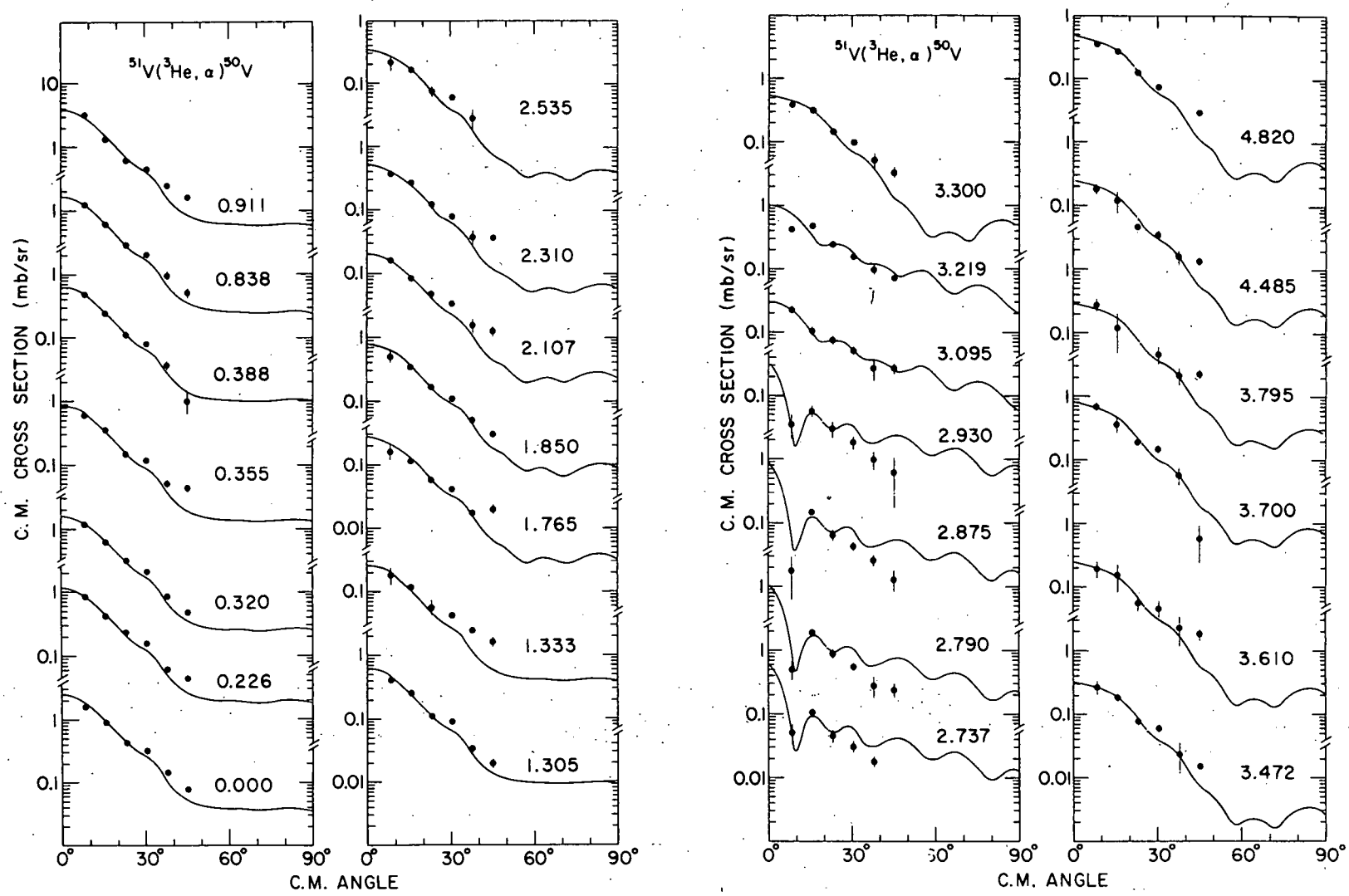

Fig. III-8. Angular distributions and DWBA fits from the $^{51}V(^{3}He,\alpha)^{50}V$ reaction.

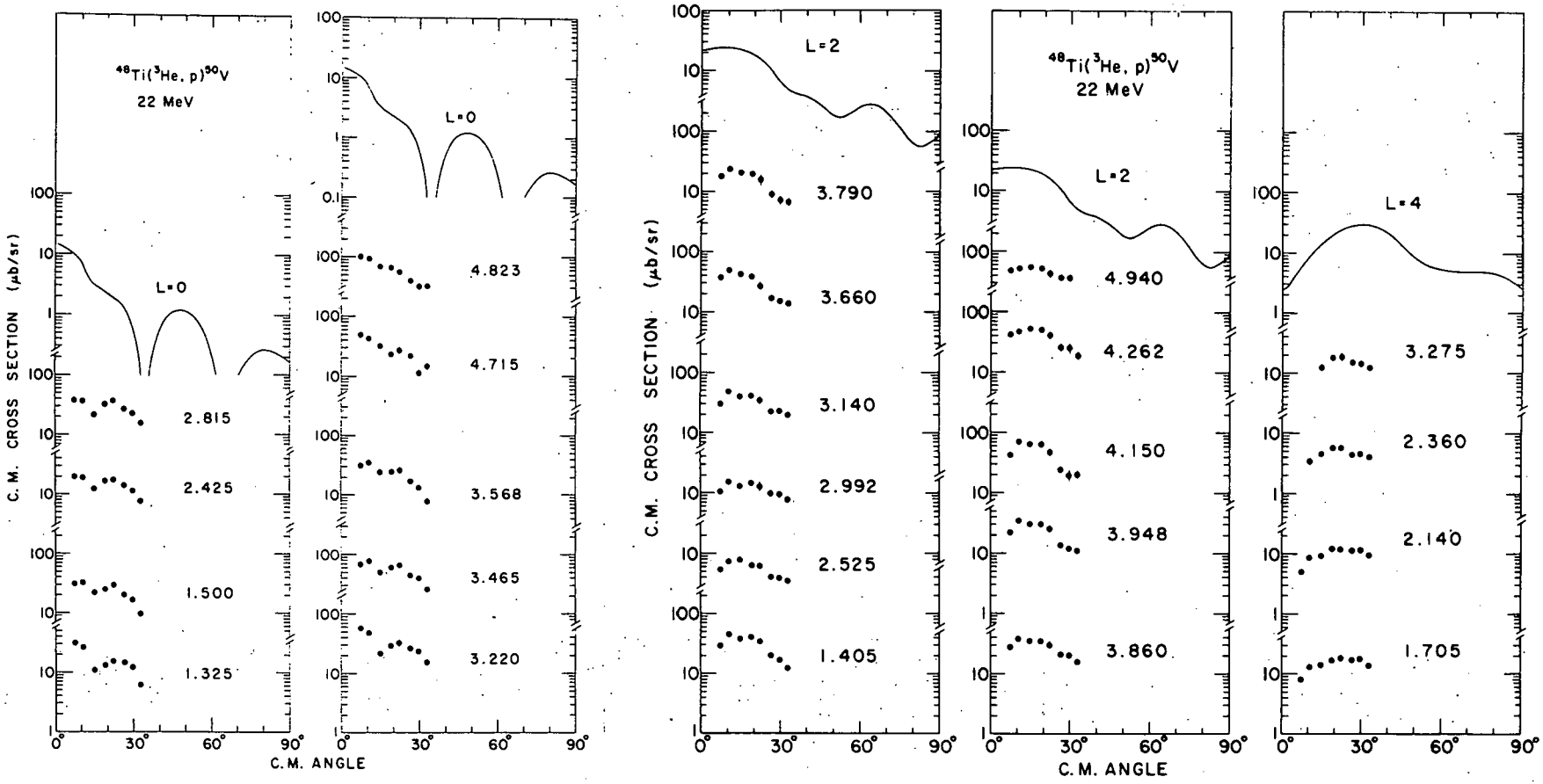

Fig. III-9. Experimental and DWBA angular distributions from the $^{48}Ti(^{3}He,p)^{50}V$ reaction induced by 22-MeV ^{3}He.

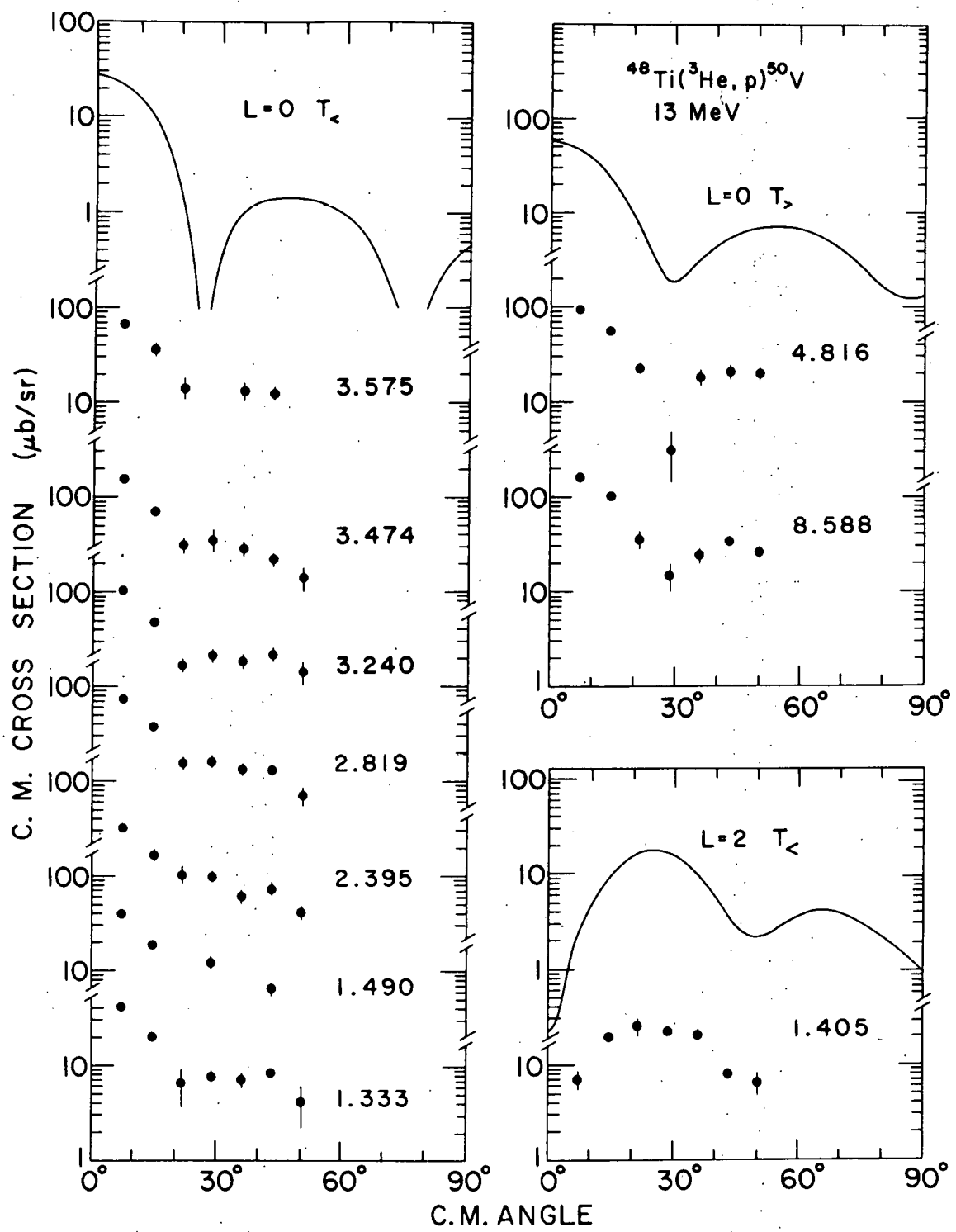

Fig. III-10. Experimental and DWBA angular distribution from the $^{48}Ti(^{3}He,p)^{50}V$ reaction induced by 13-MeV ^{3}He.

The $^{49}Ti(^{3}He, d)^{50}V$ reaction is special in two respects. First ^{49}Ti is a rare isotope of natural titanium and a very pure target cannot be made. (Our "^{49}Ti" target is only 76% ^{49}Ti, whereas our ^{51}V and ^{48}Ti targets are more than 99% pure.) The impurities in the ^{49}Ti target result in contaminants in our spectrum from the reactions $^{48}Ti(^{3}He, d)^{49}V$ and $^{50}Ti(^{3}He, d)^{51}V$. Spectral peaks resulting from these contaminants were identified by carefully measuring the Q values of peaks as a function of the scattering angle and examining the results for kinematic energy shifts that were inconsistent with a mass-49 target. Since the inconsistency would be of the order of 1 part in 50, plates were exposed at eleven angles up to 90^{o}. This has been sufficient to identify spectral peaks resulting from the $^{48, 50}Ti$ contaninants in the target. These are marked with X in Fig. III-3.

Second, the $^{49}Ti(^{3}He, d)^{50}V$ measurement has recently been published by Bishop et al. (Bi70). The measurement reported here will be seen (Table III-1) to be in agreement with the work of Bishop except for the levels at 1305 and 1333 keV excitation. We observed these levels to be partially obscured by contaminant peaks corresponding to the 90- and 150-keV levels populated in the $^{48}Ti(^{3}He, d)^{49}V$ reaction, and this suggests these levels are also obscured in Bishop's work. Chapter VI of this work will show the spin and parity of the 1333-keV state in ^{50}V to be $J^{\pi} = 1^{+}$, but this is inconsistent with Bishop's conclusions. However, the discrepancy can be understood if a small yield from the ^{48}Ti contaminant is obscuring the peaks of interest at forward angles in his angular distribution.

The energy dependence of the absolute cross section at the maximum of the ground-state angular distribution revealed another discrepancy. The ratio of the value Bishop et al. obtained

TABLE III-1. Experimental data on ^{50}V.

Level number	$^{50}V(p,p')^{50}V$ [a]	$^{49}Ti(^3He,d)^{50}V$ [b]		$^{49}Ti(^3He,d)^{50}V$ [c]			$^{51}V(d,t)^{50}V$ [d]			$^{51}V(^3He,\alpha)^{50}V$ [e]			$^{48}Ti(^3He,p)^{50}V$ [f]						J^π
	E_x (MeV)	E_x (MeV)	l_p	E_x (MeV)	l_p	$\frac{2l+1}{2J+1}S$	E_x (MeV)	l_n	$S_{l=3}$	E_x (MeV)	l_n	S	E_x (MeV)	22 MeV L_{np}	22 MeV $\frac{d\sigma}{d\Omega}\Big)_{max}$ (μb/sr)	E_x (MeV)	13 MeV L_{np}	13 MeV $\frac{d\sigma}{d\Omega}\Big)_{max}$ (μb/sr)	
1	0.0	0.0	3	0.0	3	0.91	0.0	1 + 3	1.57	0.0	3	1.9							6^+
2	0.226	0.226	1 + 3	0.226	1 + 3	0.023 + 0.38	0.228	1 + 3	0.66	0.226	3	0.9							(5^+)
3	0.321	0.318	3	0.320	3	0.60	0.321	1 + 3	0.99	0.320	3	1.3							(4^+)
4	0.358	0.350	1 + 3	0.355	3	0.55	0.357	1 + 3	0.56	0.355	3	0.7							(3^+)
5	0.390	0.388	3	0.388	1 + 3	0.01 + 0.38	0.387	1 + 3	0.32	0.388	3	0.5							(2^+)
6	0.838	0.836		0.838	1 + 3	0.01 + 0.36	0.838	1 + 3	1.01	0.838	3	1.3							
7	0.911	0.911	3	0.911	3	1.3	0.911	1 + 3	2.67	0.911	3	3.1							7^+
8	1.305	1.307	1 + 3	1.305	1 + 3	0.005 + 0.18	1.301	1 + 3	0.33	1.305	3	0.5							
9	1.330	1.347	1 + 3	1.333	3	0.25	1.330	1 + 3	0.23	1.333	3	0.2	1.325	0	31	1.333	0	41	1^+
10	1.404						1.402	1					1.405	2	45	1.405	2	25	
11													1.500	0	32	1.490	0	39	1^+
12	1.519			1.515						1.515									
13	1.561												1.570						
14	1.701									1.710									
15	1.725																		
16	1.753												1.750	4	18				
17	1.760			1.757						1.765	3	0.2							
18	1.808			1.810															
19	1.884																		
20	1.937																		
21	1.957									1.950	3	0.6	1.950						
22	2.038			2.030						2.040									
23	2.112			2.110	1	0.02				2.107	3	0.11							
24	2.133												2.140	4	12				
25	2.162			2.115						2.150									
26	2.314	2.300	1	2.300	1	0.04				2.310	3	0.3							
27	2.342	2.348	1	2.350	1	0.13				2.350			2.360	4	6				
28	2.399												2.425	0	20	2.395	0	34	(1^+)
29	2.422	2.427	0	2.420	0	0.22				2.422									
30	2.456	2.467	1	2.460	1	0.11				2.460									
31	2.481																		
32	2.492			2.495															

TABLE III-1. (Con't.)

Level number	$^{50}V(p,p')^{50}V$ [a] E_x (MeV)	$^{49}Ti(^3He,d)^{50}V$ [b] E_x (MeV)	ℓ_p	$^{49}Ti(^3He,d)^{50}V$ [c] E_x (MeV)	ℓ_p	$\frac{2I+1}{2J+1}S$	$^{51}V(d,t)^{50}V$ [d] E_x (MeV)	ℓ_n	$S_{\ell=3}$	$^{51}V(^3He,\alpha)^{50}V$ [e] E_x (MeV)	ℓ_n	S	$^{48}Ti(^3He,p)^{50}V$ [f] 22 MeV E_x (MeV)	L_{np}	$\left(\frac{d\sigma}{d\Omega}\right)_{max}$ (μb/sr)	13 MeV E_x (MeV)	L_{np}	$\left(\frac{d\sigma}{d\Omega}\right)_{max}$ (μb/sr)	J^π
33	2.512																		
34[g]	2.533	2.542	0	2.535	0	0.17				2.535	3	0.2	2.525	2	8				
35	2.600			2.595						2.595									
36	2.655	2.658	1	2.650	1	0.05				2.645									
37	2.738									2.737	0	0.5							
38	2.763																		
39	2.792									2.790	0	0.9							
40	2.815	2.814		2.810	1	0.013							2.815	0	37	2.819	0	75	(1^+)
41	2.828																		
42	2.849																		
43										2.875	0	0.7							
44	2.931									2.930	0	0.3							
45	2.958																		
46	2.965	2.966	1 + 3	2.960	1	0.07													
47	2.992	2.996		2.990	1	0.022				2.985			2.992	2	15				
48	3.011																		
49	3.099	3.101	1	3.100	1	0.02													
50										3.095	2	0.4							
51	3.111																		
52	3.142	3.140		3.138	1	0.05				3.135			3.140	2	45				
53	3.169																		
54[g]	3.202									3.217	2	1.3	3.220	0	56	3.240	0	105	
55				3.255	1	0.02													
56	3.274												3.275	4	19				
57	3.297	3.285		3.295	1	0.2													
58	3.312									3.300	3	0.4							
59	3.433																		
60	3.482									3.472	3	0.2	3.465	0	77	3.474	0	155	(1^+)
61		3.537		3.540	1	0.056													
62	3.566												3.568	0	35	3.575	0	68	(1^+)
63				3.595						3.610	3	0.2							

TABLE III-1. (Con't.)

Level number	$^{50}V(p,p')^{50}V$ [a]	$^{49}Ti(^3He,d)^{50}V$ [b]		$^{49}Ti(^3He,d)^{50}V$ [c]			$^{51}V(d,t)^{50}V$ [d]			$^{51}V(^3He,\alpha)^{50}V$ [e]			$^{48}Ti(^3He,p)^{50}V$ [f]						J^π
	E_x (MeV)	E_x (MeV)	ℓ_p	E_x (MeV)	ℓ_p	$\frac{2I+1}{2J+1}S$	E_x (MeV)	ℓ_n	$S_{\ell=3}$	E_x (MeV)	ℓ_n	S	E_x (MeV)	22 MeV L_{np}	$\frac{d\sigma}{d\Omega}_{max}$ (μb/sr)	E_x (MeV)	13 MeV L_{np}	$\frac{d\sigma}{d\Omega}_{max}$ (μb/sr)	
64	3.671			3.655									3.660	2	49				
65	3.700	3.713		3.700	1	0.02				3.700	3	0.6							
66	3.722																		
67	3.730																		
68	3.749									3.795	3	0.2	3.790	2	23	3.790			
69		3.813	1	3.813	1	0.047													
70										3.840									
71		3.885	1	3.883	1	0.028				3.885			3.860	2	38	3.870			
72		3.939	1	3.915	1	0.01													
73				3.955	1	0.01				3.950			3.948	2	34				
74										4.035									
75		4.081	1	4.080	1	0.027				4.095			4.072						
76		4.124		4.115						4.137									
77		4.151	1	4.150	1	0.065							4.150	2	69	4.145			
78		4.213																	
79										4.240			4.262	2	50	4.245			
80		4.282								4.300									
81										4.340			4.345						
82		4.407								4.395									
83										4.430			4.427						
84		4.441														4.445			
85										4.485	3	0.2							
86		4.513.																	
87										4.555			4.562						
88		4.581								4.585									
89		4.602								4.615									
90		4.664		4.650															
91													4.715	0	49	4.720			
92		4.774								4.770									
93 [h]		4.833		4.820						4.820	3	0.37	4.823	0	95	4.816	0	98	0^+
94		4.898																	
95		4.928		4.920									4.940	2	55				
96		5.018																	

TABLE III-1. (Con't.)

Level number	$^{50}V(p,p')^{50}V$ [a] E_x (MeV)	$^{49}Ti(^3He,d)^{50}V$ [b] E_x (MeV)	ℓ_p	$^{49}Ti(^3He,d)^{50}V$ [c] E_x (MeV)	ℓ_p	$\frac{2I+1}{2J+1}S$	$^{51}V(d,t)^{50}V$ [d] E_x (MeV)	ℓ_n	$S_{\ell=3}$	$^{51}V(^3He,\alpha)^{50}V$ [e] E_x (MeV)	ℓ_n	S	$^{48}Ti(^3He,p)^{50}V$ [f] 22 MeV E_x (MeV)	22 MeV L_{np}	22 MeV $\frac{d\sigma}{d\Omega}_{max}$ (μb/sr)	13 MeV E_x (MeV)	13 MeV L_{np}	13 MeV $\frac{d\sigma}{d\Omega}_{max}$ (μb/sr)	J^π
97		5.058		5.070									5.042						
98		5.090																	
99		5.326																	
100		5.409																	
101		5.531																	
102		5.645																	
103		5.755																	
104		5.786																	
105		5.820																	
106		5.893																	
107		5.951																	
108																6.560			
109																6.610			
110 [h]																8.588	0	160	0^+
111																9.115			
112																9.164			

[a] Bu 69.

[b] Bi 70.

[c] This work. The quantity $[(2J_f + 1)/(2J_i + 1)]$ S was calculated on the assumption that $J = \ell + \frac{1}{2}$ for the transferred proton.

[d] So 69.

[e] This work. S was calculated on the assumption that $J = \ell + \frac{1}{2}$ for the transferred neutron.

[f] This work.

[g] Possible doublet.

[h] Isobaric analog state.

at E(^{3}He) = 15 MeV to our value at E(^{3}He) = 22 MeV was 8:9, whereas the DWBA calculation to be discussed in Chap. IV predicts a ratio of ~1:2. Since there currently is speculation on the possible breakup of nuclei such as the ^{3}He and the deuteron in high energy (>20 MeV) reactions, and since this would result in inaccuracies in the DWBA predictions, we have remeasured the absolute cross section at the ground-state maximum at E(^{3}He) = 15 MeV (maximum at 25°) and 22 MeV (maximum at 21°) under the same conditions so far as the uncertainties listed in Sec. F of this chapter allow. The result is that the ratio is 1:2.2, in agreement with the DWBA prediction (to within the 20% uncertainty in the DWBA calculation).

1. ^{49}Ti(^{3}He, d)^{50}V Reaction Induced by 22-MeV Incident ^{3}He

Forty-three peaks in the spectrum up to 5.1 MeV excitation are seen strongly enough to assign as levels in ^{50}V. These are listed in Table III-1 and are plotted in Fig. III-3.

Of the 43 observed ^{50}V levels, 31 are seen strongly enough to determine their angular distributions. These are presented in Fig. III-7. Three shapes may be distinguished by the position of the first maximum. A maximum at 0° and the first minimum at 12° is characteristic of the level at 2.535 MeV; and this shape will be identified with $\ell_p = 0$ in Chap. IV. The second shape is distinguished by the position of the first maximum at 10° and is examplified by the level at 2.650 MeV ($\ell_p = 1$). The third shape has its first maximum at 22° and may be observed in the ground state ($\ell_p = 3$). In Chapter IV several low-lying levels will be shown to be combinations of $\ell_p = 1$ and 3.

2. $^{51}V(^{3}He, \alpha)^{50}V$ Reaction Induced by 22-MeV Incident ^{3}He

Fifty-three levels up to 4.82 MeV excitation in ^{50}V are seen in this reaction, but only 27 (including all 9 levels below 1.4 MeV) are strongly populated. All observed levels are listed in Table III-1.

The angular distributions (Fig. III-8) from the $(^{3}He, \alpha)$ reaction have an exponential-like decrease which masks the details of their shape and the positions of their first maximum. However, four of the angular distributions may be distinguished from the rest on the basis of the cross section at 9°. For the level at 2.790 MeV, for example, the differential cross section at 9° is an order of magnitude less than would be predicted by an exponential extrapolation. This minimum at 9° will be interpreted in Chapter IV as characteristic of an $\ell_n = 0$ transfer.

3. $^{48}Ti(^{3}He, p)^{50}V$ Reaction Induced by 22-MeV Incident ^{3}He

Thirty-one levels are observed up to 5.0 MeV, as listed in Table III-1. Angular distributions are obtained for 24 well-resolved levels. However, at excitation energies above 4.0 MeV the number of states becomes so large that structure in the angular distribution of one peak tends to be washed out by the contributions from overlapping neighboring peaks.

Three different shapes of angular distribution may be discerned. Those having a sharp minimum near 14° are represented by the state at 1.500 MeV ($L_{np} = 0$). An angular distribution with a wide maximum at about 14° is exemplified by the state at 1.405 MeV ($L_{np} = 2$). Finally an angular distribution with a very wide maximum in the vicinity of 22° is seen in the distribution of the state at 1.705 MeV ($L_{np} = 4$).

4. $^{48}Ti(^{3}He, p)^{50}V$ Reaction Induced by 13-MeV Incident ^{3}He

Measurements on the $^{48}Ti(^{3}He, p)^{50}V$ reaction at $E(^{3}He) = 13$ MeV were undertaken to gain the good resolution needed to identify the ^{50}V levels observed in the $^{48}Ti(^{3}He, p\gamma)^{50}V$ reaction and to obtain the neutron-proton orbital-angular-momentum transfer. Fifteen levels, including all 11 levels seen in the gamma decay, are seen well enough to assign excitation energies. Ten of these 11 levels were seen strongly enough to obtain angular distributions. (The angular distribution of the level at 3.240 MeV is the sum of the distributions of the 3.205- and 3.225-MeV levels seen in the γ-decay measurements.)

The levels seen in the gamma decay (all those presented in Fig. III-10 except the state at 1.405 MeV excitation) all have a peak towards 0° and a minimum from 20° to 30° ($L_{np} = 0$). On the other hand, the angular distribution of the state at 1.405 MeV shows a wide maximum at 25° ($L_{np} = 2$). The ten angular distributions with $L = 0$ may be divided into two groups distinguished by the sharpness of the minimum. The minima for the two isobaric analog states at 4.816 and 8.588 MeV (which are $J^{\pi} = 0^{+}$ and must be pure $L_{np} = 0$) are distinctly sharper than those for the seven other L_{np} angular distributions for which the minimum can be seen; in the case of the remaining $L_{np} = 0$ angular distribution (for the state at 3.575 MeV), the angular distribution is obscured at 29° where the minimum would be. These seven angular distributions could be mixtures of $L_{np} = 0$ and $L_{np} = 2$ (which would fill in the $L_{np} = 0$ minimum) and would then necessarily be $J^{\pi} = 1^{+}$ levels. This mixture of L values will be discussed in Chapter IV.

IV. THE DISTORTED-WAVE BORN-APPROXIMATION (DWBA) ANALYSIS

A. Nature of the Analysis

The purpose of the DWBA analysis is to allow the extraction of spectroscopic factors for one-nucleon transfer reaction by comparing the experimental angular distributions with those calculated with the DWBA. The spectroscopic factor of a final state is defined as the squared magnitude of the overlap integral of the wave function of the core nucleus plus the one transferred nucleon. The DWBA allows the calculation of the angular distribution of a one-nucleon transfer reaction in which the initial state is an inert core plus the transferred nucleon in a single-particle state. By comparing the experimental angular distribution with those calculated by the DWBA, one is often able to identify the major single-particle states and to extract the strengths (spectroscopic factors) for final nuclear states.

Section B of this chapter will describe the formalism of the DWBA analysis used to calculate the transition amplitude. The major approximations used in developing the analysis will be listed, but no evaluation of their effect on the DWBA will be undertaken. Many such evaluations have already been given (Gl65, Bo67, Wa68) mostly in the form of Ph. D. theses. In most applications of the DWBA, consistent results for the shapes of the angular distributions and for the magnitudes of the relative spectroscopic factors for one-nucleon transfer reactions are obtained so long as sufficient care is taken in the selection of input parameters. Also this work has included no attention to the difficulties of actually calculating the DWBA angular distribution via computer codes. Such problems exist but have been reviewed elsewhere (Ba62, Bo67).

Section C of this chapter will discuss the results of the DWBA calculation and the parameters used in the calculations. The DWBA fits to the experimental angular distributions presented in Chapter III and the extracted spectroscopic factors and angular-momentum-transfer values will be presented in Section D.

B. DWBA Formalism and Approximations

The transition amplitude for the reaction $A(\tau,\beta)B$ may be written (Pr62)

$$T_{\tau\beta} = \langle \phi_{\beta B}\, \chi_{\beta B} | V_{INT} | \Psi_{\tau A} \rangle, \qquad \text{(IV-1)}$$

where $\Psi_{\tau A}$ is the exact total wave function with incoming wave for the particle τ only and outgoing waves in all open channels, $\phi_{\beta B}$ is a function of only the internal coordinates of the β and B nuclei, and $\chi_{\beta B}$ describes the relative motion of the pair β-B. The wave function $\chi_{\beta B}$ is defined by

$$\left\{ \nabla^2 + \frac{K_{\beta B}^2}{\hbar^2} - \frac{2\mu_{\beta B}}{\hbar^2} [U_{\beta B}(r_{\beta B}) + V_c(r_{\beta B})] \right\} \chi_{\beta B}(\vec{K}_{\beta B} \vec{r}_{\beta B}) = 0, \qquad \text{(IV-2)}$$

in which $\vec{K}_{\beta B}$ is the relative momentum, $\mu_{\beta B}$ the reduced mass, $\vec{r}_{\beta B}$ the displacement vector, and V_c the Coulomb potential for the pair β-B (Ba62). The potential $U_{\beta B}$ has been introduced to approximate the interaction between β and B.

In order to get $U_{\beta B}$, let us consider the total nuclear Hamiltonian

$$H = H_0 + \sum_{i<j} V_{ij} = H_0 + V_{\beta B} \qquad \text{(IV-3a)}$$

in which

$$H_0 = \nabla^2 - \frac{2\mu_{\beta B}}{\hbar} V_c(r_{\beta B}), \qquad \text{(IV-3b)}$$

where the V_{ij} are the two-body potentials among all the nucleons in the β-B system. Introducing $U_{\beta B}$ into the Hamiltonian, we obtain

$$H = (H_0 + U_{\beta B}) + (V_{\beta B} - U_{\beta B}). \qquad \text{(IV-4)}$$

To the extent that the two-body potential $U_{\beta B}$ may be made equivalent to the many-body potential $V_{\beta B}$, the second term may be made small. If it is assumed that elastic scattering is the dominant process when β and B interact, and if $U_{\beta B}$ (and hence $\chi_{\beta B}$) are selected to reproduce the elastic scattering, the second term is expected to be small.

Now that the procedure for approximating $\chi_{\beta B}$ has been established, one can state the Born approximation to allow calculation of the initial state in Eq. (IV-1). If the total energy of a particle is everywhere large compared with the scattering potential V_{INT}, then the form of the incident wave cannot be greatly perturbed by the scattering field. One can then assume that each volume element within the scattering field produces a scattered wavelet whose amplitude is jointly proportional to the scattering potential and to the amplitude of the incident wave at the volume element. The wave function $\Psi_{\tau A}$ is then approximated by $\psi_{\tau A}$, which is a solution of an equation analogous to (IV-2). The potential $U_{\tau A}$ is chosen such that $\psi_{\tau A}$ reproduces the elastic scattering of τ on A. With the above introduction, the Born approximation will now be developed quantitatively.

The Hamiltonian of the τ-A system, written in analogy to Eq. (IV-4), is

$$H = (H_0 + U_{\tau A}) + (V_{\tau A} - U_{\tau A}). \qquad \text{(IV-5)}$$

Now let

$$K = (H_0 + U_{\tau A}) \quad \text{and} \quad W = (V_{\tau A} - U_{\tau A}),$$

where K is a Hamiltonian that reproduces the elastic scattering of τ on A, and W is the potential of the interaction leading to all other channels. Then $\Psi_{\tau A}$ and $\psi_{\tau A}$ are solutions of the equations

$$H\Psi_{\tau A} = (K + W)\,\Psi_{\tau A} = E\Psi_{\tau A} \qquad \text{(inhomogeneous equation)}$$

and

$$K\psi_{\tau A} = E_{\tau A}\psi_{\tau A}, \qquad \text{(homogeneous equation)}$$

whose respective Green's function solutions are

$$G = 1/(E - H),$$

$$G_0 = 1/(E - K).$$

Then

$$\Psi_{\tau A} = (1 + GW)\psi_{\tau A} \qquad \text{(IV-6)}$$

is a solution of the inhomogeneous equation. From the identity $1/A - 1/B = (1/B)(B - A)(1/A)$, it follows that

$$G = G_0 + G_0 WG. \qquad \text{(IV-7)}$$

Then using Eqs. (IV-6) and (IV-7) yields a series approximation for $\Psi_{\tau A}$ known as the Born series, namely

$$\Psi_{\tau A} = (1 + G_0 W + G_0 WG_0 W + \cdots)\psi_{\tau A}$$

If $U_{\tau A}$ is chosen properly, the series will converge. The Born series and its convergence is discussed in more detail by Goldberger (Go64, p. 114). The DWBA assumes that the series converges and that using the first term is sufficient (i.e., that W is small) if $U_{\tau A}$ is chosen to provide wave functions that reproduce the elastic scattering of τ on A (i.e., if $U_{\tau A}$ is chosen on the same basis as $U_{\beta B}$).

The remaining step is to approximate the interaction potential in a form that will allow calculation of the transition amplitude. The potential V_{INT} in Eq. (IV-1) is by definition the potential of the interaction that causes the transition from the initial to the final state. Since $\Psi_{\tau A}$ is approximated by $\psi_{\tau A}$, the "elastic" wave function W has been ignored in Eq. (IV-5) and hence W must be the potential that produces the transition, i.e.,

$$V_{INT} = W = V_{\tau A} - U_{\tau A}.$$

Let the nucleus A be composed of the nucleus β plus the transferred nucleon p. Then

$$V_{INT} = (V_{\tau p} + V_{\tau B}) - U_{\tau A},$$

from which, if it can be assumed that $V_{\tau B} = U_{\tau A}$, it follows that

$$V_{INT} = V_{\tau p}.$$

Then

$$T_{\tau\beta}(DWBA) = \langle \phi_{\beta B}\, \chi_{\beta B} | V_{\tau p} | \psi_{\tau A} \rangle.$$

If the wave function $\psi_{\tau A}$ is divided into its wave function of internal coordinates $\phi_{\tau A}$ and relative coordinates $\chi_{\tau A}$ just as βB has been, the final distorted-wave Born-approximation transition amplitude is found to be

$$T_{\tau\beta}(DWBA) = \iint \chi^{*}_{\beta B} \langle \phi_{\beta B} | V_{\tau p} | \phi_{\tau A} \rangle \chi_{\tau A} d\vec{r}_{\tau A} d\vec{r}_{\beta B}, \qquad \text{(IV-8)}$$

where the angular parenthesis is called the form factor.

The cross section is defined in terms of the transition amplitude as

$$\frac{d\sigma}{d\Omega} = \frac{\mu_{\tau A}\mu_{\beta B}}{(2\pi\hbar^2)^2} \frac{K_{\beta B}}{K_{\tau A}} \sum |T|^2, \qquad \text{(IV-9)}$$

where $\sum|T|^2$ represents a sum over the final states and an average over the initial states.

The approximations that go into the DWBA calculations will now be enumerated.

1) The Born approximation. The approximation is to take only the first term in a series expansion (Born series) in the "powers" of the potential. The criterion for validity of the Born approximation is that the series converge sufficiently rapidly. For the cases of interest here, Goldberger (Go64) shows that the series does converge, but he gives no estimate of the error introduced by taking only the first term in the series.

2) The locality assumption. An implicit assumption is that the potential observed by the wave function that represents the state is a local potential; that is, the potential depends only on one (3-dimensional) coordinate $\vec{r}$. A more realistic assumption would reflect the fact that the presence of a particle at $\vec{r}$ influences the probability of finding another particle at $\vec{r}$ in the neighborhood of $\vec{r}$, and hence affects the potential. There is some evidence that such nonlocal effects account for the observed energy dependence of local optical-model potentials (Bo67). In order to obtain potentials at one incident energy and use them at other incident energies, and to take the nonlocality into account, one may assume (a) that the nonlocality is describable as a function with reasonable behavior so that the local-energy approximation (LEA) is valid (Bo67) and (b) that the nonlocality has a Gaussian shape of width Γ. Then the ratio of the wave function from the nonlocal potential to the wave function from the local potential is

$$\frac{\chi_{NL}}{\chi_L} = \left[1 - \frac{\Gamma^2 \mu}{2\hbar^2} U_2\right]^{-1/2} .$$

The χ_{NL} may now be used instead of χ_L in Eq. (IV-8). No estimates of the improved accuracy are available (Gl65, Bo67, Ku69).

3) The zero-range assumption. To enable a digital computer to calculate the transition amplitude within an acceptable time, Eq. (IV-8) is reduced to a single integral by use of the zero-range assumption. This corresponds to assuming that the outgoing particle β is created where the incoming particle τ is absorbed, and may also be treated in the LEA. If the potential $V_{\tau p}$ is assumed to have a Gaussian dependence on the relative position $\vec{r}_{\tau p}$, rather than to be a delta function, the result is to modify the form factor (i.e., the wave function of the bound particle p) by the factor

$$\left\{1 + \frac{2}{\hbar^2} \frac{m_\beta m_p}{m_\tau} R^2 [U_{\tau A} - U_{\beta B} - V_p - E_{BIND}]\right\}^{-1} ,$$

where R is the range of the Gaussian τ-p interaction, m_β, m_p, and m_τ are masses, E_{BIND} is the separation energy of particle p in nucleus β, and V_p is the potential that binds the particle p to the nucleus B.

4) The assumption of an average potential. The potential that binds nucleon p to the nucleus B is assumed to be adequately represented by an average potential of Woods-Saxon shape. The depth of the well is adjusted to produce the experimentally observed p-B separation energy, but little else of this potential is experimentally justifiable. Even this adjustment of the well depth has been shown to be in error for reactions that leave the nucleus B in an analog state (Bo67).

5) The assumption of a spherically-symmetric potential. Equation (IV-2) assumes a spherical form of the optical-model potential although some nuclei are thought to be statically deformed (Ma66).

6) The assumption of a real potential. The optical-model potential that represents the scattering of τ on nucleus A is assumed to be equal to the real potential between τ and the nucleus B. Some implications of this assumption are currently under investigation (Ku70). We can reasonably suppose that a careful choice of optical-model potentials will minimize errors due to this approximation.

7) Ambiguities in choosing the optical potential. The careful choice of optical-model potentials means that the elastic-scattering angular distribution obtained at the appropriate energy is fitted with the optical model. This may be carried out generally on the target nucleus A; however, in addition to the familiar optical-model ambiguities, an uncertainty in the optical-model parameters is introduced by uncertainty in the experimental angular distribution. Even if it is demonstrated that a change in parameters does not change the elastic scattering by more than the experimental uncertainty, there is no guarantee that the same parameter change will not have a great effect on the wave function generated in Eq. (IV-2) and hence greatly change the DWBA calculation results. This difficulty is heightened by the fact that the fit to elastic scattering only puts requirements on the asymptotic behavior of the wave functions χ; their behavior in the region of the nuclear interior is undetermined. Some of this indeterminancy may be taken into account by assuming that there is no contribution to the transition amplitude from the nuclear interior and therefore that the integration of Eq. (IV-8) can be restricted to the nuclear

exterior. A common experimental difficulty encountered in fitting the optical-model curves to the data on elastic-scattering from the residual nucleus is that often the residual nucleus is unstable.

The correctness of approximation 7) will be partially reflected by the ability of the DWBA to calculate the experimental angular distribution in Sec. D. The DWBA calculations for the reactions (^{3}He,d) and (^{3}He,α), in which one nucleon is transferred, are more likely to reproduce the experimental distribution than are calculations for the (^{3}He,p) reaction, in which a neutron-proton pair is transferred. The n-p pair may be considered to act as one quasi-elementary nucleon (a deuteron) but certainly some of the preceding assumptions will be further stretched.

C. DWBA Input Parameters and Results

The philosophy guiding the selection of input parameters for the potentials U assumes that if a set of parameters has been successfully used by others 1) for the same reaction, 2) at about the same particle energies, and 3) for nuclei close to mass 50, then it will be successful also for these measurements. For each of the reactions described in this work there are several sets of parameters satisfying the above requirements, as might be expected because of the ambiguities in fitting the parameters of the potential U to elastic scattering.

For both one-nucleon transfer reactions, several of the available parameter sets have been tried and they produce almost identical shapes for the angular distribution of the reaction. For the (^{3}He,p) reaction in which an n-p pair is considered to be transferred as a deuteron, one observes some differences between the shapes of the reaction angular distributions calculated with different parameter sets. Section IV D will show that the DWBA

fits for deuteron transfer are considerably worse than for one-nucleon transfer, and the small differences in predicted shape are comparatively unimportant.

The final parameters chosen are listed in Table IV-1. A local potential was used and finite ranges R = 0.770 F for (^{3}He,d) and R = 2.0 F for (^{3}He,α) were chosen. For the one-nucleon transfer, the parameter set chosen was the one that best satisfied the sum rule for the ℓ=3 spectroscopic factor (to be discussed in Chap. V). Since it is not possible to extract spectroscopic factors for the n-p transfer reaction, the chosen parameter set was the one that gave the best fit to the data at both 13 MeV and 22 MeV incident ^{3}He.

1. ^{49}Ti(^{3}He,d)^{50}V

Figure IV-1 shows the results of the DWBA calculations for the ^{49}Ti(^{3}He,d)^{50}V reaction; the orbit of the transferred proton is indicated. For each orbital, a curve is shown for each of two different excitations in ^{50}V, namely at 0.0 and 4.0 MeV—the extremes of the experimental excitations. The slight differences observed between the angular distributions for the different excitations result from 1) the different binding energy between the transferred proton and the ^{49}Ti core and 2) the different energy of the outgoing deuteron.

The calculated angular distributions for different orbital-angular-momentum transfer show distinct shapes which are independent of the total angular-momentum transfer j, so only $j = \ell + \frac{1}{2}$ states are shown in the figure. Thus by comparing the experimental distributions with the calculated ones, the transferred orbital angular momentum ℓ is obtained. Once ℓ is known, the change of parity is known and the possible spins of the final states are limited.

TABLE IV-1. DWBA input parameters for the potential

$$V(r) = V\left[f(x_R) + \frac{\lambda}{45.2}\frac{1}{r}\frac{d}{dr}f(x_R)\,\vec{L}\cdot\vec{S}\right]$$

$$+ i(W + W'\,d/dx_I)f(x_I) + V_c(r, r_c),$$

$$f(x_i) = \left(1 + \exp\frac{r - r_{0i}A^{1/3}}{a_i}\right)^{-1}.$$

	- V (MeV)	λ	r_{0R} (F)	a_R (F)	W (MeV)	W' (MeV)	r_{0I} (F)	a_I (F)	r_c (F)
				$^{49}Ti(^3He,d)^{50}V$ [a]					
^{3}He	-167.9	0.0	1.07	0.775	-16.79		1.611	0.600	1.4
d	-112.	0.0	1.0	0.900	0.0	72.	1.55	0.47	1.3
p	d	0.0	1.1	0.65	. . .	. . .	. . .	. . .	1.25
				$^{51}V(^3He,\alpha)^{50}V$ [b]					
^{3}He	-168.0	0	1.07	0.775	-16.79	0.0	1.610	0.600	1.4
α	-140.1	0	1.480	0.529	-22.9	0.0	1.480	0.529	1.4
n	d	25.	1.20	0.65	. . .	. . .	. . .	. . .	1.25
				$^{48}Ti(^3He,p)^{50}V$ [c]					
^{3}He	-173.77	0	1.14	0.734	-16.21	0	1.604	0.753	1.4
p	-53.6	0	1.217	0.6	0	68.4	1.264	0.31	1.25
d	d	0	1.2	0.65	. . .	. . .	. . .	. . .	1.2

[a] Based on Ref. (Do67).

[b] Based on Ref. (Bo67).

[c] Based on Ref. (Ra70).

[d] Adjusted to reproduce the experimental binding energy.

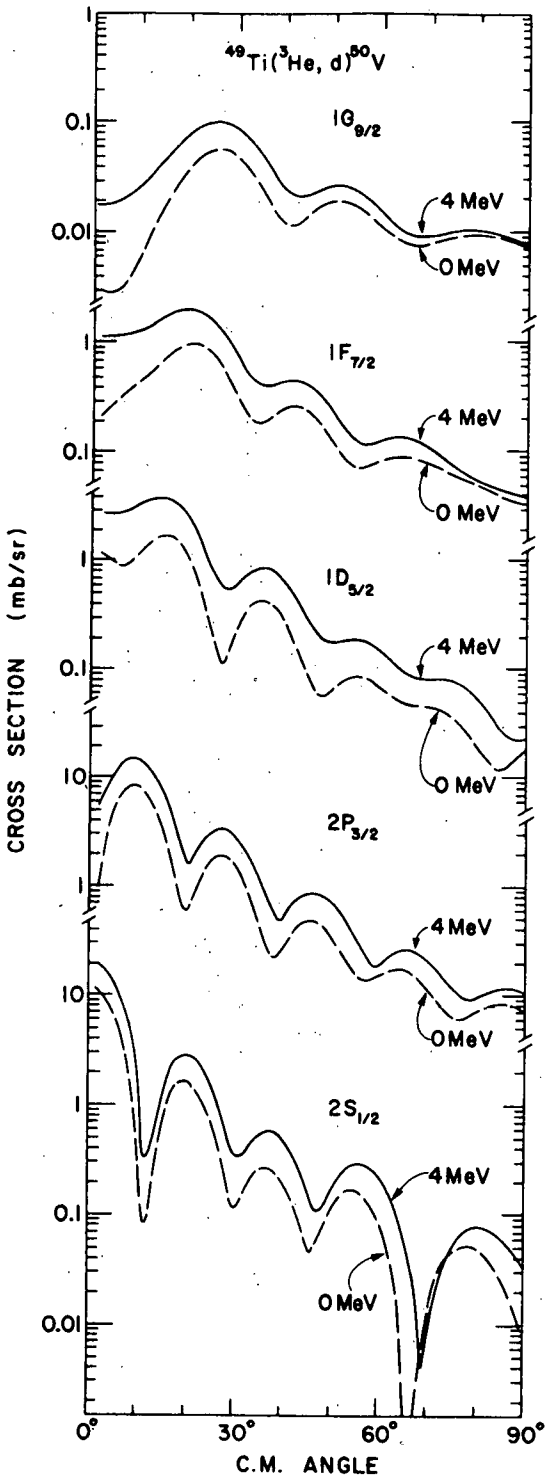

Fig. IV-1. DWBA angular distributions for the $^{49}Ti(^3He,d)^{50}V$ reaction.

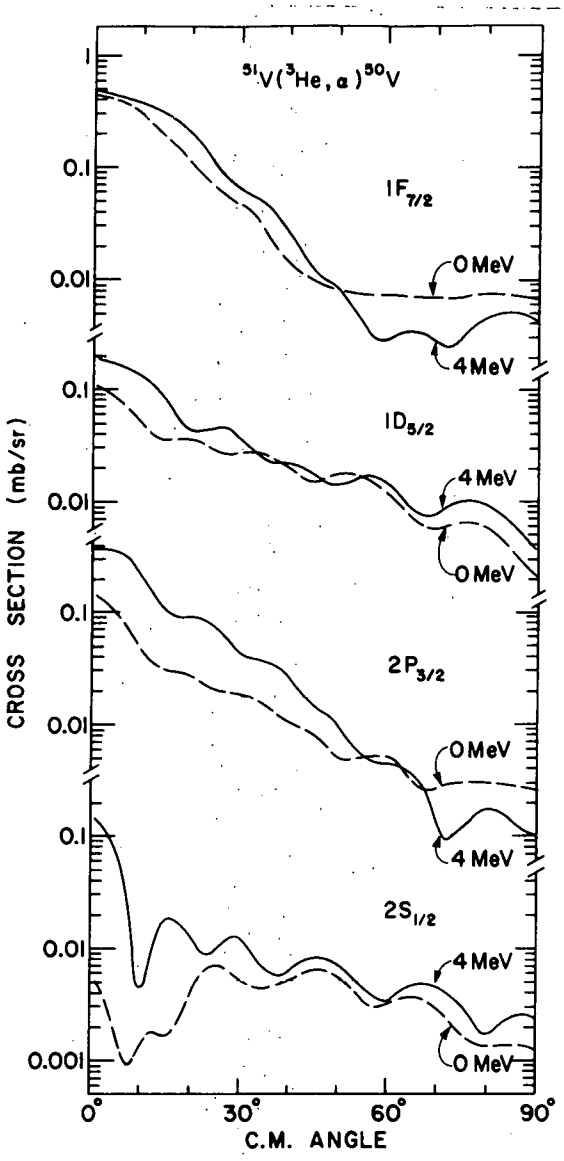

Fig. IV-2. DWBA angular distributions for the $^{51}V(^3He,\alpha)^{50}V$ reaction.

There also exists the possibility that a level of ^{50}V may be populated with two different ℓ transfers, so long as that is allowed by parity conservation. For example a p and f mixture is allowed, but a d and f mixture is forbidden. In case of an allowed mixture, Eq. (IV-9) predicts that the angular distribution will be the sum of the two angular distributions. In favorable cases we expect to be able to tell if an experimental angular distribution includes a significant amount of a second orbital angular-momentum transfer.

2. $^{51}V(^{3}He,\alpha)^{50}V$

Figure IV-2 shows the DWBA calculations for the neutron-hole transfer. The structure is seen to differ from one ℓ transfer to another, but it is somewhat obscured by the exponential decrease with increasing angle. Although the different ℓ transfers may be distinguished by the differences in the slope and by the structure, mixtures of two ℓ transfers in the ^{50}V wave function will not be discernible.

3. $^{48}Ti(^{3}He,p)^{50}V$

Figures IV-3 and 4 show the DWBA calculation for the transfer of a deuteron as a single particle into the ^{48}Ti core for $E(^{3}He)$ = 22 and 13 MeV, respectively. If the largest angular momentum for each nucleon is 3 (i.e., an f orbit), the deuteron may find itself absorbed with L = 0, 2, 4, or 6. As in the $(^{3}He,d)$ calculation, the shapes of the angular distributions are distinctive and one may expect to be able to assign the L value for each experimentally observed level.

One might also be able to discern mixtures of two L values. For instance, mixtures of L = 0 and L = 2 might look

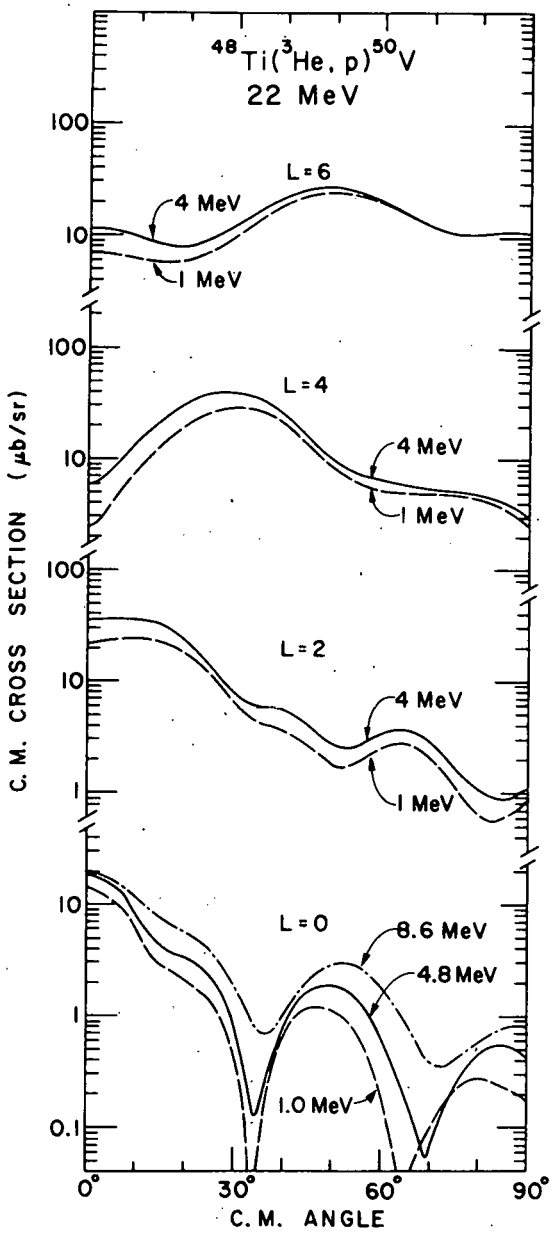

Fig. IV-3. DWBA angular distributions for the ^{48}Ti(^{3}He,p)^{50}V reaction induced by 22-MeV ^{3}He.

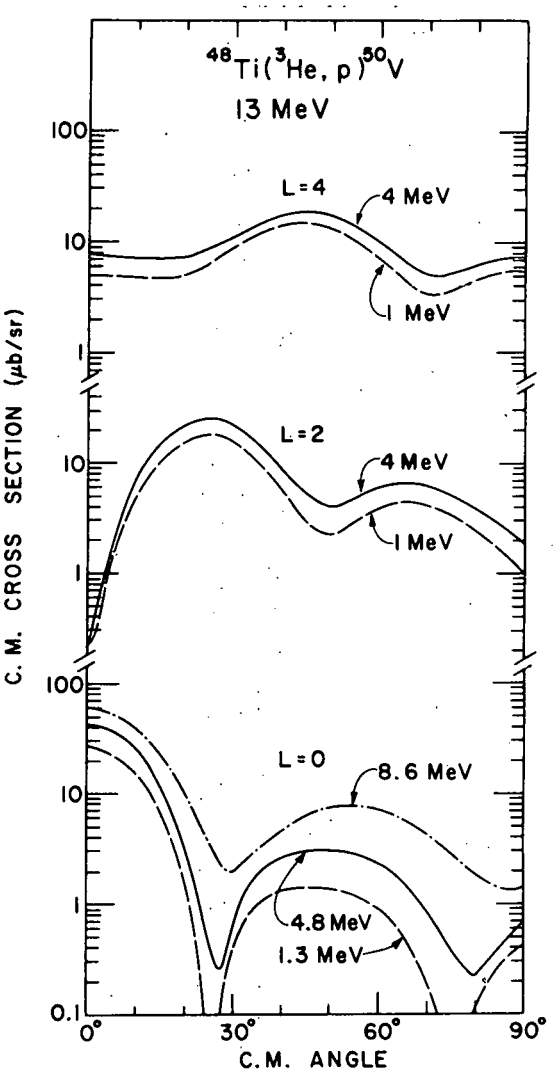

Fig. IV-4. DWBA angular distributions for the ^{48}Ti(^{3}He,p)^{50}V reaction induced by 13-MeV ^{3}He.

like the L = 0 distribution except that the L = 2 distribution would fill in the first L = 0 minimum. Because ^{48}Ti has a 0^+ ground state and the deuteron has spin 1, admixtures of L = 0 + 2 can lead only to states of $J^\pi = 1^+$. Unfortunately the greater uncertainties associated with the DWBA calculations for two-nucleon transfer make the procedure questionable. In fact Rao (Ra70) has shown that even in a more precise treatment of the DWBA for two nucleons (each bound to the core separately instead of as a deuteron), some legitimate parameterizations of the potentials U cause the first minimum of the pure L = 0 angular distributions to fill in. On the other hand, if one pure L = 0 angular distribution with the deep minimum (such as is observed for the 0^+ isobaric analog state in this work) can be found experimentally for comparison, then it may be that one can tentatively assign 1^+ to states for which the angular distributions are similar in shape to those for L = 0 except that the first minimum is shallow.

D. Extraction of the Spectroscopic Value and ℓ Transfer

The procedure for extracting the orbital momentum transfer by DWBA is obvious from the discussion in Chap. III. The fits of DWBA calculations to the experimental angular distribution, shown as smooth curves in Figs. III-7 to III-10 allow the extraction of the spectroscopic factors by the relations

$$\frac{2J_f + 1}{2J_I + 1} S = \frac{2J + 1}{4.42} \left[\left(\frac{d\sigma}{d\Omega} \right)_{EXP} \Big/ \left(\frac{d\sigma}{d\Omega} \right)_{DWBA} \right] \qquad \text{(IV-10)}$$

for ^{49}Ti(^{3}He,d)^{50}V and

$$S = \frac{2J + 1}{23} \left[\left(\frac{d\sigma}{d\Omega} \right)_{EXP} \Big/ \left(\frac{d\sigma}{d\Omega} \right)_{DWBA} \right] \qquad \text{(IV-11)}$$

for ^{51}V(^{3}He,α)^{50}V.

In Eqs. (IV-10) and (IV-11), J_f and J_i are the total angular momenta of the final and initial states, respectively, J is the total angular momentum of the single-particle state (taken as $J = \ell + \frac{1}{2}$ in spectroscopic-factor calculations in this work). The numbers 4.42 in Eq. (IV-10) and 23 in Eq. (IV-11) are empirically determined normalizing factors. The isospin Clebsch-Gordan coefficient has been absorbed into the spectroscopic factor S so that $S = C^2 \delta$. In Eq. (IV-10), the product $[(2J_f + 1)/(2J_i + 1)]S$ as a whole will be used as equivalent to the spectroscopic factor S in Eq. (IV-11). The ratio of cross sections is evaluated at the most forward maximum.

1. ^{49}Ti(^{3}He,d)^{50}V

The ℓ values and spectroscopic values are extracted from the data on the levels of ^{50}V (plotted in Fig. II-7 and listed in Table III-1). Several cases identified as mixtures of $\ell = 1$ and $\ell = 3$ are indicated in the levels below 1 MeV.

Figure IV-5 displays the spectroscopic factor as a function of excitation energy for $\ell = 3$, 1, and 0. The $\ell = 3$ strength lies wholly below 1.5 MeV. The $\ell = 1$ strength is split over the whole level scheme but is strongest around 3 MeV. The dots in the $\ell = 1$ plot represent spectroscopic factors less than 0.1. The $\ell = 0$ angular distributions seen for the two levels near 2.5 MeV indicate that these are negative-parity states. These levels presumably have configurations with holes in the $2s_{1/2}$ shell.

2. ^{51}V(^{3}He,α)^{50}V

The ℓ values and spectroscopic factors were also extracted from the data on the ^{50}V levels (plotted in Fig. III-8 and listed in Table III-1). Figure IV-6 shows the spectroscopic factor

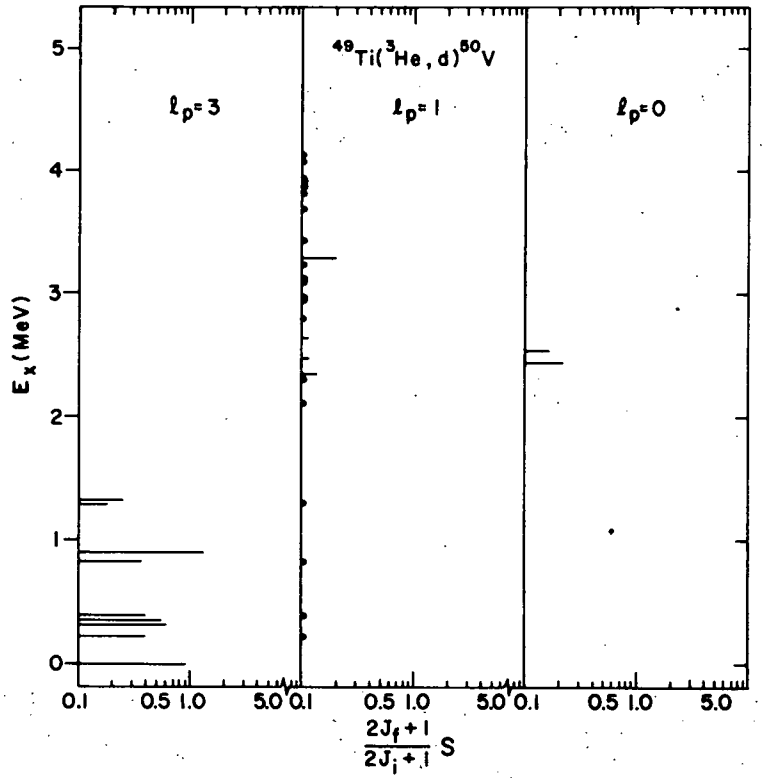

Fig. IV-5. The spectroscopic factors obtained from a DWBA analysis of the data on the ^{49}Ti(^{3}He, d)^{50}V reaction. The results for ℓ_p = 3, 1, and 0 are plotted as a function of excitation energy.

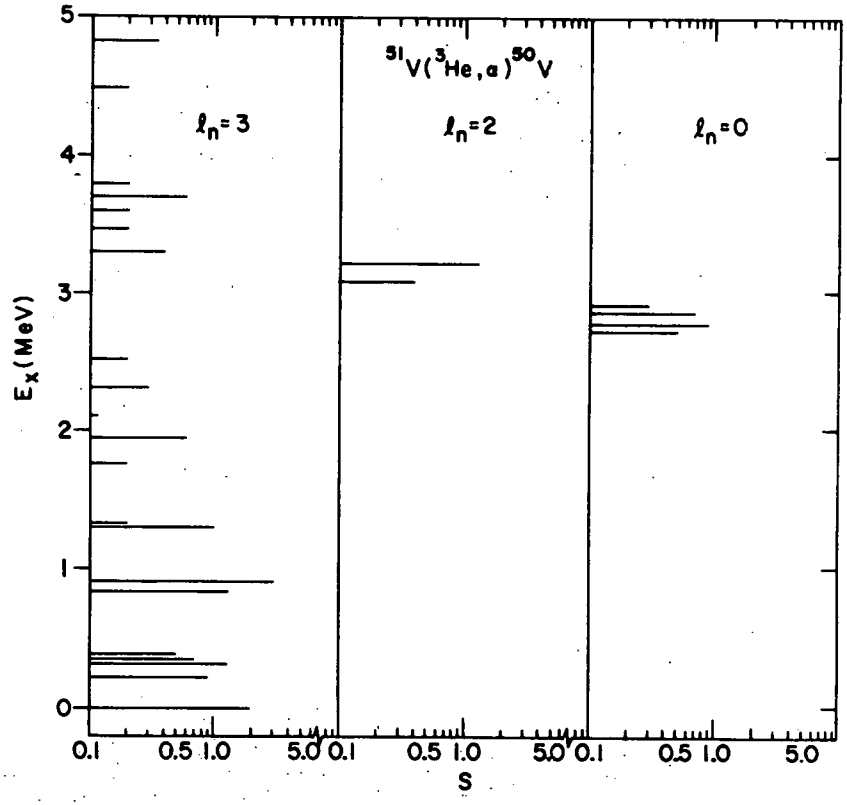

Fig. IV-6. The spectroscopic factors obtained from a DWBA analysis of the data on the ^{51}V(^{3}He, α)^{50}V reaction. The results for ℓ_n = 3, 2, and 0 are plotted as a function of excitation energy.

for the $^{51}V(^{3}He,\alpha)^{50}V$ reaction for ℓ = 3, 2, and 0 as a function of the excitation energy in the final state. A great deal of ℓ = 3 strength is observed throughout the whole range of excitation but is most concentrated below 1.5 MeV. The ℓ = 3 strength is thought to be overestimated as a result of our inability to separate admixtures of ℓ = 1 strength. That some levels in ^{50}V are populated through ℓ = 1 transfer is known from recent work (De71) on the $^{51}V(d,t)^{50}V$ reaction, in which angular distributions with distinctive shapes characteristic of ℓ = 3 and ℓ = 1 were measured.

Negative-parity states populated with ℓ = 0 and 2 are seen near 3 MeV. These states must have configurations corresponding to holes in the 2s-1d shell.

3. $^{48}Ti(^{3}He,p)^{50}V$

Although spectroscopic factors are not extracted for the $(^{3}He,p)$ reaction, the L_{np} were identified and the maximum observed cross sections of the levels are displayed on a scale of excitation energy for each value of L. For the 22-MeV data (Fig. IV-7), there are displays for L = 0, 2, and 4; but for the 13-MeV data (Fig. IV-8), only L = 0 is presented. The relative magnitudes of the cross sections for L = 0 transfer at $E(^{3}He)$ = 13 and 22 MeV are seen to be similar, as expected.

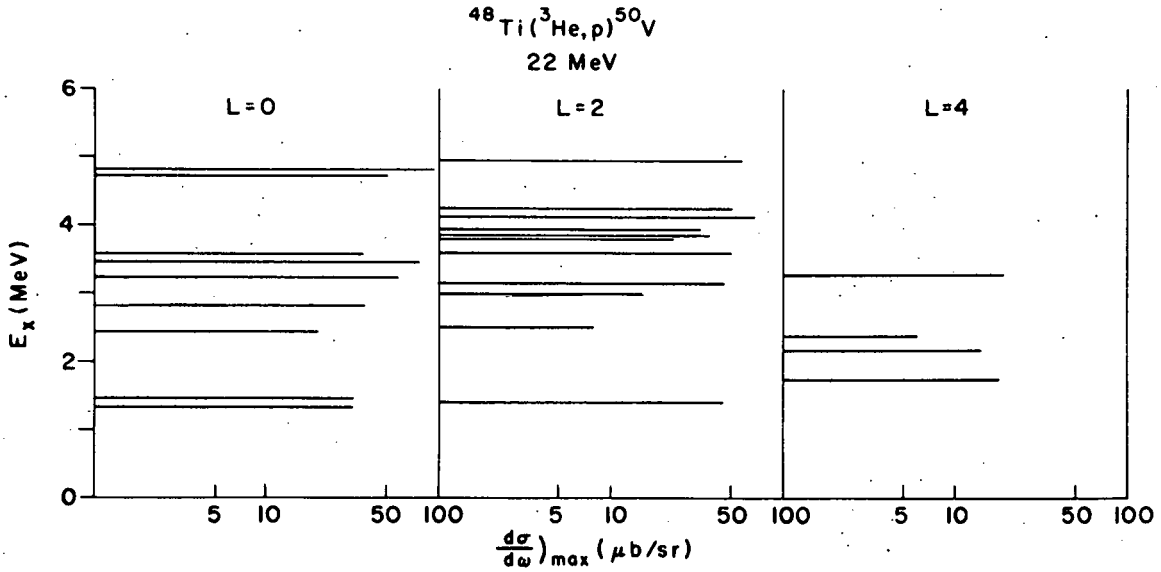

Fig. IV-7. The maximum cross section of the ^{48}Ti(^{3}He,p)^{50}V reaction induced by 22-MeV ^{3}He. The results for L = 0, 2, and 4 are plotted as a function of excitation energy.

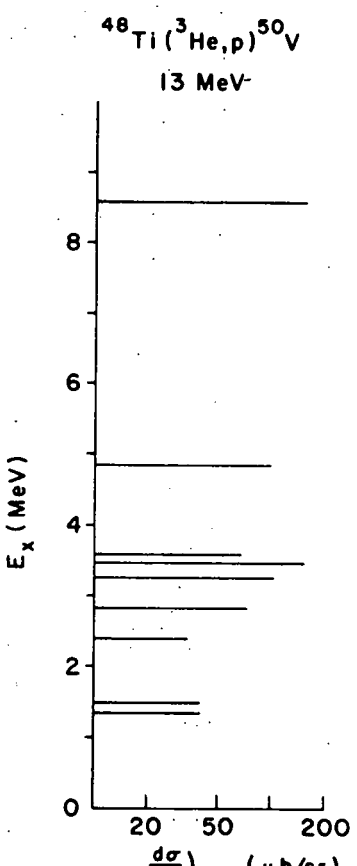

Fig. IV-8. The maximum cross section of the ^{48}Ti(^{3}He,p)^{50}V reaction induced by 13-MeV ^{3}He. The results for L = 0 are plotted as a function of excitation energy.

V. NUCLEAR MODELS

A. Introduction

In the absence of a complete theory, nuclear models provide the basis for interpreting the results of nuclear reaction experiments. Numerous models have been proposed but the present discussion includes only two current models that have had some success in the mass region near ^{50}V. They are (1) the McCullen, Bayman, and Zamick (MBZ) calculation for $1f_{7/2}$ nuclei in terms of the spherical shell model (Mc64) and (2) the rotational-particle coupling (RPC) or Coriolis-coupling deformed shell model developed by Wasielewski and Malik (Wa70a). This work is restricted to calculations with these models and to comparisons with level energies, spins, and spectroscopic factors extracted from experimental measurements on ^{50}V. Inasmuch as both models are variants of the shell model, the latter will be discussed first to provide a basis for further specialization. Each model and its prediction will then be discussed separately.

B. The Shell Model

Since exact calculations of the N-body problem are beyond our abilities, some approximations must be made in order to reproduce observed experimental phenomena, such as the magic numbers. The basis of the approximation is that the nucleons are bound in a nucleus whose radius is of the same order of magnitude as the range of the nuclear force and that the most important portion of the nuclear forces is a two-body force. The central approximation is that the potential V_i felt by the ith nucleon in the nucleus is the resultant of the individual forces of all the other nucleons and may be suitably approximated by a central

potential which is the average of the potentials due to all the nucleons. Some elements of the individual potentials cannot be so represented, but these may be treated as perturbations. The resulting single-particle Hamiltonian is

$$H_{sp} = \sum_{i=1}^{A} (T_i + V_i). \qquad (V-1)$$

where T_i is the kinematic energy of the ith nucleon.

In order to reproduce the values of the magic numbers, one must also introduce a spin-orbit potential

$$V_{so} = a\vec{\ell} \cdot \vec{s}. \qquad (V-2)$$

With Eqs. V-1 and V-2, the nucleon has the orbital angular momentum ℓ and the total angular momentum j as good quantum numbers. The value of a that reproduces the magic numbers forces the levels with $j = \ell + \frac{1}{2}$ to be lower in energy than the levels $j = \ell - \frac{1}{2}$ for the same ℓ.

With several nucleons forming a nucleus, the spin of the ground state could be any of the large number of values consistent with the rules for addition of angular momenta. However the ground-state spins of even-even nuclei are observed to be $J = 0$, whereas those of the odd-even nuclei are observed to be just the shell-model value of j for the (unpaired) last nucleon added. This is the basis for introducing a pairing potential, which lowers the excitation of levels for which nucleons in the same $n\ell j$ orbit are paired such that their angular momenta add up to 0. The pairing potential is another name for the short-range nuclear force and may be approximated by a $\delta(r - r')$ function. The seniority quantum number ν is introduced as a measure of the number of unpaired nucleons.

Nuclear levels with $\nu = \nu_{g.s.} + 2$ (i.e., one pair is broken compared to the ground state) are observed to be at some hundreds of keV. This implies that any unpaired nucleons are energetically much more available than paired nucleons and may be expected to interact more readily with other nucleons or nuclei. All the paired nuclei then act as a core and might be ignored. If the paired nuclei fill a shell up to a magic number, they are energetically even more unavailable and the even more inert core is usually omitted in any interaction calculation. This omission is called the truncation assumption, which is that the space spanned by the wave function excludes the space spanned by the inert core.

1. Spectroscopic Sum Rules

French and Macfarlane (Fr61) have derived simple relations to describe the total spectroscopic factor for exciting the $T_<$ and $T_>$ states in a single-nucleon transfer reaction into the orbit $n\ell j$. For stripping reactions, the sum rule is given by the equation

$$\sum \frac{2J_f + 1}{2J_i + 1} S_{n\ell j}(T_<) = \pi - \frac{\nu}{2T + 1} ,$$

$$\sum \frac{2J_f + 1}{2J_i + 1} S_{n\ell j}(T_>) = \frac{\nu}{2T + 1} , \qquad \text{(V-3)}$$

where J_i and J_f are the spins of the target and final states, respectively, and $T_<$ is the isospin of the ground state of the residual nucleus ($T_> = T_< + 1$) and π and ν are the numbers of proton and neutron holes, respectively, in the target nucleus whose isospin is T and whose quantum numbers n, ℓ and j are the same as those of the transferred nucleon. For a proton transferred

into the $1f_{7/2}$ orbit in the $^{49}Ti(^{3}He, d)^{50}V$ reaction, the sum rules are

$$\sum \frac{2J_f + 1}{2J_i + 1} S_{n\ell j}(T_<) = 5.833,$$
$$\sum \frac{2J_f + 1}{2J_i + 1} S_{n\ell j}(T_>) = 0.167. \qquad \text{(V-4)}$$

For pickup reactions, on the other hand, the sum rules become

$$\sum S_{n\ell j}(T_<) = \nu - \frac{\pi}{2T + 1},$$
$$\sum S_{n\ell j}(T_>) = \frac{\pi}{2T + 1}, \qquad \text{(V-5)}$$

where the symbols retain the same meaning as before except that π and ν refer to the number of particles instead of holes. For the reaction $^{51}V(^{3}He, \alpha)^{50}V$ with the neutron picked up from the $1f_{7/2}$ orbit, Eq. (V-5) becomes

$$\sum S_{n\ell j}(T_<) = 7.50,$$
$$\sum S_{n\ell j}(T_>) = 0.50. \qquad \text{(V-6)}$$

As seen in Table III-1, the sum rule for the $^{49}Ti(^{3}He, d)^{50}V$ reaction to final states at excitations below 1.5 MeV (the experimental limit of the $1f_{7/2}$ states) gives $\sum[(2J_f + 1)/(2J_i + 1)]S(T_<) = 4.91$, which agrees with Eq. (V-4)

within the 20% DWBA uncertainty. For the $^{51}V(^{3}He,\alpha)^{50}V$ reaction to final states with excitations below 1.5 MeV, the experimental result is $\sum S(T_<) = 10.4$. This value is 30% over the sum rule prediction (V-6), but the excess is understood as being due to our inability to detect admixtures of other ℓ transfers in the angular distributions. For the $T_>$ states, which lie at high excitation energy, there is insufficient information to allow the evaluation of the sum rule for $S(T_>)$ or for $[(2J_f + 1)/(2J_i + 1)]\, S(T_>)$.

2. Calculations with the Shell Model

When all the perturbation potentials are collected into the single interaction potential V_{ij}, the nuclear Hamiltonian may be expressed as

$$H = H_{s.p.} + \sum_{i<j=1}^{A} V_{ij}. \qquad (V-7)$$

The V_{ij} are related to the real nucleon-nucleon potentials V_{ij}^{real} by $\sum V_{ij} = \sum V_{ij}^{real} - \sum V_i$. The solution of a nuclear problem now proceeds in three steps. First the completely asymmetric wave function Φ_{TOTAL} of all the nucleons is written

$$H_{s.p.}\, \Phi_{TOTAL} = E\, \Phi_{TOTAL},$$

$$\Phi_{TOTAL} = \Phi_{CORE}\Phi_{ACTIVE}.$$

By the truncation assumption, the interaction V_{ij} will act only on Φ_{ACTIVE}. The subscript ACTIVE will be omitted in the future as unnecessary. Second, the interaction matrix between all states r and s is written as

$$H_{INT} = \langle \Phi_r | \sum_{i<j=1} V_{ij} | \Phi_s \rangle . \qquad (V-8)$$

The matrix H_{INT} is then diagonalized. Finally, the eigenfunctions are extracted and used as the wave functions of the nuclear states. These wave functions with the appropriate operators may be used to calculate the properties of the nuclear states.

This three-step program involves two major uncertainties: (1) the uncertainty about the space spanned by Φ and (2) the uncertainty about the residual interaction V_{ij}. Correspondingly, there are two principal approaches to shell-model calculations: the choice between them depends on which uncertainty is felt to be the most serious. If uncertainty (1) is felt to dominate the problem, a detailed residual interaction V_{ij} is assumed and wavefunctions are used from as many single-particle shell-model states as one feels capable of diagonalizing with the available computing facilities. In principle then, only uncertainties of type (2) remain. The parameters of V_{ij} are then adjusted to reproduce the experimental data. This is the approach of the RPC model which proposes a source of the interaction, and therefore V_{ij}. The RPC model will be discussed in Sec. V D.

If, on the other hand, the type (2) uncertainties in the residual interaction are felt to be the most serious, one might make very restrictive assumptions on the space spanned by Φ so that the interaction matrix elements are determined by only a few numbers that may be extracted from experimental measurements. Then to the extent to which uncertainties in the experimental measurement can be neglected, the calculation is free of uncertainties of type (2) but may be incorrect due to uncertainties of type (1). The spin-orbit interaction (V-2) leads to an energetically isolated $1f_{7/2}$ orbit.

Thus limiting Φ to the space of $1f_{7/2}$ active nucleons will minimize uncertainties of type (1) in such a calculation. This has been the approach of McCullen, Bayman, and Zamick and will be discussed in Sec. V C.

Given experimental measurements and two applicable models, one is tempted to compare the predictions of each model with the experimental measurements in order to determine which model best represents the real world. However, the critical difference between the two models presented here is in the method of extracting H_{INT} from the experimental data; they are both the shell model. Conclusions from comparisons between the data and the predictions of the models must reflect successes and failures of the calculation of H_{INT} by the two methods.

C. The Scheme of McCullen, Bayman, and Zamick (MBZ)

By limiting the space of wave functions to the $1f_{7/2}$ orbit only and by extracting the nucleon-nucleon interaction energies from the levels in ^{42}Sc (in which the ^{40}Ca core is assumed to be inert), MBZ establish the matrix for H_{INT} in Eq. (V-7) for two $1f_{7/2}$ nucleons (Mc64). Fractional-parentage expansions then establish the matrix H_{INT} for more than two $1f_{7/2}$ nucleons. The eigenvectors of the nuclear state are then extracted from the diagonalized H_{INT} and may be expressed as a linear combination of all the states of allowed total angular momentum of neutrons and protons. We will use the notation of MBZ in which $j \equiv \frac{7}{2}$ and [ ] represents angular momentum coupling, i.e.,

$$[\Psi(J)\Phi(K)]^{I}_{M} = \sum_{m_1 m_2} (J\ K\ m_1 m_2 | IM)\Psi(Jm_1)\Phi(Km_2). \quad (V-9)$$

In the MBZ scheme, a state of ^{50}V ($Z = 23$, $N = 27$) is described as three protons coupled to a neutron hole. Since the nucleons are limited to the $1f_{7/2}$ orbit, the neutron-hole wave function may have only total angular momentum $j \equiv \frac{7}{2}$. However the three protons may couple to any one of the total angular momenta $L = \frac{3}{2}, \frac{5}{2}, \frac{7}{2}, \frac{11}{2}$, or $\frac{15}{2}$ and seniority ν. The states of ^{50}V are then combinations of

$$[\psi_{123}(j^3 \nu L)\psi_n(j^{-1})]^I_M ,$$

where ψ_{123} is the wave function of the three protons coupled to total angular momentum L and seniority ν and is written first. Then the wavefunction ψ_n of the neutron hole is written. The spin of the state is $\vec{L} + \vec{j} = \vec{I}$. The wave function of the ath state of spin I is then

$$\Psi(^{50}V, aI) = \sum_{\nu, L} C^{aI}(\nu L)[\psi_{123}(j^3 \nu L)\psi_n(j^{-1})]^I_M . \quad (V\text{-}10)$$

The coefficients $C^{aI}(\nu L)$ are given in Ref. Mc64a. Wave functions such as those in Eq. (V-10) may be used with the appropriate operators in calculating observable quantities.

1. Predictions with the MBZ Wave Functions

The calculations of the spectroscopic factors for the $^{49}Ti(^3He, d)^{50}V$ and $^{51}V(^5He, \alpha)^{50}V$ reactions with MBZ wave functions is given in Appendix B, and the results are presented in Table V-1.

In Fig. V-1 the experimental results are compared with the MBZ predictions for the $^{49}Ti(^3He, d)^{50}V$ reaction. Part (a) presents the results of the present work, (b) the work of

TABLE V-1. MBZ Spectroscopic Factors.

E_x (MeV)	$I(T_<)$	$(^3He, d)$ $\frac{2I+1}{2J+1} S$	$(^3He, \alpha)$ S
1.5811	1	0.24967	0.14036
2.950	1	0.03819	0.06716
4.2158	1	0.12138	0.16743
0.3197	2	0.55630	0.45796
1.6144	2	0.01167	0.05689
2.8483	2	0.00040	0.00837
4.7346	2	0.00011	0.03229
0.0347	3	0.53315	0.39420
2.0748	3	0.08034	0.25439
2.8265	3	0.03227	0.13098
3.2223	3	0.01897	0.06512
5.5033	3	0.00455	0.03027
0.1078	4	0.29265	0.27144
0.8849	4	0.39089	0.67553
2.3402	4	0.00242	0.00376
3.3368	4	0.00134	0.00425
5.7210	4	0.00007	0.04504
0.2248	5	0.43933	0.53539
0.8676	5	0.30427	0.63917
2.3367	5	0.00103	0.00010
3.1923	5	0.00004	0.07619
4.8217	5	0.00049	0.11836
6.5980	5	0.00000	0.00576
0.0000	6	1.06561	1.14580
2.0335	6	0.01105	0.10951
3.3129	6	0.00044	0.07779
4.3418	6	0.00014	0.11146
1.2104	7	1.68001	1.69825
2.6533	7	0.00896	0.08435
3.8585	7	0.00048	0.04669
5.9291	7	0.00019	0.04563

TABLE V-1 (Cont'd)

E_x (MeV)	$I(T_<)$	$(^3He, d)$ $\frac{2I+1}{\beta J+1} S$	$(^3He, \alpha)$ S'
1.9521	8	0.0	0.0
3.7164	8	0.0	0.0
4.1531	8	0.0	0.0
2.8601	9	0.0	0.0
4.4192	9	0.0	0.0
4.6291	10	0.0	0.0
4.9049	11	0.0	0.0
4.6447	0 ($T_>$)	0.13900	0.12500
6.1537	2 ($T_>$)	0.02744	0.06940
2.6427	4 ($T_>$)	0.00006	0.12500
8.0447	6 ($T_>$)	0.00004	0.18000

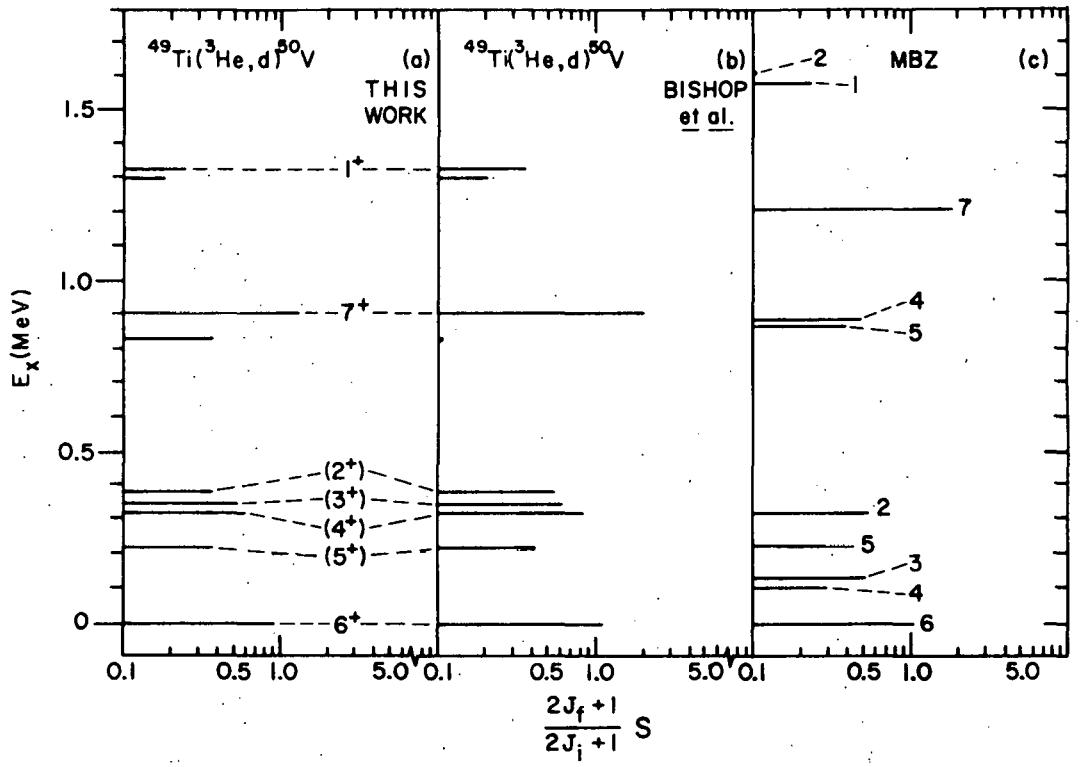

Fig. V-1. Spectroscopic factors as obtained from the DWBA analysis of the ^{49}Ti(^{3}He,d)^{50}V reaction and as predicted from the MBZ theory, plotted as functions of excitation energy.

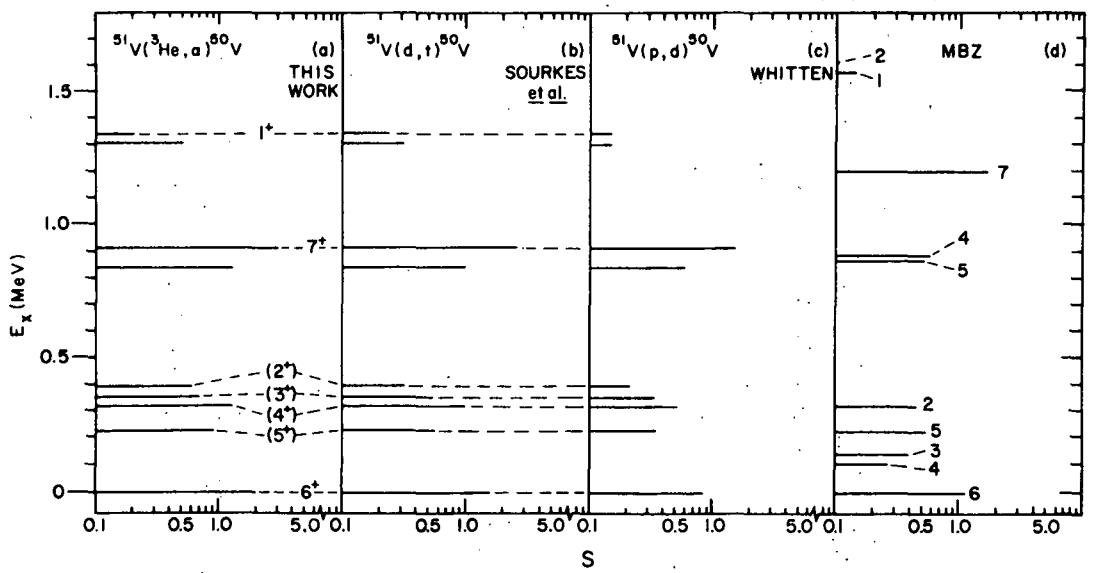

Fig. V-2. Spectroscopic factors as obtained from the DWBA analysis of the ^{51}V(^{3}He,α)^{50}V, ^{51}V(d,t)^{50}V, and ^{51}V(p,d)^{50}V reactions and as predicted from the MBZ theory, plotted as functions of excitation energy.

Bishop et al. (Bi70), and (c) the MBZ predictions. The MBZ proton-transfer spectroscopic factors are taken from Table V-1. The two experimental measurements are in agreement, as pointed out in Chap. III, and the MBZ energy level scheme is seen to be qualitatively right. The MBZ spectroscopic factors for the three ^{50}V states of known spin— g.s. (6^+), 0.91 MeV (7^+) and 1.333 MeV (1^+)— are closely predicted. The energy level for the first, second, third, and fourth excited states are roughly right, and the spectroscopic factors are of the correct magnitude. MBZ predict two states near 0.900 MeV, one of spin 5 and one of spin 4, whereas the only known state in this neighborhood is one of undetermined spin at 0.838 MeV. It is not clear which, if either, of the MBZ states should be identified with the 0.838-MeV state. Above about 1.0—1.5 MeV, the MBZ predictions become rapidly less meaningful because of the increasing admixtures of $2p_{3/2}$ configuration (as seen in Fig. IV-5). The exception to this is the 0^+ isobaric analog state at 4.645 MeV, whose configuration is pure $[\psi_{123}(j^3 0\ 7/2)\psi_n(j\ 7/2)]^0_0$. Experimentally, the 0^+ IAS is at 4.820 MeV.

Figure V-2 is a comparison between experimental results and MBZ predictions for the neutron-pickup reaction. Part (a) presents the results for the $^{51}V(^3He, \alpha)^{50}V$ reaction (this work), (b) for $^{51}V(d, t)^{50}V$ (So69), and (c) for $^{51}V(p, d)^{50}V$ (Wh66); and part (d) presents the predictions of the MBZ theory from Table V-1. Of course the MBZ energy levels are the same as are shown in Fig. V-1c. The experimental spectroscopic factors obtained from the different reactions agree with each other and are in qualitative agreement with the MBZ predictions for the 6^+ and 7^+ states. The rest of the spectroscopic factors predicted by MBZ are of the right magnitude but are not distinctive enough to allow levels assignments.

2. The Nucleon-Nucleon Interaction Used in the MBZ Calculation

In order to obtain the MBZ wave function, the matrix elements of the neutron-proton interaction V_{ij} were needed. These were obtained from the ^{42}Sc energy levels, which are listed in Table V-2. This procedure is justified on two assumptions: (1) the energies and spins of the ^{42}Sc states have been accurately determined and (2) that the ^{42}Sc nucleus is well represented as a ^{40}Ca inert core plus a neutron and a proton.

Table V-2 presents the MBZ values (Mc64a) for the ^{42}Sc energy levels in column 1 and the current best values (Mo69) in column 2. The rms deviation between these two columns is about 350 keV and is due mostly to differences in the excitation energies of the odd-J levels. This 350 keV is taken as the uncertainty in the predicted level energies if ^{40}Ca is an inert core.

If ^{40}Ca is not considered to be a good inert core (Mo69), one might use ^{48}Ca as an inert core and extract the neutron-proton interaction matrix from the excitation energies of neutron-hole — proton-particle states in ^{48}Sc via the Pandya transformation (Pa56), i.e., via

$$E_J(f_{7/2}f_{7/2}) = -\sum_{J'}(2J'+1)W(\tfrac{7}{2},\tfrac{7}{2},\tfrac{7}{2},\tfrac{7}{2};JJ')E_{J'}(f_{7/2}f_{7/2}^{-1}).$$

The equivalent (Pandya transform) neutron-proton interaction energies deduced from the ^{48}Sc excitation energies of Ref. Mo69 are presented in column 3 of Table V-2. The rms deviation between column 2 and 3 of Table V-2 is ~500 keV. The conclusion is that ^{40}Ca and ^{48}Ca cannot both be good inert cores. The ^{48}Ca is generally believed to be a better doubly-closed-shell nucleus (and hence a better inert core) than ^{40}Ca. Then the rms deviation between column 1 and 3 of Table V-1 represents the difference

TABLE V-2. Nucleon-nucleon interaction energies for the $1f_{7/2}$ orbit.

J	MBZ values (MeV)[a]	Current ^{42}Sc (MeV)[b]	Pandya transf. of ^{48}Sc (MeV)[c]
0			
1	1.035	0.615	0.002
2	1.509	1.593	1.307
3	2.248	1.498	1.075
4	2.998	2.800	2.183
5	1.958	1.518	1.254
6	3.400	3.200	2.394
7	0.617	0.625	-0.157

[a] Reference Mc64a.

[b] Reference Mo69.

[c] Reference Mo69.

between the values used by MBZ and the current best values. The size of this difference is ~800 keV, which is comparable to the average interaction energy of ~1200 keV. One cannot know the effects of the discrepancy in neutron-proton interaction energies, and perhaps the whole MBZ calculation should be redone.

D. The Rotational-Particle Coupling (RPC) Model

Suppose an odd-odd nucleus such as ^{50}V may be described as a statically deformed core surrounded by the two odd nucleons. The Hamiltonian then is the sum of the rotational energy and the particle excitation energy, i.e.,

$$H = H_{rot} + H_{part}.$$

The particle Hamiltonian can be divided into the excitation energy H_p of the proton alone, the energy H_n of the neutron alone, and their mutual interaction H_I, i.e.,

$$H_{part} = H_p + H_n + H_I .$$

The rotational energy can be expressed as

$$H_{rot} = \sum_{k=1}^{3} \frac{R_k^2}{2\mathcal{I}_k}$$

where $\mathcal{I}_k$ is the moment of inertia about axis k in the body-fixed coordinates and where

$$\vec{R} = \vec{J} - \vec{j}$$

is the angular momentum of the statically deformed core. Here $\vec{J}$ is the total angular momentum of the nucleus and $\vec{j}$ is the total angular momentum of the proton and neutron so that

$$\vec{j} = \vec{j}_p + \vec{j}_n \quad \text{and} \quad j_3 = j_{p3} + j_{n3}.$$

If the deformed core has a symmetry axis (say the k = 3 axis), i.e., if

$$I_1 = I_2 \equiv I,$$

then

$$H_{rot} = \sum_{k=1}^{3} \frac{(J_k - j_n)^2}{2\mathcal{I}_k} = \frac{\hbar^2}{2\mathcal{I}}[(J - j)^2 - (J_3 - j_3)^2] + \frac{\hbar^2}{2\mathcal{I}_3}(J_3 - j_3)^2.$$

If one separates out the individual contributions to the rotational energy by defining

$$H_r = (\hbar^2/2\mathcal{I})[J^2 - J_3^2 - j_{p3}^2 - j_{n3}^2] + (\hbar^2/2\mathcal{I}_3)(J_3 - j_{p3} - j_{n3})^2,$$

$$H_{rpc} = (\hbar^2/2\mathcal{I})[J_+ j_- + J_- j_+],$$

$$H_{pp} = (\hbar^2/2\mathcal{I})[j_{p+} j_{n-} + j_{p-} j_{n+}],$$

where the subscripts + and - indicate the usual raising and lowering operators, then

$$H_{rot} = H_r + H_{rpc} + H_{pp} + (\hbar^2/2\mathcal{I})(\vec{j}_p^{\,2} + \vec{j}_n^{\,2}).$$

The total Hamiltonian, now divided into six parts, therefore becomes

$$H = H_r + (H_p + (\hbar^2/2\mathcal{I})j_p^2) + (H_n + (\hbar^2/2\mathcal{I})\vec{j}_n^2) + H_{rpc} + H_{pp} + H_i. \quad (V-11)$$

The first, second, and third terms are the Hamiltonians of the rotating core, the proton particle, and the neutron particle. The term H_{rpc} is the rotational-particle coupling or Coriolis potential, H_{pp} is the rotating particle-particle coupling potential, and H_i is the static proton-neutron interaction.

The first three terms of Eq. (V-11) are certainly the ones of greatest importance since they represent the energy of the three components of the system— the core, the proton, and the neutron, respectively, whereas the last three terms are interactions between these different components of the system. The next step therefore is to obtain a wave function that satisfies the Schrödinger equation for the first three terms. Following Nilsson (Ni55), we parameterize H_p and H_n in the form

$$H_p \text{ or } H_n = -(\hbar^2/2\mu)\nabla^2 + \tfrac{1}{2}\mu(w_1^2X_1^2 + w_2^2X_2^2 + w_3X_3^2)$$

$$+ C\vec{\ell}\cdot\vec{s} + D\ell^2. \quad (V-12)$$

The parameters C and D for both proton and neutron are chosen to reproduce the shell-model energy-level ordering at zero deformation, and μ is the effective mass. For symmetry about the (body-fixed) k = 3 axis, one defines the oscillator frequencies w_1 and w_2 in terms of w_0 and the deformation parameter β. Then

$$w_1^2 = w_2^2 = w_0^2 (1 + \tfrac{1}{2}B),$$

$$w_3^2 = w_0^2 (1 - B),$$

where

$$B = 2F(2 - F/(4 - F^2)) \quad \text{and} \quad F = (5/4\pi)^{1/2} \beta .$$

The wave function of the proton is then χ_{Ω_p} such that

$$[H_p + (\hbar^2/2\mathcal{J}) j_p^2] \chi_{\Omega_p} = \epsilon_p \chi_{\Omega_p}.$$

Then in terms of a basis function in which j_p is a good quantum number, χ_{Ω_p} may be expanded in the form

$$\chi_{\Omega_p} = \sum_{j_p} C_{j_p \Omega_p} \chi_{j_p \Omega_p}.$$

By a similar process, the wave function of the neutron is found to be

$$\chi_{\Omega_n} = \sum_{j_n} C_{j_n \Omega_n} \chi_{j_n \Omega_n}.$$

The wave function Ψ which satisfies Schrödinger's equation

$$[H_R + (H_p + (\hbar^2/2\mathcal{J}) j_p^2) + (H_n + (\hbar^2/2\mathcal{J}) j_n^2)] \Psi = E\Psi \qquad (V-13)$$

may be written (Pr62) as

$$\Psi(JMK\Omega_p\Omega_n) = [(2J+1)/16\pi^2] \sum_{j_p, j_n} C_{j_p\Omega_p} C_{j_n\Omega_n}$$

$$\{D^J_{MK}\chi_{j_p\Omega_p}\chi_{j_n\Omega_n} + (-1)^{J-j_p-j_n} D^J_{M-K}\chi_{j_p-\Omega_p}\chi_{j_n-\Omega_n}\}, \qquad (V-14)$$

where $J(J+1)$, M, K, Ω_p, and Ω_n are the quantum numbers of the operators J^2, J_z, J_3, j_{p_3}, and j_{n_3} — J^2 being the square of the total angular momentum of the system, J_z the space-fixed projection of J, J_3 the body-fixed projection of J, the j_{p_3} the body projection of the total angular momentum of the proton, and j_{n_3} the body projection of the total angular momentum of the neutron. Note that Ψ is properly asymmetrized.

The standard diagonalization of the matrices of the neglected potentials H_{rpc}, H_{pp}, and H_i yields the final wave functions. The matricesof H_{rpc} and H_{pp} are easily obtained from the wave function (V-14). The matrix of H_i is obtained independently by calculation with two-particle forces.

1. The Parameters of the Potential in the RPC Model

The parameters for which values must be obtained before the matrix H_{INT} can be diagonalized and the eigenvalues and eigenfunction extracted are the Nilsson spin-orbit parameter C, the Nilsson ℓ^2 (well-flattening) parameter D, the effective mass μ of the proton or neutron in the field of the deformed core, oscillator strength $\hbar w_0$, the moment of inertia parameter $\hbar^2/2\mathcal{I}$ of the core, the softening parameter Q of the rigid core, the core deformation β, and the matrix elements of the residual interaction H_i. The parameter C is well known from the spin-orbit splitting between the $1f_{7/2}$ and $1f_{5/2}$ levels in Sc^{41} and Sc^{49}.

The well-flattening parameter D is not so well defined, but values in the range -0.8 MeV $\leq D \leq -0.3$ MeV preserve the level ordering of the spherical shell model (Wa70). The oscillator strength $\hbar\omega_0 = 41A^{-1/3}$ varies with the mass A of the nucleus in such a way as to preserve the nuclear volume.

The moment of inertia $\mathcal{I}$ that appears in the core parameter $\hbar^2/2\mathcal{I}$ is obtained from the excitation energy of the first 2^+ states in the nearby even-even nuclei. The core is not expected to remain rigid, however; it is expected to change with the proton or neutron excitation. In calculating the matrix H_{INT} the core overlap between two states (the row and column in the matrix) is multiplied by Q (≤ 1) if the proton or neutron are in different configurations and by Q^2 if both the proton and the neutron are in different configurations from the initial to final state. Values $0.5 \leq Q \leq 1$ are obtained in calculations (Ma66). The deformation parameter β is varied freely from nucleus to nucleus.

Two sets of the 195 matrix elements of the residual interaction H_i are obtained (1) from the work of Kuo and Brown, who based their calculations on the hard-core Hamada-Johnston potential derived from two-nucleon scattering data (Ku68a) and (2) from the work of Wasielewski and Vary (Wa70a), who calculated it by use of a Yukawa potential with a Rosenfeld exchange mixture.

These parameters are divided into two groups depending on how well their values are known or on how much their variation affects the calculated energy levels. Parameters C, D, μ, $\hbar\omega_0$ and $\hbar/2\mathcal{I}$ are well known or have little effect, but Q, β and H_i have considerable effect as shown by the considerable differences among the different predictions plotted in Fig. V-3 c—e.

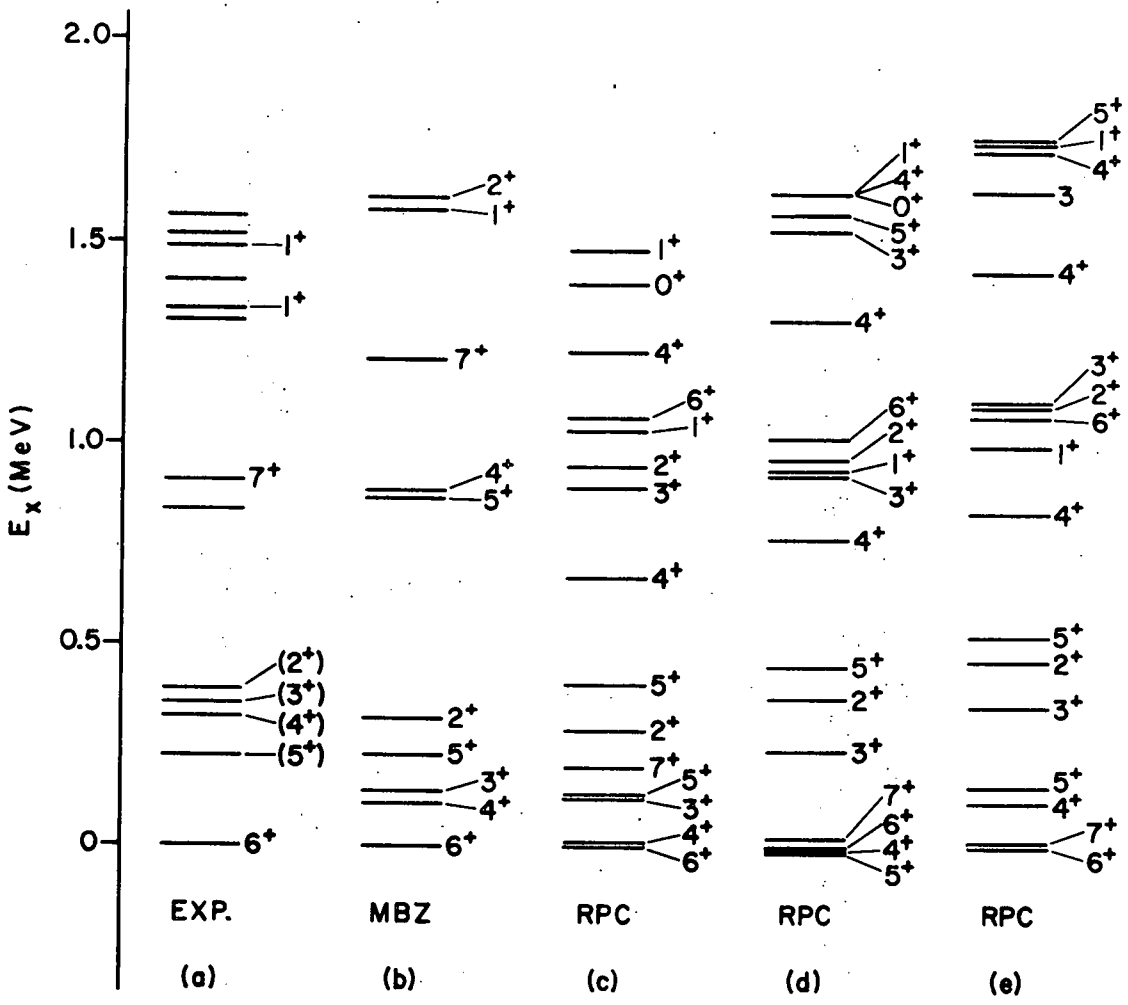

Fig. V-3. Energy levels in ^{50}V. (a) Experimental levels up to 1.6 MeV. (b) MBZ predicted levels up to 2.0 MeV. The last three level schemes were calculated with the rotational-particle-coupling model with the parameters A = 0.2 MeV, C = -0.28 $\hbar\omega_0$, D = -0.06 $\hbar\omega_0$, and $\hbar\omega_0$ = (41 MeV)/$A^{-1/3}$. They differ in that (c) was obtained with Q = 0.9, β = -0.25, and the Kuo-Brown matrix elements (Ku68a); (d) was obtained with Q = 0.9, β = -0.3, and the Yukawa-Rosenfeld matrix elements (Wa70a); and (e) was obtained with Q = 0.95, β = -0.3, and the Yukawa-Rosenfeld matrix elements (Wa70a).

2. Predictions of Energy Levels with the RPC Model

Figure V-3 presents some calculations with various values of Q and β for the Kuo-Brown matrix elements and for the Rosenfeld matrix elements and compares their level schemes with the experimental values and with the MBZ scheme. The energy levels are normalized to the ground state and are carried to high enough excitation to show two 1^+ levels. A broad minimum is observed in the energy of the ground state for $-0.3 \leq \beta \leq -0.2$. The best energy level ordering is produced with $0.9 \leq Q \leq 1$. The low-lying 2^+, 3^+, 4^+, 5^+ and 6^+ states usually are reproduced, and the two 1^+ levels are seen also. The 7^+ state can be made to lie higher but only at the cost of raising the 6^+ above the ground state. Predicted 4^+ and 5^+ states are not observed, as in the MBZ scheme. Spectroscopic factors cannot now be calculated from the wave functions obtained by the diagonalization, but the experimental magnetic dipole moment is well reproduced.(Li64).

VI. DISCUSSION OF ^{50}V LEVELS

A. Information Available from the Reactions Studied

The best available information on energy levels and spectroscopic studies of ^{50}V is presented in Table III-1, which was prepared at the end of December 1970. Generally the (p, p) reaction may be expected to populate ^{50}V levels with protons in such configurations as $(\pi 1f_{7/2})^2(\pi 2p1f_{5/2})$ or $(\pi 1f_{7/2})^4(\pi 2s1d)^{-1}$ but not in such configurations as $(\pi 1f_{7/2})(\pi 2p1f_{5/2})^2$ (two-particle excitation for protons). Likewise the (^{3}He, d) may excite levels with the transferred proton entering a 1f or 2p orbit such as $(\pi 1f_{7/2})^2(\pi 2p1f_{5/2})$ but will lead to no two-particle excitations such as described above. Similarly the (^{3}He, α), (d, t), and (p, d) reaction should produce hole levels in the $1f_{7/2}$, 2s, or 1d orbits but no two-particle excitations.

On the other hand, the two-nucleon transfer reaction (^{3}He, p) can populate these two-particle excitations. With the target nucleus ^{48}Ti ($J^\pi = 0^+$, T = 2), two-particle excitations with $J^\pi = 0^+$ or 1^+ may be populated with $L_{np} = 0$. (The transferred neutron-proton pair np may also enter the $f_{7/2}$ orbit with $L_{np} = 0$ and thereby form a state that is not a two-particle excitation according to our definition.) Since the np pair may be transferred with S = 0 T = 1 or with S = 1 T = 0, the $J^\pi = 0^+$ states so formed may either be T = 2 or 3 (the T = 3 are the 0^+ analog states) but the $J^\pi = 1^+$ states must be T = 2. The $L_{np} > 0$ transfer may also populate levels in which the members of the transferred neutron-proton pair enter different single-particle orbitals and therefore cannot be thought of as a pair.

The gamma-decay operator is a one-nucleon operator (a sum of all possible products of one creation and one annihilation

operator with appropriate angular-momentum coefficients and may be expected to connect levels whose configurations differ only in the change of one nucleon. Angular-momentum conservation requires the transitions of the one nucleon from the 2p to the $1f_{7/2}$ orbit to proceed via a gamma of multipolarity ≥ 2. However, the $1f_{5/2} \rightarrow 1f_{7/2}$ transition could be M1. It is characteristic of γ decays that they often proceed to final states whose spin differs from the initial spin by one unit. As a result, J = 0 or 1 states populated in the (^{3}He, p) reaction would be expected to γ decay to states with J = 0, 1, or 2 (barring collective motion).

B. The ^{50}V Levels

1. The 0^+ Analog States

Two 0^+ IAS at 4.820 and 8.588 MeV excitation in ^{50}V are populated by the (^{3}He, p) reaction. Their parent states are known (Sh69) to be at 0.0 and 3.88 MeV excitation in ^{50}Ti. The wave function of an analog state may be determined from the wave function of its parent state by operating on the parent wave function with the isospin lowering operator T_- (which changes neutrons into protons unless that would violate the Pauli principle).

The configuration of the ground state of ^{50}Ti is expected to be $[(\pi f_{7/2})^2(\nu f_{7/2})^8]$ coupled to $J^\pi = 0^+$, T = 3 plus an inert core. When T_- operates on such a configuration, the result is the same inert core plus $[(\pi f_{7/2})^3(\nu f_{7/2})^{-1}]$ coupled to $J^\pi = 0^+$, T = 3. All the active nucleons still are $1f_{7/2}$. This is taken as the configuration of the 4.820-MeV analog state of ^{50}V.

The parent of the 8.588-MeV analog state of ^{50}V is unusual in its cross section in the (t, p) reaction (Hi67). Fig. VI-1 (from Ref. Hi66) shows the ratio of the (t,p) cross section for the first 0^+ excited state of a nucleus to that for its ground state as

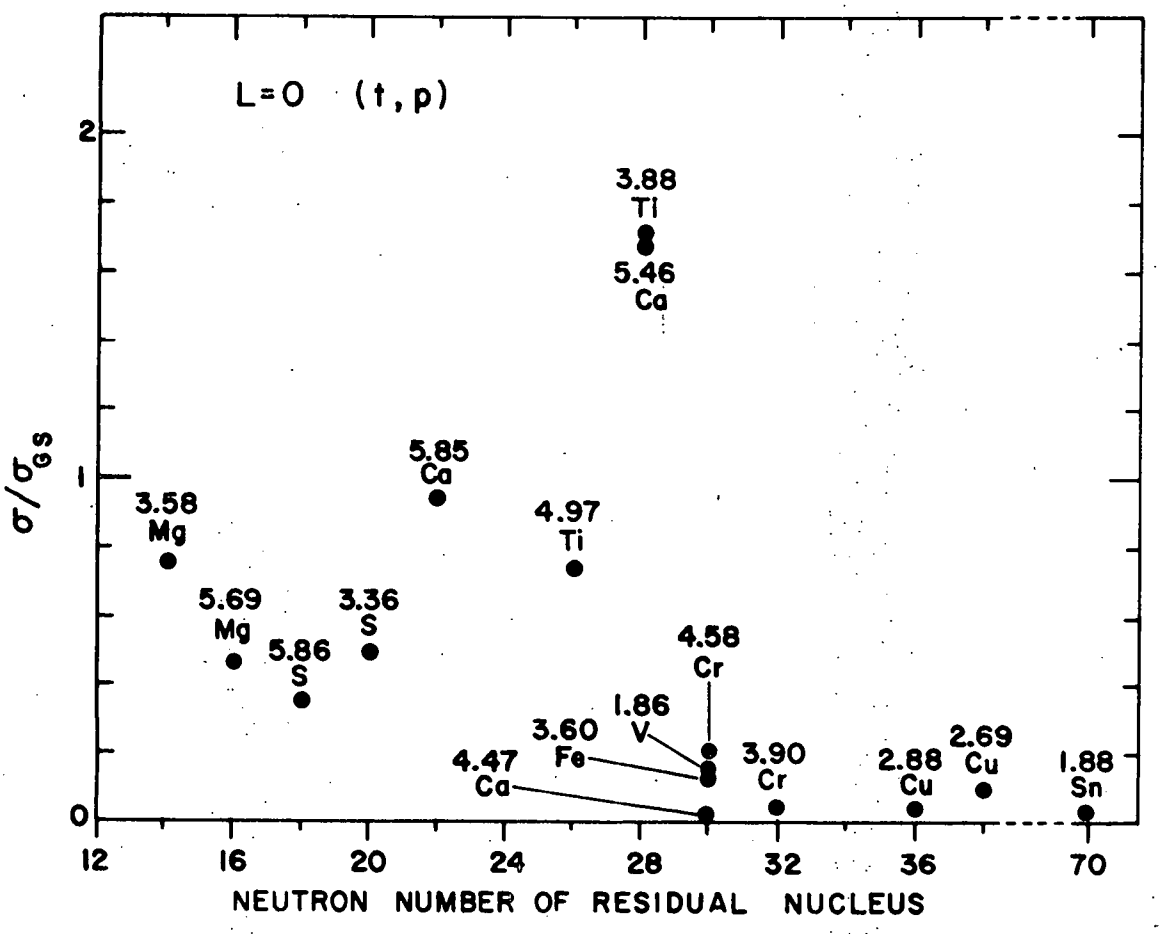

Fig. VI-1. The ratio of the cross section of the first $J^{\pi} = 0^{+}$ excited state to the 0^{+} ground state in the (p,t) reaction with angular-momentum transfer L = 0, plotted as a function of neutron number. The data are from Ref. Hi67.

a function of neutron number for $L_{nn} = 0$. The fact that the ratio reaches a peak at N = 28 (^{50}Ti) and then drops suddenly at N = 30 is taken as evidence that the 3.88-MeV state of ^{50}Ti is a two-particle excitation (Hi67) of neutrons into some mixture of the $1f_{5/2}$ and 2p orbits (since they are almost degenerate) so that the resulting configuration is $[(\pi 1f_{7/2})^2(\nu 1f_{7/2})^{-2}(\nu 1f_{5/2}2p)^2]$ coupled to J = 0, T = 2. Operating on the 3.88-MeV state of ^{50}Ti with T_- then places the extra proton in a mixture of the $1f_{7/2}$ and $1f_{5/2}2p$ orbits. The configuration of the 8.588-MeV state of ^{50}V is then the two-particle excitation

$$\sqrt{2}/3\,[(\pi 1f_{7/2})^3(\nu 1f_{7/2})^{-3}(\nu 1f_{5/2}2p)^2]^{T=3}_{J^\pi=0^+}$$

$$+\sqrt{1}/3\,[(\pi 1f_{7/2})^2(\pi 1f_{7/2}2p)(\nu 1f_{7/2})^{-2}(\nu 1f_{5/2}2p)]^{T=3}_{J^\pi=0^+}.$$

The configurations of both analog states are then approximately known, and both should be populated in the (^{3}He, p) reaction with $L_{np} = 0$. This is shown is Fig. III-6.

If the ground state of the ^{48}Ti target is assumed to be wholly $1f_{7/2}$ configuration, then the (^{3}He, d) reaction should populate the 4.820-MeV state by $\ell_p = 3$ transfer (since it is wholly $1f_{7/2}$ configuration) but not the state at 8.588 MeV (which is a two-particle excitation). The 4.820-MeV level is seen but contaminants (carbon) in the target prevent the extraction of an angular distribution to certify that the proton is transferred with $\ell_p = 3$. No (^{3}He, d) measurement was made at 8.58 MeV excitation. The (^{3}He, α) reaction should populate the 4.820-MeV level by $\ell_n = 3$ transfer, as is observed in Fig. III-8 but should not populate the level at 8.588 MeV (the two-particle excitation) which is not observed (Br66) in the ^{51}V(^{3}He, α)^{50}V spectrum at 26° and 13 MeV.

2. The 1^+ Levels at 1.333 and 1.490 MeV

The levels at 1.333 and 1.490 are populated by the γ decay of the 4.820- and 8.588-MeV $J = 0$ analog states, respectively, and hence cannot be $J = 0$ themselves. They are populated in the $^{48}Ti(^3He, p)^{50}V$ reaction with momentum transfer $L_{np} = 0$; and this means that they can be only $J^\pi = 0^+$ or 1^+. They are then $J^\pi = 1^+$.

The γ decay from the 0^+ analog state at 4.820 MeV to the 1^+ state at 1.333 MeV must be M1. Further, the wholly $1f_{7/2}$ configuration of the 4.820-MeV level implies that the 1.333-MeV level is wholly $1f_{7/2}$ configuration. If the level is wholly $1f_{7/2}$, the (^{3}He, d) and (^{3}He, α) reactions should populate it with $\ell = 3$ transfer, as is observed (Table III-1). The 1^+ member of the $(\pi f_{7/2})(\nu f_{7/2}^{-1})$ octet in ^{48}Sc is seen to lie at an excitation of a few MeV, and by analogy we tentatively assign the 1.333-MeV level as the 1^+ member of the $(\pi f_{7/2})(\nu f_{7/2})^{-1}$ octet in ^{50}V.

The γ decay from the 0^+ analog state at 8.588 MeV to the 1^+ level at 1.490 MeV must also be M1. However, the level at 8.588 MeV was seen to be a two-particle excitation and, since the p orbit and f orbit may not be connected by an M1 transition, the 1.490-MeV level is also a two-particle excitation. (The M1 operator may connect $1f_{5/2}$ to $1f_{7/2}$ but we assume that is negligible.) Such a two-particle excitation would not be observed in the (^{3}He, d) nor (^{3}He, α) reactions studied here nor in the $^{50}V(p, p')^{50}V$ studied by Buhl et al. (Bu69). The 1.490-MeV level is indeed unobserved in all these reactions and we take it to be a low-lying 1^+ two-particle excitation.

3. The Levels at 0.388 (2^+), 0.355 (3^+), 0.322 (4^+), and 0.266 MeV (5^+) and the 6^+ Ground State

The fact that the (^{3}He, d) and (^{3}He, α) reactions reported in this work have populated the low levels with a large $\ell = 3$ spectroscopic factor (Figs. IV-5, 6) implies they are mostly $1f_{7/2}$ configuration. (A very small admixture of $\ell = 1$ transfer was observed in the (^{3}He, d) reaction to some final states.) Unfortunately the spins of these levels cannot be extracted from the spectroscopic factors because of the configuration mixing (wholly $1f_{7/2}$) that is present (Mc64a).

The (^{3}He, p) reaction with angular-momentum transfer $L_{np} = 0$ cannot populate levels with $J^\pi \geq 2^+$, and these low levels are not in fact observed to be populated. However, the (^{3}He, p) reaction would populate a $J^\pi = 1^+$, $1f_{7/2}$ configuration (e.g., the level at 1.333 MeV) so that probably none of these levels are 1^+, in agreement with the tentatively assigned spins of Ref. (B169). The γ decay of levels populated by (^{3}He, p) with momentum transfer $L_{np} = 0$ is expected to proceed to levels with $J^\pi = 0^+$, 1^+, or 2^+; and we see (Fig. II-12) that only the (2^+) level at 0.388 MeV is populated by the γ decay. The observation of these but not the lower levels ($J^\pi \geq 3^+$) again supports the tentative spins.

The lowest five levels in ^{50}V are assgined as the $2^+ - 6^+$ members of the $(\pi f_{7/2})(\nu f_{7/2}^{-1})$ octet on the basis of this evidence.

4. The (2^+) Levels at 1.305 and 1.515 MeV

Because the (^{3}He, p) reaction is expected to proceed directly to the $J^\pi = 0^+$ and 1^+ levels with momentum transfer $L_{np} = 0$ and because the levels populated by the (^{3}He, p) reaction

with $L_{np} = 0$ are expected to γ decay to levels with $J^\pi = 0^+$, 1^+, and 2^+, the levels at 1.305 and 1.515 MeV are tentatively assigned $J^\pi = (2^+)$. They are not populated directly ($J^\pi \neq 0^+$, 1^+) but are populated in the γ decay of levels populated directly ($J^\pi = 0^+$, 1^+, or 2^+).

5. The Levels of Odd Parity

Six levels in (^{3}He, a) are seen (Table III-1) to proceed by a transfer of $\ell = 0$ or 2. These states have large spectroscopic strengths ($\sum S_{\ell=0} = 2.4$ and $\sum S_{\ell=2}$ 1.7) and are taken as levels with $2s_{1/2}$ and $1d_{3/2}$ hole configurations, respectively.

The (^{3}He, d) reaction may not populate a hole configuration directly but only by a two-step process. None the less, two levels are formed with an $\ell = 0$ transfer. The spectroscopic strength ($\sum [(2J_f + 1)/(2J_i + 1)]S = 0.37$) is small as a result of the non-direct nature of the transition.

6. Possible Levels of a Collective 1^+ Mode

Fleming's recent evidence (Fl70) for a collective 1^+ mode in ^{50,48}Sc is based on a large number of levels in ^{50,48}Sc strongly excited by (^{3}He, p) reactions with L = 0 + 2 mixtures. In the present ^{48}Ti(^{3}He, p)^{50}V angular distributions (Fig. III-10), the filling of the minima (possibly a characteristic of L = 0 + 2 mixtures) is as prominent as it is in the angular distributions of Fleming. From this we conclude that the levels at 1.333, 1.490, 2.395, 2.819, 3.240, and 3.474 MeV may also be collective 1^+ excitations. Some reservation is warranted on the grounds that DWBA calculations of two-nucleon transfer are not as straightforward as those of one-nucleon transfer, as noted in Chap. IV. As a result, there remains a question whether the filling of the

L = 0 minimum is due to the L = 2 admixture or to some component of the wave function of the state. The nature of these possible 1^+ states cannot be made more definite without microscopic calculations to examine how different admixtures of wave functions affect the angular distributions predicted by the DWBA.

VII. CONCLUSIONS

The ^{50}V nucleus, whose ground-state configuration is $(\pi f_{7/2})^3(\nu f_{7/2})^{-1}$, is subject to investigation by analyzing experimental data to determine the matrix elements of operators and, since these are not overly complex, to draw some inferences about the wave functions underlying these matrix elements. The experiments and analyses reported here are the γ decay of levels populated by the (^{3}He, p) reaction with angular-momentum transfer $L_{np} = 0$ and the DWBA analysis of the single-nucleon transfer reactions (^{3}He, d) and (^{3}He, α) and of the two-nucleon transfer reaction (^{3}He, p).

The experimental methods necessary to measure the $^{48}Ti(^3He, p\gamma)^{50}V$ reaction at high counting rate and high resolution have been described along with the methods used to accumulate, manipulate, and reduce the 10^6 channel data from a two-parameter pulse-height analyser. The use of the Argonne split-pole magnetic spectrograph for measuring the angular distributions of charged particles and the operation of the automatic track-plate scanner to read off the data on the resulting photographic record were also discussed.

Spectroscopic factors S were extracted via DWBA analyses of the angular distributions of charged particles from single-nucleon transfer reactions. Comparison between the absolute cross sections measured at 15—22 MeV and DWBA predictions showed no breakup phenomena. The sum rule for the L = 3 spectroscopic factors is seen to be satisfied to within 25%. On the assumption that the neutron-proton pair was transferred as a deuteron, the DWBA analysis of the (^{3}He, p) reaction has allowed the assignment of angular-momentum transfers L_{np} for this reaction, but no spectroscopic values were extracted.

This work has resulted in the assignment of $J^{\pi} = 1^{+}$ to the ^{50}V levels at 1.333 and 1.490 MeV. The level at 1.490 MeV is seen to be a two-particle excited state with two nucleons in the degenerate $1f_{5/2}$ and 2p orbits, whereas the 1.333-MeV level is purely $1f_{7/2}$. The spins of the lowest four excited states had been tentatively assigned by Blasi (BL69) and Del Vecchio (De71), and these are supported. These four states of spin 2^{+}—5^{+}, the 6^{+} ground state, the 7^{+} state at 0.911 MeV, and the 1^{+} state at 1.333 MeV are thought to be seven members of the $(\pi f_{7/2})(\nu f_{7/2})^{-1}$ octet.

The isobaric analog states at 4.82 and 8.58 MeV are observed to be populated in the (^{3}He, p) reaction with pure L = 0 transfer of the np pair. Many other levels above 1.3 MeV and below 4.0 MeV are also observed, and the angular distributions of some could be interpreted as mixtures of L = 0 + 2. Such an angular distribution is observed for the $J^{\pi} = 1^{+}$ level at 1.333 MeV. A mixture of L = 0 + 2 necessitates a $J^{\pi} = 1^{+}$ state. In the work of Fleming (FL70), such a group of 1^{+} levels with a large (^{3}He, p) cross sections has been interpreted as evidence for a collective 1^{+} mode in ^{48,50}Sc. Since the ground state of ^{50}Sc has the configuration $(\pi f_{7/2})(\nu p_{3/2})$, which is very similar to the $(\pi f_{7/2})^{3}(\nu f_{7/2})^{-1}$ configuration of the ground state of ^{50}V, such a collective 1^{+} mode might be expected if two protons are considered to be paired to S = 0. However, the present work yields no evidence of strong enough population to confirm a collective excitation.

Two nuclear models are evaluated by comparison with the available experimental data. The truncated $1f_{7/2}$-orbit spherical shell model of McCullen, Bayman, and Zamick (Mc64) predicts energy levels and wave functions for ^{50}V. These wave functions are used to calculate the spectroscopic factors for the

levels populated by $\ell = 3$ transfer in the (^{3}He, d) and (^{3}He, α) reactions. The energy levels below 1 MeV are seen to be well reproduced, although the calculations predict an extra 4^+ and an extra 5^+ level. The comparison of the predicted spectroscopic factors is hindered by the uncertainty in the assigned spins of the four lowest excited states. The predicted values are in the right neighborhood for the lowest states, even though the (^{3}He, d) results show that an admixture of the 2p orbit is present in some of the levels and this orbit is outside the wave-function space of the MBZ calculations.

The other model evaluated is the rotational particle coupling model with two particles outside a deformed core (Wa70a). This model has been able to reproduce the experimental energy levels about as well as the MBZ calculations; it even predicts the extra 4^+ and 5^+ levels. We cannot calculate spectroscopic factors with the RPC model at this time. Such a calculation could prove interesting inasmuch as the spectroscopic values depend more critically on the wave function used than do the level energies.

The most serious impediment in this study of ^{50}V has been the uncertainty of the spin assignments of levels. Such assignments are necessary if one wishes to compare model calculations with experimental measurements in order to identify the corresponding levels. Also missing are γ-decay transition rates, which constitute a sensitive measure of the wave functions of nuclear levels. The decay of the level at 1.490 MeV is expected to be especially slow (much slower than the 1.333-MeV decay), since the annihilation and creation operator connecting the wave functions of the initial and final states is thought to act only through minor components in these wave functions. The γ decay of the $(\pi f_{7/2})(\nu f_{7/2})^{-1}$ octet (via the 1.333 → 0.388 → 0.355 →

0.322 → 0.226 → 0.0 cascade) should proceed readily since at each step the proton particle and neutron hole merely recouple to a total angular momentum decreased by one unit.

Microscopic DWBA calculations of two-nucleon transfer could help to establish if some of the levels excited by (^{3}He, p) in the excitation range 1.3—4.0 MeV are in fact populated by L = 0 + 2 and are therefore 1^+ states. If they are 1^+ levels of very large strength, a 1^+ collective mode would be further supported.

ACKNOWLEDGMENTS

I would like to thank my thesis supervisors Dr. Luise Meyer-Schützmeister of Argonne National Laboratory and Dr. Paul Singh of Indiana University not only for their invaluable assistance and guidance on the work reported here but also for the moral encouragement and friendship given through my term as a graduate student. My thanks also go to Drs. G. Hardie and T. H. Braid for their assistance in the experimental phase of this work. For the program ODD-ODD, I am grateful to Drs. J. R. Comfort, P. Wasielewski, and F. B. Malik. I am indebted to Dr. Comfort for discussions on the application of ODD-ODD to the ^{50}V nucleus.

I would like to acknowledge the kindness and assistance shown to me by the whole Argonne Physics Division staff. The fine condition of the Argonne split-pole spectrograph and its associated equipment, which is under the supervision of Dr. J. R. Erskine and C. Bolduc, has greatly simplified the accumulation of high-quality angular distributions. The efforts of J. R. Wallace, P. Billquist, and the crew of the tandem in providing the ^{3}He beam is gratefully acknowledged. The excellence of the electronics arrangement used in the γ-decay measurements was in large measure due to the efforts of R. Larson and M. Strauss of the Argonne Electronics Division. The careful work of J. Franklin in setting up the hardware for the γ-decay measurement is appreciated.

The physical form of this work is largely due to the careful draftsmanship of D. Kurth and B. Greenberg, the editing of Dr. F. E. Throw, and the careful typing of the Physics secretaries.

The financial support I received from the Argonne Universities Association, Indiana University, and the U. S. Atomic Energy Commission is gratefully acknowledged. I am grateful to Dr.

L. M. Bollinger for the opportunity to use the facilities of the Argonne Physics Division in the measurements and analyses reported here.

APPENDIX A. PROGRAM FOR TWO-PARAMETER PULSE-HEIGHT ANALYSIS

A. Purpose of the Programs

The purpose of the program GROUP to be described is to provide a speedy and convenient way to accumulate, manipulate, and reduce data from up to two two-parameter pulse-height analyzers of 10^6 channels each. Previous experience with the program DIDJERIDOO (Ge65) has shown that a single program subdivided into many basic functions, which may be executed singly or in automatic sequences, provides the experimenter with a versatile tool for data handling. In program GROUP there are 50 basic functions. It is assumed that any operation the experimenter wishes to perform may be accomplished as a sequence of these. A statement of what GROUP can do is clearly impractical because each possible task corresponds to one combination of functions selected from these 50, and the number of such combinations is extremely large. Rather, the approach will be to discuss what each of the functions does by itself and to illustrate the capabilities of GROUP by presenting a few examples in which functions are combined to accomplish a task. Experience indicates that the user will then be able to select the appropriate sequence of functions for his own problem.

Section B of this appendix details the control of GROUP by computer interrupts and sense-switch options. Section C discusses each of the basic functions of GROUP in detail.

Although GROUP may be used to form the two-parameter 10^6-channel pulse-height array from the magnetic-tape output of function TAKE 2 (via TPTSLC), GROUP is necessarily slow to make the 10^6-channel array. Another program called

DIMWIT has been written to make the array (that is perform the pulse-height analysis) about 30 times faster than GROUP can. DIMWIT requires about 300 μsec per event. The input-output requirements and sense-switch options of DIMWIT are discussed in Sec. D.

The operator often finds he would like to add two 1024 × 1024-channel arrays (or subarrays thereof) element by element. This process may be performed with an appropriate sequence of functions with GROUP but may be done much faster and with less chance of operator error with program ADDUP. The input-output requirements and sense-switch options of ADDUP are detailed in Sec. E.

Although GROUP is limited to spectra of 1024 channels (because of the limited storage available in the computer), this does not imply that the 10^6-channel arrays must be only 1024 × 1024. Other array sizes such as 512 × 2048 and 256 × 4096 are perfectly usable; however, only 1024 channels of the 2048 or 4096 may be investigated at one time. Section F of this report explains the use of GROUP with such rectangular arrays.

B. Program Control

The program GROUP uses six of the available program interrupts (specifically A, B, C, S, M, and OP). Operation of the interrupts C or OP (C will be used in following examples) will instruct the program that the operator wishes to have the program execute one (only) of the functions. The program will type out "FUNCT" and the experimenter is expected to type in the six-letter mnemonic name of a function (plus a carriage return). If that mnemonic name is one of the 50 allowed, the program executes the corresponding function. If that mnemonic is not one of the 50

allowed, the program types "AGAIN" and waits for the operator to type in an allowed mnemonic name.

Operation of the program interrupts B, S, or M will instruct the program to execute the automatic sequence B, S, or M, respectively. Any of these three sequences (B will be used in the following example) may be changed by the experimenter at his convenience—for example, by executing the function ENTB5B (i.e., enter a B sequence as explained in detail in Sec. C). The experimenter must then enter a list of up to ten function mnemonics to be executed when the interrupt B is operated; e.g., the sequence, MT1TSL, SLTPTR will read a 1024-channel spectrum from magnetic tape and print it on the line printer every time the B interrupt is operated. This list is terminated by a carriage return and stop.

The interrupt A is reserved for starting and stopping the function TAKE 2 (described in Sec. C) as a result of some necessary hardware associated with the transmission of analog-to-digital converted words from the analyzer to the computer.

There are six sense switches on the computers. Four of these (2—5) take on different meanings in different functions as detailed in Sec. C. Sense switches 1 and 6 are reserved for the system control of the program. Sense switch 1 must remain on at all times to indicate to the program that the operator wishes to communicate with it via the console typewriter (mostly for historical reasons). Turning on sense switch 6 indicates to the program that it is in the process of being loaded and that no functions are to be executed. Sense switch 6 should be off for normal program operation. This use of switch 6 is not necessary from a systems point of view but allows a considerable saving of time in executing the program.

The program GROUP was written in a sublanguage of Fortran II documented by Holland (Ho67). Because the program is many times too large for the computer memory, it is linked and executed in segments. The segments not being used are stored in the external core memory. Since Holland clearly explains the linkage principles of which program GROUP is built, no further explanation is given here.

The array sizes in GROUP limit the projections of the two-parameter measurements to 1024 channels. GROUP includes an array of 1024 computer words called SLICE (usually SL or SLC in a mnemonic) which is used by GROUP to save a one-parameter projection of one of the two-parameter arrays. Many references to the array SLICE will be found in Sec. C. GROUP also reserves a 51200 word array BLOCK in the external core memory (usually called EM in a mnemonic). This BLOCK of computer words may be thought of as 50 of the 1024-channel slices which might at some point in the execution of the program be placed in the array SLICE; or this BLOCK may be considered as a 50×1024-channel subarray of the 1024×1024-channel two-parameter spectrum. This 51200-word array will be referred to in Sec. C as the BLOCK in the external core memory, and each of the fifty 1024-word arrays will be referred to as a slice (numbered 1 to 50) in the BLOCK of external core memory.

C. The Functions of GROUP

This section contains a discussion of each of the 50 functions of GROUP. Each individual description starts with the mnemonic name (except for the first function which has the null name and is called by typing only a carriage return and a stop code) followed by a short description of the purpose of the function. Next

comes a detailed description of the use of the function. Finally any sense-switch options are enumerated. All typewriter input-output is in integer format with a six-digit maximum. GROUP uses only the magnetic tape (usually MT1 or TP in a mnemonic) with logical unit zero (0).

1. This function orders a return to the waiting loop. If it is executed after a C interrupt, it acts as a do-nothing statement. It serves to end an "enter sequence" function (function 2, 3, or 4).

2. ENTB5B

3. ENTERS

4. ENTERM allows the operator to enter a sequence of up to 10 function mnemonics to be executed when the interrupts B, S, or M are operated, respectively. The program types out "TYPE IN SEQ." The operator types in up to 10 mnemonic names. The list of function mnemonics is terminated by function 1, a carriage return and a stop code.

5. TYPE_B

6. TYPE_S

7. TYPE_M types out the list of mnemonics corresponding to the function sequence in sequence B, S, or M, respectively.

8. CYCLEB is a special function that forces the program to keep repeating the sequence of functions in the B (only) automatic sequence until sense switch 6 is turned on. Then after the current function is

finished, the program will go to the wait loop before the next function is started. Sense switch 6 must now be turned off.

9. RUNNUM — allows the operator to type in a number that will subsequently be used to identify data (a run number). The program types out "TYPE RUN NO" and the operator must type in an integer of up to 6 digits plus a carriage return.

10. WOTRUN — request a type-out of the run number used to identify the data.

11. AUGRUN — augments by 1 the current run number and types the result.

12. AUGHND — augments the current run number to the next higher hundred. The new run number is typed out.

13. SRCHT1 — searches forward on the magnetic tape (0) for a given run number. The program requests the input of the desired run number by typing "GIVE RUN NUMBER REQD." The operator must supply a run number by typing in up to 6 digits. The tape is left positioned immediately before the file corresponding to the input run number and "FOUND IT" is typed. If the entered run number is not found, either "MT POSITIONED" is typed (as explained for function 14: POSNT1) or an end of tape is encountered.

14. POSNT1 — searches forward on magnetic tape (0) to find the end of data (EOD) mark (specified in function

20: SLTMT1), then backspaces over the EOD mark and types "MT POSITIONED." The next record will be written over the EOD mark.

15. RDRUN1 — reads and types out the run number which is next on magnetic tape (0) and then backspaces to its original position. The typed-out run number becomes the current run number.

16. FRWDSP — advances magnetic tape (0) one record.

17. BK1RCD — backspaces magnetic tape (0) one record.

18. BK1RUN — backspaces magnetic tape (0) one file.

19. WRTEOF — writes a file mark on magnetic tape (0), follows this with an EOD mark, and backspaces over the EOD mark.

20. SLTMT1 — writes a file of three records onto magnetic tape (0). The first record is two words; the current run number and a second word which ordinarily is unused. The second record is 1024 words long and is read from the array SLICE. The third record is the file mark. An EOD mark is written after the file mark and is backspaced over.

21. MT1TSL — reads a three-record file from magnetic tape (0). The first record is two words. The first word is read as the run number and becomes the current run number. The second record is 1024 words and is read into the array SLICE. The third record is a file mark.

22. TPDUMP transfers data from magnetic tape (0) to the 51200-word BLOCK in external core memory. This BLOCK in external memory is broken into fifty 1024-word slices and the tape is read (as up to 50 files) exactly as function MT1TSL. The program asks for the run number of the last file to be transferred to the BLOCK in external memory by typing "GIVE LAST RUN." Next, by typing "GIVE INITIAL SLICE," the program asks for the first slice (1—50) in the BLOCK in external memory into which the first file from tape is to be read. The next file on magnetic tape is read in and the 1024-word array is put into the slice number entered. Finally the run-number record (from the file read from magnetic tape) is typed out. The next file is read into the next slice and this process is continued until the last run number typed out is identical to the desired last run as originally typed in by the operator. The current run number is unchanged. If sense switch 5 is on, the typeout is bypassed.

23. EMDUMP transfers data from the BLOCK in external core memory to magnetic tape (0) exactly as function SLTMT1. The program asks for the first slice number (1—50) to be transferred as a file to magnetic tape (0) by typing "GIVE INITIAL SL NO." Next to ask for the last slice number (1—50) to be transferred the program types "GIVE FINAL SL NUMBER." The current run

number is written as the run number in the first file written on tape, and that number is printed on the lineprinter. Then the run number is augmented by 1. Files are written onto tape until the last slice (as typed in) is written.

24. ZEROEM — sets to zero the contents of the 51200-word BLOCK in the external core memory.

25. EMTSLC — transfers one of the 50 slices from the BLOCK in external core memory to the contents of SLICE. The program asks for the number of this slice by typing "GIVE NO OF SLC." The operator must respond by typing a number from 1 to 50.

26. SLCTEM — transfers the contents of SLICE into one of the 50 slices in the BLOCK in external core memory. The program asks which one of the 50 slices is to be written by typing "GIVE POSN FOR STORE." The operator must respond by typing in a number from 1 to 50.

27. SLTPTR — prints the contents of SLICE onto the line printer. First is written the current run number. Next the contents of the 1024-word SLICE array are written, 16 channels to a line. The leftmost column is a number indicating how many channels have been printed (to and including the previous line).

28. ADDSPC — causes the spectrum in SLICE to be added channel by channel to one of the 50 slices in the BLOCK in external core memory and puts

the results in SLICE. The coincident channel limits written in the second and third spectral channels (lower limit and upper limit, respectively, as explained in connection with function 48: TAKE-2), are preserved. The lower limit in channel 2 is taken from SLICE and the upper limit in channel 3 is taken from the slice in the BLOCK in external core memory. For example, with this function the operator can construct the gamma spectrum in coincidence with proton channels 1—4 from the gamma spectra in the BLOCK in external core memory (i.e., the channels in coincidence with proton channels 1—1, 2—2, 3—3, and 4—4). When the addition is done in this order, the limits are 1—4. Since SLICE is not necessarily zero at the start, the first function should be EMTSLC (function 25). The program types "GIVE SLC NOS" to ask for the slice number of the BLOCK in external memory that is to be added. The operator must call ADDSPC once for each spectrum to be added.

29. ADTPEM — adds the 1024-channel spectra from the files on magnetic tape to the slices in the BLOCK in external core memory one by one. The program asks for the last number on the tape by typing "GIVE LAST NO ON TAPE" and for the first slice number by typing "GIVE FIRST SLC." The next file from magnetic tape is read into the computer array SLICE, and the slice from

the BLOCK in external core memory is read from the slice specified. The two are added channel by channel except channel 2 (lower limit) comes from the magnetic tape and channel 3 (upper limit) comes from the slice of the BLOCK in external core memory. The result of the addition is written back into the slice of the BLOCK in external core memory from which the original slice was taken. The current run number becomes the last one read from tape, and the line printer prints out the slice number and the run number. Addition of sequential pairs of spectra continues until the last run number, as specified, is read from magnetic tape and processed.

30. PEAKEY displays the contents of SLICE as a one-parameter pulse-height spectrum of 1024 channels on the memory-display oscilloscope as a series of 1024 points. In addition to the spectrum, an axis is displayed with a point every 32 channels. Four displayed control points cause operations to be performed if they are sensed by the light pen. 1) The point in the upper left-hand corner ends the function. 2) The one in the upper right-hand corner is unused. 3) The one just below point 2 cuts the maximum scale of the display in half and thereby magnifies the display. 4) The point just below point 3 doubles the maximum scale of the display and thereby shrinks the display.

The function PEAKEY may be operated in either of two modes, which are named for the interrupts S and M that send the function into their respective modes when operated. The function starts in the S mode. While this is in effect, penning a point in the displayed spectrum causes either the energy corresponding to that point or alternatively some parametric number depending on the numbers entered in the CONSTS array (as explained in connection with function 31: CALPAR) to be written on the display scope. Three points in the spectrum are brightened, namely the penned point and the points corresponding to its energy ±1.022 MeV (providing that energy constants were entered) in order to identify the double-escape peak (-1.022 MeV) or the full-energy peak (+1.022 MeV) in a γ-ray spectrum. If one operates the M interrupt, the M mode is entered and the full scale of the display is typed out on the typewriter. If any points of the spectrum are light penned, their channel numbers are entered into a list in the computer and may be used by other functions. In addition, these channel numbers are typed out on the typewriter. The operator may return to the S mode by operating the S interrupt.

31. CALPAR performs a least-squares fit (linear or quadratic) to two sets of numbers (of up to 10 elements

each) that convert the member of one set into the members of the other set. Most commonly the conversion from channel number (independent set) to energy (dependent set) is desired. The program asks if the channel numbers are to be entered via typewriter or display scope by typing "TYPE OR SCOPE." The operator must type in "TYPE" or "SCOPE." If he types in "TYPE," the program types out "CHAN" and the operator must type in the independent variable; then the program types "ENERGY" and the operator must type in the corresponding dependent variable. This list of up to 10 pairs is terminated when both the independent and dependent variables are entered as 0.

If the operator has chosen SCOPE, the spectrum from SLICE is displayed and the operator must first push the M interrupt and then light-pen the independent variable set and finally terminate the display as in PEAKEY by penning the point in the upper left corner. The typewriter types "ENERGY" and the operator must type in the dependent variable set in the order corresponding to the independent variable set.

After either of these processes is finished, the program types "LNR OR PBRL" for linear fit (LNR) or quadratic fit (PBRL). If the operator types in "LNR" or "PBRL" (and carriage return stop) the program does a

2- or 3-parameter fit to the respective sets. The typewriter paper always serves as a log of the input. The numbers resulting from the fit are saved in an array dimensioned 4 × 3, since there are up to 3 numbers for the conversion and 4 one-parameter spectra (two from each two-parameter measurement). The results from any CALPAR are stored in the section of the 4 × 3 array corresponding to the one-parameter spectrum stored in SLICE. The contents of the 4 × 3 array may be interrogated by executing function WOTCON.

32. CONSTS allows the entry of constants, as would be calculated by CALPAR, directly into the array described in CALPAR. The program asks for which one-parameter spectrum the constants should be entered by typing "ADC X OR Y." The operator must type in 1X, 1Y, 2X, or 2Y to indicate not only the two-parameter set 1 or 2 but also the axis X or Y of the one-parameter spectrum. The operator must then type in three numbers (which, for the case of conversion from channel number to keV, have the units given in parentheses), namely 1) ten times the constant term (tenths of keV), 2) a thousand times the linear term (eV per channel), and 3) a million times the quadratic term (meV/channel^2). Note that if the constants entered are 0, 1000, 0, the conversion will be the identity transformation and may be used to

display channel number with PEAKEY.

33. WOTCON — types out the constants entered by CALPAR or CONSTS. The program asks "ADC X OR Y" and the operator must type in "1X," "1Y," "2X," or "2Y." The constants are typed out in the same units as were listed in function 32: CONSTS.

34. ENTLMT — allows the operator to enter up to 50 pairs of numbers (from 1—1024) that will be used as pairs of lower and upper channel limits by other functions. The channel limits are defined as LL $\leq$ channel $\leq$ UL. The program asks "ADC X OR Y" to which the operator must respond "1X," "1Y," "2X," or "2Y," to specify the analog-to-digital-converter number. If "1X" is typed, the limit pairs will produce a 1Y spectrum in coincidence with 1X events between the entered channel limits. The program next asks "TYPE OR SCOPE" to which the operator must respond "TYPE" or "SCOPE." If he enters "TYPE" the program types "LL" to invite him to type in a lower limit and then "UL" to request an upper limit. The pairs of numbers are entered at the end of a list until either 50 paris have been entered or the list is terminated by entering a pair having zero for both limits. If an upper limit is less than its corresponding lower limit, then "AGAIN" is typed and the operator must re-enter the pair.

If "SCOPE" was typed on the other hand, the program displays the spectrum in SLICE, if that spectrum corresponds to the ADC number typed in. If there is no correspondence, the program types "WRNG SPCTR, IF OK SS6, RUN" and halts. When the computer RUN button is pressed and sense switch 6 (SS6) is off, the function terminates. If sense switch 6 is on, however, the program displays the contents of SLICE on the scope. (Sense switch 6 must then be turned off.) The M interrupt must be operated to enter the channel numbers in the list by light-penning; no entry takes place unless the scope display is in the M mode. The energies represented by the points may be interrogated in S mode just as in function 30: PEAKEY. The program assumes that the limits are penned in pairs consisting of lower and an upper limit, in that order. The channel numbers of the penned points are also typed out. After 50 pairs are entered or the display is terminated (as in function 30: PEAKEY) the function inserts these limit pairs into the limit list after any limit pairs already present. The number of the pair after the word SLICE will be typed out whenever an upper limit is less than the associated lower limit. Each pair of 50 limit pairs will correspond to a slice in the 50 $\times$ 1024-word BLOCK in external memory, and hence they

are numbered by their slice numbers. If an odd number of limits has been entered, "ODDLMT" is typed and many limit pairs may be incorrect because the operator entered an upper limit into a lower limit or vice versa. The sense-switch-6 option has just been discussed.

35. LSTLMT — prints the whole limit list on the line printer. Each line has first the word SLICE, then the number of the limit pair followed by 1X, 1Y, 2X, or 2Y to specify the corresponding analog-to-digital converter, and finally the characters LL= and the lower limit followed by UL= and the upper limit. There are up to 50 such lines, one for each pair.

36. CHGLMT — allows the operator to change one of the limit pairs in the limit list. The program asks for the number of the desired pair by typing "SLICE" and the operator must enter its slice number. The pair is then entered, just as it would be in function 34: ENTLMT except only one pair will be accepted and this limit pair will replace that of the slice number typed in.

37. ERASER — allows the operator to erase all or part of the limit list and reorder the remainder of the limits and slices so there are no vacant slices in the BLOCK in external memory nor vacant slots in the limit list. The program asks "ALL OR PART." If "ALL" is typed in, the

whole limit list is erased but the slices in the BLOCK in external core memory are untouched. (The latter can be set to zero by use of the function ZEROEM.) If "PART" is typed in, the program types "SLICE" to invite the operator to type in the slice number. The program then moves all the limit pairs above the entered number down one pair, and similarly all the slices in the 50 × 1024-word BLOCK in external core memory above slice corresponding to the entered number are moved down one slice. The effect is to erase both the limit pair and its corresponding 1024-channel slice in the BLOCK in external memory. The program will continue to ask for slices to erase until the number zero is entered to terminate the function.

38. SETPLT — allows the operator to tell the program the number of channels and the number of inches per channel to be plotted on the Calcomp plotter if a plot function is called. The program asks for the number of channels to be plotted in by typing "GIVE NO CHANNL." (The effective limit is 1024 because of the dimension of SLICE.) The program next asks "GIVE NSTEP," and the operator replies by stating the step size (in hundredths of an inch per channel) to be used by the plotter.

39. SETSCL — allows the operator to set the number of events that are to occupy full scale (10 in.) on the

Calcomp plotter. The program invites the operator to type in the full-scale value by typing "FULL SCALE." If the operator types in a zero the program will inspect the spectrum in SLICE each time a plotting function is called and will take the full scale to be the number of events in the channel with the most events.

40. WOTSCL — types out the number specifying the number of events taken as the full-scale excursion (10 in.) on the Calcomp plotter when a plotting function is executed.

41. PLOTSL — plots the contents of the array SLICE as a pulse-height spectrum (in the form of a histogram) according to the parameters entered in functions 38 and 39: SETPLT and SETSCL. In the lower left-hand corner of the plot, numbers are written in three rows. Reading left to right, the top row has the number of events corresponding to full scale on the plotter. The second row has the current run number and the number of the analog-to-digital converter (1X = 1, 1Y = 2, 2X = 3, and 2Y = 4). The third row has first the lower limit and then the upper limit corresponding to the channels in the conjugate spectrum with which the plotted spectrum was in coincidence.

42. PLOTEM — causes the Calcomp plotted to plot a histogram of the data from selected slices from the BLOCK in external core memory according to

the parameters entered in functions 38 and 39: SETPLT and SETSCL. The program types "FIRST" to ask for the first of the 50 slices in external core memory to be plotted. The program next types "LAST" to ask for the final slice in external core memory to be plotted. Finally the program types "NO OF SUMS." This number is the number of spectra to be added together channel by channel (just as in function 28: ADDSPC). If the number of sums is 1, no addition takes place. The plot output is just like that from function 41: PLOTSL. If the number of sums is greater than 1 and the slices have been read into the BLOCK in external core memory with the lowest limit first and there are no gaps in the list, then the limits will be written correctly on the plot. For example, if FIRST = 5, LAST = 11, NO OF SUMS = 5, then the three plots corresponding to slices 5+6+7+8+9, 6+7+8+9+10, and 7+8+9+10+11 will be added channel by channel.

43. PLOTGM causes the 1024-channel spectrum obtained in function 50: ANALYZ (i.e., the 1024-channel spectrum in coincidence with some specified part of the 50-channel spectrum) to be reconstructed in SLICE and plotted on the Calcomp plotter. If PLOTGM is executed after ANALYZ, the 1024-channel spectrum will be plotted on the same scale as was used for the display on the memory oscilloscope in ANALYZ. The

current run number, maximum scale, limits, and analog-to-digital-converter number are written on the plot just as in function 41: PLOTSL. The plot is always 1024 channels long and the step is 0.01 in. per channel.

44. SETANA — allows the operator to type in a list of up to seven numbers that indicate the order in which the seven 1-parameter multichannel analyzers are to transmit the contents of their memories into the array SLICE in function 45 or 48: DUMPAN or TAKE_2. Each analyzer has a number in the range 1—7, and the order in which these numbers are entered into the list in SETANA is the order in which the analyzer memory will be transmitted. The list is ended after seven numbers are entered or a zero is entered.

45. DUMPAN — transfers the contents of the one-parameter multichannel analyzer memories into SLICE and onto magnetic tape (0) (if sense switch 5 is off) in the order of the SETANA list until (as specified in function 44) until seven spectra are transferred or a zero is encountered in the SETANA list. The file on magnetic tape is in the same format as in function 20: SLTMT1, and the run-number record contains the current run number as the first word and the negative of the analyzer number as the second word. Before the file is written on magnetic tape (0) the run number and analyzer number are typed

out. After the file is written on magnetic tape (0), the current run number is augmented by one. If sense switch 5 is on, nothing is written onto magnetic tape (0).

46. 1KDUMP — transfers a 1024-word subarray of the 4096-word memory attached to the Nuclear Data two-parameter analyzer to the array SLICE. The 1024-channel subarray is switch-selected on the Nuclear Data memory, and the Nuclear Data memory mode must be in stop 2. Since the dual analog-to-digital-converted results of converter number 1 may be routed into this memory (a 4096-channel subarray from the 10^6-channel array), 1KDUMP may be used to transfer events that have been pulse-height analyzed by the Nuclear Data memory. The operator should realize that one-parameter spectra such as can be stored in the memory of the Nuclear Data analyzer may be obtained with the limit pair 1 and 1024 by using function 48: TAKE_2. If 1KDUMP is used, the operator should execute function 47: SETADC immediately afterward. Failure to do so will almost certainly result in future errors.

47. SETADC — allows the operator to instruct the program that he wishes the contents of SLICE to be identified as originating from analog-to-digital converter 1X, 1Y, 2X, or 2Y. The program asks "ADC X OR Y," to which the operator must respond "1X," "1Y," "2X," or "2Y." Channels

2 and 3 (the lower and upper limits) of the spectrum in SLICE are altered.

48. TAKE_2 accumulates events from up to two (if sense switch 2 is on) Nuclear Data ND160 dual analog-to-digital converters on magnetic tape (0), sorts pulse-height information according to the limit list and enters it into the BLOCK in external memory, displays the results of the sorting on the scope as data are accumulated, reads the contents of up to four ASI scalers, and controls the beam shutter. When TAKE_2 is called, the program types first "TAKE_2" and then the run number. If sense-switch 4 is on, the operator next is requested to "GIVE NUMBER OF RECORDS" (containing 256 analog-to-digital-converted events) at which intervals the beam shutter will be closed, the scalers will be stopped, and a one-parameter analyzer memory will be transferred as in function 45: DUMPAN according to the first element of the list from function 44: SETANA. The scalers will then be restarted and the beam shutter opened. The above process from closing to opening of the shutter will also occur any time the B interrupt is operated during the data-transfer process in TAKE_2. Next the program types out "ANALYZER NO I WILL BE DUMPED EVERY J RECORDS," where I is the first element of SETANA list (function 44) and J is the number of records

entered. (If sense switch 4 was off, if a 0 was entered, or if I = 0, the analyzer contents will not be transferred.)

The program now waits for the Nuclear Data two-parameter analyzer to transmit 256 words which will fill one buffer array in the computer. When the buffer array is filled, another is opened and the contents of the first are written onto magnetic tape (unless sense switch 5 is on). Next in accordance with the limit list entered by ENTLMT (function 34), the words in the buffer are sorted into one-parameter spectra in the BLOCK in the external memory. The result of the sorting of a one-parameter pulse-height spectrum corresponding to a limit pair is displayed on the display scope. In the upper right-hand corner is the number of the limit pair (1—50) that produced the spectrum. Below that number is a number that represents the full scale on the scope display. The full scale is taken as the number of events in the channel with the most events when the display scope first displays the spectrum number. This scale factor may be halved by operating the S interrupt. Every time the M interrupt is operated, the spectrum number to be displayed increases by 1. The spectrum is displayed on the scope only when the computer is not busy changing buffer areas or writing on magnetic tape (0).

In order to terminate the flow of data into buffer arrays, the operator must operate the blue A interrupt button on the BØ-5 unit. No other interrupt button will terminate the transfer of data because of hardware limitations in instructing the computer that the buffer is full. If sense switch 3 is off, the shutter is closed, the scaler is turned off, and the contents of the scalers are typed out. The current run number, the negative of the first element of the analyzer list, the number of records written onto tape (0) unless sense switch 5 is on, and the number of current integrator interrupts is typed out.

Putting sense switch 2 on implies that form will be taken from 2 two-parameter experiments; turning it off implies that only the one two-parameter analyzer attached to the Nuclear Data memory unit will be used.

The off position of sense switch 3 implies that the beam shutter, scaler control, and 1-parameter-analyzer control will proceed automatically; putting it in the on position implies that these operations must be performed manually. If sense switch 3 is off and the magnetic tape fails while words converted from analog to digital are being recorded, the beam shutter is closed, the scaler is turned off, the one-parameter analyzer are halted, and the computer halts and types out "RCRD NO. X." If RUN on the computer is operated, everything

will continue as normal.

The on and off positions of sense switch 4 respectively imply that the operator does and does not desire the contents of the one-parameter analyzer appearing first in the analyzer list to be transmitted to magnetic tape (0) after a given number of records are written on that tape.

The on position of sense switch 5 implies that all output to magnetic tape (0) will be bypassed, off implies that magnetic tapes will be written. This sense-switch-5 option is convenient for accumulating the one-parameter spectra from the Nuclear Data analyzer in the BLOCK in the external core memory according to the limit list; the process then is not slowed down by the magnetic tape (which can only handle an input rate of about 4 records per second). The operator can conveniently accumulate the singles spectra (i.e., spectra with no coincidence requirement) with sense switch 5 on and limits of 1 and 1024 in the limit list for 1X, 1Y, 2X, and 2Y.

The format in which words from the analog-to-digital converter are written onto magnetic tape by TAKE_2 consists of a two-word record of the current run number and then 256-word records of analog-to-digital-converter words, and finally an end of file followed by an end-of-data mark (which is backspaced over).

49. TPTSLC performs the sorting (pulse-height analysis of words from the analog to digital converter) of one file of information on magnetic tape written by TAKE_2 (function 48) according to the limits currently in the limit list. The results are stored in the 50 × 1024-word BLOCK in external core memory. After the end of file is read, the program compares the number of records sorted against the number written. If the numbers are equal, the function terminates. If they are unequal, the program types "RCD COUNT ERR" followed first by the number of records read by TPTSLC (function 49) and then by the number written by TAKE_2 (function 48).

Because TPTSLC is limited to a block of 51 200 words, and because it uses the same sorting routine as TAKE_2 (which allows the events to occur randomly—as they actually do when the data are taken), the sorting by TPTSLC requires about 4.5 msec/event. A factor of 30 in speed may be gained by using the full 98 304 words of the external core memory and by requiring the limit list to be sequential. To do this, program DIMWIT (described in Sec. D) was written.

50. ANALYZ allows two-parameter pulse-height data to be reduced to the information of interest. That is, one may find which peaks in one of the parameters are coincident with peaks in the other

parameter; further, one may get the number of events under such two-dimensional peaks. The operator should transfer into the 51 200 word BLOCK in external core memory fifty 1024-channel γ-ray spectra coincident with protons so that if first gamma spectrum is in coincidence with proton pulses of some energy E to $E + \Delta E$ the i^{th} gamma spectrum is in coincidence with protons having energies from $E + (i - 1)\Delta E$ to $E + i\Delta E$ for $1 \leq i \leq 50$. ΔE is the energy width of each of the 50 channels. (The programs DIMWIT (Sec. D) and ADDUP (Sec. E) normally produce their results in a form so that this condition is automatically met and one may use TPDUMP to read the BLOCK in external memory). Call the 50 gamma spectra P1, · · ·, P50. ANALYZ will consider the 51 200-word BLOCK in external core memory as a two-parameter pulse-height spectrum of 50×1024 channels.

From this BLOCK two 1-parameter spectra are creaded. A coincidence gamma spectrum is obtained by summing gamma spectra in the BLOCK in external core memory from Pi to Pj, where Pi and Pj are the selected proton channel numbers from $E + (i - 1)\Delta E$ to $E + j\Delta E$. Likewise, a spectrum of protons in coincidence with a given γ ray may be obtained. If for proton channel Pk the coincident gamma spectrum contains a peak from gamma spectrum channel γi to γj (the lowest and highest channel

in the peak, respectively) and if a low channel background may be taken from γk to $\gamma i-1$ and a high channel background may be taken as $\gamma j + 1$ to $\gamma \ell$, then ANALYZ will fit the background points with a quadratic fit (or with a linear fit if sense switch 2 is on) and take the area from γi to γj minus the background from γi to γj as the number of events for the Pk element of the proton spectrum. Repeating the same process for k = 1—50 results in the 50 channel proton spectrum in coincidence with the gamma peak in channels γi to γj. The background correction in the gamma spectrum is necessary because of the Compton scattering of gammas of higher energy would produce spurious peaks in the proton spectrum.

These two spectra (proton and gamma) are displayed on the memory display oscilloscope. The 50-channel proton spectrum is on the left; and depending on whether sense switch 3 is off or on, the right-hand position displays respectively the first or the last 960 channels of the 1024-channel γ spectrum. In addition, the points Pi, Pj, γi, γj, γk, and $\gamma \ell$ are brightened in the displayed spectra and their channel numbers are listed along the top of the display screen. Each of these channel numbers is entered by light-penning the corresponding point in the appropriate spectrum of the display scope. A few precautions on the

points which may be light penned are taken, viz. $Pi < Pj$, $\gamma k < \gamma i \leq \gamma j < \gamma \ell$ and when light penning the proton spectrum (to get a coincident gamma spectrum) the gamma spectrum cannot be light penned until both Pi and Pj are penned, likewise for light penning the four gamma spectrum points.

By reducing the two-parameter data to one-parameter spectra over narrow limits, one can find which proton peaks are in coincidence with which gamma peaks. For identification of the channel numbers or energies of the proton spectrum or the gamma spectrum (if the correct constants have been entered via function 32: CONSTS or function 31: CALPAR) another mode has been built into ANALYZ. The experimenter may change modes by operating either the M or S interrupt. In mode 2, the numbers Pi, Pj, γi, γj, γk, and $\gamma \ell$ are not displayed, and if a channel in the gamma spectrum is light-penned its channel number or energy is displayed. If a proton channel is penned, the scope displays its channel number or energy (depending on the number entered in CONSTS); and in the upper right-hand corner is displayed the result of integrating the proton spectrum from the last proton point penned to the current one, inclusive.

Putting sense switch 2 on forces the gamma background to be fitted with two

variable quantities (i.e., it calls for a linear fit). When sense switch 3 is on, the last 960 channels of the 1024-channel gamma spectrum are displayed.

D. Program DIMWIT

Program DIMWIT performs the pulse-height analysis (sorting) of words which TAKE_2 (function 48 of GROUP) accepted from an analog-to-digital converter and stored on magnetic tape (0). DIMWIT is capable of sorting a 96 × 1024-channel subarray of the 1024 × 1024 array produced by any pair of the dual analog-to-digital converters. The input magnetic tape is logical unit 0 and the output magnetic tape is logical unit 2. The program types "ENTER RUN NO FOR OUTPUT" and the operator must type in the identifying number to be written on magnetic tape (2) for the first of the 96 output files. These files are the 1024-channel spectra from the external core memory written in the same format as SLTMT1 (function 20 from GROUP). If 1001 is entered, for example, the 96 output spectra will be numbered 1001—1096. Next the DIMWIT types "FIRST" and expects the operator to type in the lowest channel number of the subarray to be formed. Next DIMWIT types "STEP," to which the experimenter must respond with the number of input channels to be integrated to form an output channel. Then DIMWIT asks "ADC X OR Y," to which the experimenter must respond "1X," "1Y," "2X," or "2Y" to indicate the analog-to-digital converter on which the sorting is to proceed. DIMWIT then prints out the list of 96 limit pairs that will be sorted into the external core memory. This input is repeated until a 0 is entered as an output number. Next DIMWIT types "RUN NO FOR INPUT" to ask for the runs to be sorted. To make his selection from among the runs written onto magnetic tape (0) by TAKE_2, the experimenter types

in a list of their run numbers. This list is ended by typing in a zero.

DIMWIT then erases (sets to zero) the external core memory (if sense switch 5 is off) and prints out the set of 96 limit pairs it will use. It then searches forward on magnetic tape (0) to find the first run number for input, whereupon "FOUND IT" is typed and the sorting proceeds. This process is repeated until the list of input run numbers is finished. The magnetic tape (0) is rewound. DIMWIT now searches magnetic tape (2) for an end-of-data mark (as written by function 20: SLTMT1). The 96 1024-word slices are now written onto magnetic tape (2), and the corresponding run numbers are printed on the line printer. After magnetic tape (0) is rewound, this process is repeated for every set of output numbers and their corresponding limit pairs.

Sense switch 1 must be on. Putting sense switch 2 on will instruct DIMWIT to pause after magnetic tape (0) is rewound and before magnetic tape (2) is written. If only one magnetic-tape handler is available, the output tape may be mounted as logical unit 2 and the output will proceed on this unit. After the output has finished, the program will again pause so magnetic tape (0) may be remounted. Putting sense switch 3 on means that the search for the input run number will be bypassed and the sorting will start immediately. Whenever TAKE_2 has written the first run number over the magnetic tape load point, this option should be used. Sense switch 3 should be turned off as soon as sorting has begun. Sense switch 4 will postpone the output on magnetic tape (2) and allow a new magnetic tape (0) to be mounted. The program then will ask for a new set by typing "RUN NO FOR INPUT." The external core memory is not erased and the subarray from several

input tapes may thus be accumulated in the external core memory. When sense switch 4 is turned off, the output will proceed normally. With sense switch 4 on, the operator should have sense switch 2 on. Turning sense switch 5 on instructs the program to skip the part of the program which erases external core memory. Use of this sense switch is not normally necessary but is sometimes convenient if the sense-switch-4 option is being used and a typing-in error requires the program to be restarted from the beginning. In this case sense switch 5 should be turned on in order to avoid erasing the data previously accumulated in external core memory.

E. Program ADDUP

Program ADDUP is capable of adding several 96 × 1024-channel subarrays channel by channel to form a total 96 × 1024-channel subarray. The input magnetic tape is logical unit 0, and the output magnetic tape is logical unit 2. ADDUP first types "OUTPUT NO" and the operator must type in an identifying number which will be used to label the files on magnetic tape (2), which are written in the standard format produced by SLTMT1 (function 20). If, for example, the operator types in 1001, the 96 output run numbers will be 1001—1096. ADDUP next types "INPUT NOS," and expects the operator to type in the first run numbers of each of the 96 × 1024 subarrays that were written on magnetic tape (0) and that are to be added channel by channel into the 96 × 1024-channel array in the external memory. The list of input numbers is ended by entering a zero. The whole input sequence is repeated until zero is entered as an output number. The process followed for each set consisting of an output number and several input numbers is as follows. First, the

external core memory is erased. Second, the first input number is searched for on magnetic tape (0) and then added into the external core memory in the first of the 96 1024-channel slices, and similarly the 2nd through 96th files are added to the correspondingly numbered 1024-channel slices. Third, the second step is repeated for each input number. Fourth, magnetic tape (0) is rewound. Fifth, magnetic tape (2) is searched for an end-of-data mark (as written by function 20: SLTMT1). Sixth, the contents of external core memory are written out on magnetic tape (2) as 96 1024-word files in SLTMT1 format. The output number is printed on the line printer after the file is written on magnetic tape (2).

Sense switch 1 must be on. If sense switch 2 is on, the program ADDUP will pause between the fourth and fifth steps and after the sixth.

F. Rectangular Arrays

The GROUP system supposes that the dual Nuclear Data analog-to-digital converter puts out one ASI computer word for each two-parameter event. The ASI word has 21 bits (labeled as B1–B21). The 21st bit (B21) indicates which of the two dual analog-to-digital converters created the event and is beyond the experimenter's control. From the remaining 20 bits, bits B1–B10 (X1–X10) are taken by GROUP as one parameter (X) and bits B11–B20 (Y1–Y10) are taken as the other parameter (Y) to form the 1024 × 1024 channel event (N. B. $2^{10} = 1024$). Should 4096 × 256 array be desired, the patch board connected must be arranged so that X1–X10 go to B1–B10, Y1–Y8 go to B11–B18, and X11 and X12 go to B19 and B20. The array created will then be four 1024 × 256 arrays, and each of the routines in Secs. C, D,

and E will use one of four 1024-channel subsection of the 4096-channel spectrum. Clearly other patch board arrangements are possible to achieve other sectioning of the 10^6-channel array.

APPENDIX B. CALCULATION OF SPECTROSCOPIC FACTORS BY USE OF THE MBZ WAVE FUNCTIONS

I. Calculations for the $^{49}Ti(^3He, d)^{50}V$ Reaction

With the square bracket [ ] used to denote angular-momentum coupling, the spectroscopic factor is defined as

$$S = Z \left| \langle \Phi^I(p_1 \cdots p_Z, n_1 \cdots n_N | [\chi^J(p_1 \cdots p_{Z-1}, n_1 \cdots n_N)\psi(p_Z)]^I \rangle \right|^2,$$

where the function Φ^I is a ^{50}V wave function of total angular momentum I, the wave function χ^J is a ^{49}Ti wave function of total angular momentum J, ψ is the wave function of the proton removed from ^{50}V to form ^{49}Ti, and Z is the number of protons in the $1f_{7/2}$ orbit of the ^{50}V nucleus. Let $j \equiv \frac{7}{2}$ represent the spin of each nucleon in the $1f_{7/2}$ orbit and let α be the serial number of a state having a given spin J. Then, as in Chap. V, a wave function of ^{49}Ti may be written

$$\chi(^{49}Ti, \alpha J) = \sum_{\nu' L'} D^{\alpha J}(\nu' L')[\psi_{12}(j^2 \nu' L')\psi_n(j^{-1})]^J \qquad (B1)$$

The $D^{\alpha J}(\nu' L')$ are the (real) coefficients of the expansion given in reference Mc64a. The $\psi_{12}(j^2 \nu' L')$ are the wave functions of two protons coupled to total angular momentum L' and seniority ν'. The neutron hole is allowed to have only the total angular momentum $j \equiv \frac{7}{2}$. The proton and neutron wave functions are coupled to total angular momentum J. Likewise,

$$[\psi_{12}(j^2 \nu' L')\psi_n(j')]^J = \sum_{\alpha} D^{\alpha J}(\nu' L')\Phi(^{47}Ti\ \alpha J). \qquad (B2)$$

On the other hand, we may write the ath state of spin I in ^{50}V as

$$\Psi(^{50}V, aI) = \sum_{\nu L} C^{aI}_{(\nu L)}[\psi_{12}(j^3 \nu L)\psi_n(j^{-1})]^I.$$

This expression for the ^{50}V wave function can be put in the desired form by successively (a) expanding in terms of fractional-parentage coefficients, (b) reordering the vector coupling, (c) recoupling by use of the Racah coefficient U, (d) reordering the vector coupling coefficient, (e) substituting from Eq. (B2), and finally (f) using the Racah coefficients. The result, shown step by step, is

$$\Psi(^{50}V, aI) = \sum_{\substack{\nu L \\ \nu' L'}} C^{aI}(\nu L)(j^2 \nu' L'; \} j^3 \nu L)[[\psi_{12}(j^2 \nu' L')\psi_3(j)]^L \psi_n(j^{-1})]^I \qquad \text{(B3a)}$$

$$= \sum_{\substack{\nu L \\ \nu' L'}} (-1)^{L'+j-L} C^{aI}(\nu L)(j^2 \nu' L'; j \} j^3 UL)$$

$$\times [[\psi_3(j)\psi_{12}(j^2 \nu' L')]^L \psi_n(j^{-1})]^I \qquad \text{(B3b)}$$

$$= \sum_{\substack{\nu L \\ \nu' L' \\ J}} (-1)^{L'+j-L} C^{aI}(\nu L)(j^2 \nu' L'; j \} j^3 \nu L) U(jL'Ij; LJ)$$

$$\times [\psi_3(j)[\psi_{12}(j^2 \ 'L')\psi_n(j^{-1})]^J]^I \qquad \text{(B3c)}$$

$$= \sum_{\substack{\nu L \\ \nu' L' \\ J}} (1)^{2j+J+L+L'-I} C^{aI}(\nu L)(j^2 \nu' L'; j \} j^3 \nu L) U(jL'Ij; LJ)$$

$$\times [[\psi_{12}(j^2 \nu' L')\psi_n(j^{-1})]^J \psi_3(j)]^I \qquad \text{(B3d)}$$

$$= \sum_{\substack{\nu L \\ \nu' L' \\ J}} (-1)^{2j+J+L+L'-I} C^{aI}(\nu L)(j^2 \nu' L'; j \} j^3 \nu L)$$

$$\times U(jL'Ij; LJ) D^{aJ}(\nu' L')[\Phi(^{49}\mathrm{Ti}, aJ)\psi_3(a)]^I \qquad \text{(B3e)}$$

$$= \sum_{aJ} \sum_{\substack{\nu' L' \\ \nu L}} (-1)^{2j+2J+2L-2I} C^{aI}(\nu L) D^{aJ}(\nu' L')(j^2 \nu' L'; j \} j^3 \nu L)$$

$$\times \left(\frac{2J+1}{2I+1} \frac{2L+1}{2L'+1} \right)^{1/2} U(jLJj; L'I)[\Phi(^{49}\mathrm{Ti}, aJ)\ \psi_3(j)]^I. \qquad \text{(B3f)}$$

Using this in the definition of the spectroscopic factor for the transition from $(^{49}\mathrm{Ti}, aJ)$ to $(^{50}\mathrm{V}, aI)$ one has

$$S_{aJ \to aI} = 3 \Big| \sum_{\substack{\nu L \\ \nu' L'}} (-1)^{2j+2J+2L-2I} C^{aI}(\nu L) D^{aJ}(\nu' L')(j^2 \nu' L'; j \} j^3 \nu L)$$

$$\times \left(\frac{2J+1}{2I+1} \frac{2L+1}{2L'+1} \right)^{1/2} U(jLJj; L'I) \Big|^2.$$

Here the spectroscopic factor for the (^{3}He, d) reaction from the ^{49}Ti ground state (^{49}Ti, α=1, J=j) to ^{50}V(aI) is expressed in terms of the coefficient of fractional parentage, the Racah coefficients, and the MBZ expansion constants. When this spectroscopic factor is multiplied by $(2J_f + 1)/(2J_i + 1)$ so that it can be compared with experimental values, the final result is

$$\frac{2I+1}{2J+1} S_{aI} = 3 \Big| \sum_{\substack{\nu L \\ \nu' L'}} (-1)^{14+2L-2I} \left(\frac{2L+1}{2L'+1} \right)^{1/2} C^{aI}(\nu L)$$

$$\times D^{1j}(\nu' L')(j^2 \nu' L'; j \} j^3 \nu L) U(jLjj; L'I) \Big|^2$$

II. Calculations for the ^{51}V(^{3}He, α)^{50}V Reaction

The calculation proceeds just as in Appendix BI. The results are

$$S = 8 \left| \langle [\chi^I p_1 p_2 p_3 \eta_1 \cdots \eta_7) \psi(\eta_8)]^I \left| \Phi^J (p_1 p_2 p_3 \eta_1 \cdots \eta_8) \right\rangle \right|^2,$$

$$\chi (^{50}\mathrm{V}, aI) = \sum_{\nu L} C^{aI}(\nu L) [\ _{123}(j^3 \nu L) \psi_{1,\,7}(j)]^I,$$

$$[\psi_{123}(j^3 \nu L) \psi_{1,\,7}(j)]^I = \sum C^{AI}(\nu L) \chi (^{50}\mathrm{V}, aI),$$

$$\Phi(^{51}\mathrm{V}, \alpha J) = [\psi_{123}(j^3 J) \psi_{1,\,8}(j^8 0)]^J$$

$$= [\psi_{123}(j^3 J) [\psi_{1,\,7}(j^7 j) \psi_8(j)]^0]^J$$

$$= \sum_I U(JjJj; I0) [[\psi_{123}(j^3 J) \psi_{1,\,7}(j^7 j)]^I \psi_8(j)]^J$$

$$= \sum_{Ia} U(jjJj; I0) C^{aI}(\nu J) [\chi (^{50}\mathrm{V}, aJ) \psi_8(j)]^J,$$

$$S_{\alpha J\text{-}aI} = 8 \left| U(JjJj;I0) C^{aI}(\nu J) \right|^2.$$

For the reaction $^{51}V(^3He, \alpha)^{50}V(aI)$ the ground state of ^{51}V has $\alpha = 1$ and $J = j \equiv \frac{7}{2}$, and the spectroscopic factor can be written

$$S_{aI} = \frac{1}{8}(2I + 1) \left| C^{aI}(\tfrac{7}{2}) \right|^2.$$

REFERENCES

Ba62 R. H. Bassel, R. M. Drisko, and G. R. Satchler, Oak Ridge National Laboratory Report ORNL-3240 (unpublished).

Ba65 J. B. Ball and R. F. Sweet, Phys. Rev. 140, B904 (1965).

Ba65a P. D. Barnes, C. K. Bockelman, O. Hansen, and A. Sperduto, Phys. Rev. 138, B597 (1965).

Ba67 B. F. Bayman and A. Kallio, Phys. Rev. 156, 1121 (1967).

Ba68 D. Bechner, R. Santo, H. H. Duhm, R. Back, and S. Hinds, Nucl. Phys. A106, 577 (1968).

Bi70 J. N. Bishop, D. J. Pullen, and B. Rosner, Phys. Rev. 2C, 550 (1970).

Bj64 J. H. Bjerregaard, P. F. Dahl, O. Hansen, and G. Sidenius, Nucl. Phys. 51, 641 (1964).

Bl69 P. Blasi, P. R. Maurinzeg, N. Joecetti, and R. A. Ricci, Phys. Letters 28, B555 (1969).

Bo67 D. D. Borlin, Ph.D. Thesis, Washington University, 1967 (unpublished).

Br66 T. H. Braid, L. Meyer-Schützmeister, and D. D. Borlin in Isobaric Spin in Nuclear Physics, edited by John D. Fox and Donald Robson (Academic Press, New York, 1966).

Br69 G. Bruge, A. Bussiere, H. Faraggi, P. Kossaniyji-Demay, J. M. Loiseaux, P. Roussel, and L. Valentin, Nucl. Phys. A129, 417 (1960).

Bu69 W. F. Buhl, D. Kovar, J. R. Comfort, O. Hansen, and D. J. Pullen, Nucl. Phys. A131, 99 (1969).

Co66 T. W. Conlon, B. F. Bayman, and E. Kashy, Phys. Rev. 144, 940 (1966).

Co70 J. R. Comfort, private communication.

Do67 W. W. Dorenbusch, J. Rapaport, and T. A. Belote, Nucl. Phys. A102, 681 (1967).

De71 R. Del Vecchio, W. Daehnick, D. L. Dittmer, and Y. S. Park, to be published.

Er66 F. C. Erné, W. A. M. Veltman, and J. A. J. M. Wintermans, Nucl. Phys. 88, 1 (1966).

Er69 J. R. Erskine, "Argonne Split-Pole Magnetic Spectrograph Manual," Argonne National Laboratory, 1969 (unpublished).

Er70 J. R. Erskine and R. H. Vonderohe, Nucl. Instr. Methods 81, 221 (1970).

Er55 R. D. Evans, The Atomic Nucleus (McGraw-Hill Book Co., New York, 1955), p. 887.

Fl70 D. G. Fleming, R. A. Broglia, K. Abdo, O. Nathan, D. J. Pullen, B. Rosner, and O. Hansen, to be published.

Fr61 J. B. French and M. H. Macfarlane, Nucl. Phys. 26, 168 (1961).

Ge65 D. S. Gemmell, "Whaddayadoo with the Didjeridoo?," Argonne National Laboratory Report ANL-6993.

Gl65 C. M. Glashousser, Ph.D. Thesis, Princeton University, 1965 (unpublished).

Go64 M. L. Goldberger and K. M. Watson, Collision Theory (John Wiley and Sons, Inc., New York, 1964).

Hi66 S. Hinds, J. H. Bjerregaard, O. Hansen, and O. Nathan, Phys. Letters 21, 328 (1966).

Hi67 S. Hinds and R. Middleton, Nucl. Phys. A42, 422 (1967).

Ho64 O. W. Howarth and R. E. Richards, Proc. Phys. Soc. (London) 84, 326 (1964).

Ho67 R. E. Holland, "Notes on Programming the ASI Computers for Data Handling," Argonne National Laboratory Physics Division Informal Report PHY-1967A (unpublished).

Ho70 R. N. Horoshko, D. Cline, and P. M. S. Lesser, to be published.

Ka64 E. Kashy, A. Sperduto, H. A. Enge, and W. W. Buechner, Phys. Rev. 135, B765 (1964).

Ku68 D. Kurath, Argonne National Laboratory Report ANL-7512 (1968) (unpublished), p. 84.

Ku68a T. T. S. Kuo and G. E. Brown, Nucl. Phys. A114, 241 (1968).

Ku69 P. D. Kunz, private communication.

Ku70 K. Kubo, Institute for Nuclear Studies, University of Tokyo, INS-Report 143 (unpublished).

La65 R. D. Lawson, "Quasi-Particle Calculations," University of Alberta, 1965 (unpublished).

Li64 I. Lindgren, Table of Nuclear Spins and Moments in Alpha, Beta and Gamma Ray Spectroscopy, Appendix 4, edited by K. Siegbahn (North-Holland Publishing Co., Amsterdam, 1964).

Li70 K. Lips and M. T. McEllistrom, Phys. Rev. 1C, 1009 (1970).

Ma66 F. B. Malik and W. Scholz, Phys. Rev. 150, 919 (1966).

Mc64 J. D. McCullen, B. F. Bayman, and L. Zamick, Phys. Rev. 134, B515 (1964).

Mc64a J. D. McCullen, B. F. Bayman, and L. Zamick, Princeton Technical Report NYO-9891 (1964) (unpublished).

Me70 L. Meyer-Schützmesiter, D. S. Gemmell, R. E. Holland, F. T. Kuchnir, H. Ohnuma, and N. G. Puttaswamy, Phys. Rev. 187, 1210 (1970).

Mo69 M. Moinester, J. P. Schiffer, and W. P. Alford, Phys. Rev. 179, 964 (1969).

Ni55 S. G. Nilsson, Kgl. Danske Videnskab. Selskab, Mat.-Fys. Medd. 29, 16 (1955).

Pa56 S. P. Pandya, Phys. Rev. 103, 956 (1956).

Pi67 Claude St.-Pierre, P. N. Makeshwore, D. Doutriaux, and L. Lamarche, Nucl. Phys. A102, 433 (1967).

Pr62 M. A. Preston, Physics of the Nucleus (Addison-Wesley Publishing Co., Reading, Mass., 1962).

Ra70 M. N. Rao, J. Rapaport, T. A. Belote, and W. E. Dorenbusch, Nucl. Phys. A151, 351 (1970).

Ri69 R. A. Ricci, "Experimental Nuclear Structure in the $1f_{7/2}$ Shell" in Nuclear Structure and Nuclear Reactions, edited by R. A. Ricci and M. Jean (Academic Press, New York, 1969).

Sc66 W. Scholz and F. B. Malik, Phys. Rev. 147, 836 (1966).

Sc67 J. J. Schwartz, D. D. Cline, H. E. Grove, R. Shen, T. S. Bhatia, and R. H. Siemssen, Phys. Rev. Letters 19, 1482 (1967).

Se65 Emilio Segre, Nuclei and Particles (W. A. Benjamin, Inc., New York, 1965).

Se69 Hiroyoshi Sekeguchi, J. Phys. Soc. Japan 26, 589 (1969).

Sh69 Chih Shin, Ph. D. Thesis, University of Heidelberg, 1969 (unpublished).

Sh69a C. Shin, B. Pouh, K. Schadewaldt, and J. P. Wurm, Phys. Rev. Letters 21, 1124 (1969).

So69 A. Sourkes, H. Ohnuma, and N. M. Hintz, University of Minnesota Tandem Laboratory Annual Report, 1969 (unpublished).

Sp65 Paulette Spink and J. R. Erskine, "A Computer Program for Automatic Decomposition of Spectra from Charged Particle Reactions," Argonne National Laboratory Physics Division Informal Report PHY-1965B.

Sp67 J. E. Spencer and H. A. Enge, Nucl. Instr. Methods 49, 181 (1967).

Wa64 J. R. Wallace, Argonne National Laboratory Report ANL-6879 (1964), p. 35.

Wa68 B. A. Watson, Ph. D. Thesis, Indiana University, 1968 (unpublished).

Wa70 P. Wasielewski and F. B. Malik, Nucl. Phys. A160, 113 (1971).

Wa70a P. Wasielewski, Ph. D. Thesis, Yale, 1970 (unpublished).

Wh66 Charles A. Whitten, Jr., Ph. D. Thesis, Princeton University, 1966 (unpublished).

Yo62 Shiro Yoshida, Nucl. Phys. 33, 685 (1962).